2018

Iron Transport Machinery: A Potential Therapeutic Target In Escherichia Coli

Clorissa L. Washington – Hughes
University of South Carolina

IRON TRANSPORT MACHINERY: A POTENTIAL THERAPEUTIC TARGET IN *ESCHERICHIA COLI*

by

Clorissa L. Washington – Hughes

Bachelor of Science
Benedict College, 2009

Submitted in Partial Fulfillment of the Requirements

For the Degree of Doctor of Philosophy in

Chemistry

College of Arts and Sciences

University of South Carolina

2018

Accepted by:

F. Wayne Outten, Major Professor

John H. Dawson, Committee Member

Sheryl L. Wiskur, Committee Member

Beth Krizek, Committee Member

Cheryl L. Addy, Vice Provost and Dean of the Graduate School

DEDICATION

Dedicated to my father, Billy Wayne Washington, Sr. and my great – grandfather, Bishop Wallace Snow

ACKNOWLEDGEMENTS

First, I would like to thank my Lord and Savior Jesus Christ for allowing me to start and complete my PhD journey.

I would like to thank my research advisor, Dr. F. Wayne Outten for accepting me into his laboratory. When I first started in the lab, I had no idea what I was in for. He was always available to help me whenever I needed it. His mentorship has developed me into a knowledgeable scientist. His continuous support has afforded me the opportunity to travel and present my research at least six conferences. As a result, I cannot say enough about how grateful I am to have him as my PhD research advisor.

I would like to thank my research committee members: Dr. John Dawson, Dr. Sheryl Wiskur, and Dr. Beth Krizek for their continuous support and mentorship. All of these faculty members have been a tremendous part of my professional development. Their feedback has helped me become a better scientific writer and presenter. Also, their guidance and mentorship has made me a better and stronger person.

I would like to thank my previous research mentor, Dr. Qian Wang. He has taught me a great deal about science and has continued to mentor and support me over the years. Other mentors include: Dr. Caryn Outten, Dr. Natalia Shustova, Dr. Parastoo Hashemi, Dr. Susan Richardson, Dr. Mythreye Karthikeyan, Dr. Thomas Makris, Dr. Maksymilian Chruszcz, Dr. Dmitry Peryshkov, Dr. Hans-Conrad zur Loye, and Dr. Ken Shimizu.

I would like to thank Dr. L. Andrew Lee for his exceptional leadership and mentorship during my postbaccalaureate research experience. Others include Dr. Geoffrey Ford for training me as a junior scientist, Dr. Angela-Nadia Albetel and Dr. Jose Amaya for their assistance with EPR. Also, Dr. Bill Cotham and Dr. Mike Walla for assistance with mass spectrometry, Evan Talib and Kevin Tabury for assistance with rt-pcr, and Swanandi Pote for her help with PyMol and Phyre2.

I would also like to thank my mother, Gayle Washington for her immeasurable guidance, support, and feedback. As a retired secretary with over 20 years of experience, she has been instrumental in editing my grants, presentations, etc. I would like to thank my husband, Ryan O. Hughes for his loving support. I would like to thank my brother, Billy W. Washington, Jr. for his support. I would like to thank my Bishop Charles J. Rush Sr. and my entire church family for their thoughts and prayers. I would also like to thank all of my aunts, uncles, and cousins for their support and understanding these past few years.

ABSTRACT

Iron metabolism is an integral part of life for most organisms. Despite its essentiality, iron can also become toxic. There are many aspects to maintaining iron balance within the cell. The aim of this work is to provide insight into the function of several components involved in bacterial iron homeostasis. This work is significant for the development of novel antibiotics for treating resistant or pathogenic bacteria. Herein, it is shown that nickel can disrupt normal bacterial iron metabolism and that bacterial resistance can be affected by expression of iron acquisition genes. Once iron is obtained by the cell, it can be used to synthesize iron-sulfur clusters which are incorporated into many metalloenzymes. The shuttling of iron-sulfur clusters is carried out by A-Type carrier proteins and glutaredoxins. This important step is required for bacterial cell survival and provides another novel target for the development of drug treatment options.

TABLE OF CONTENTS

LIST OF TABLES

LIST OF FIGURES

LIST OF ABBREVIATIONS

AAS ..... Atomic Absorption Spectroscopy

AhpC ..... Alkyl Hydroperoxide Reductase C

ATC ..... A-Type Carrier

ßME ..... ß-mercaptoethanol

B12 ..... Cobalamin

BSA ..... Bovine Serum Albumin

C or Cys ..... Cysteine

CD ..... Circular Dichroism

cDNA ..... complementary Deoxyribonucleic Acid

CEMS ..... Center for Elemental Mass Spectrometry

Cu ..... Copper

DEAE ..... Diethylaminoethanol

DNA ..... Deoxyribonucleic Acid

DTT ..... Dithiothreitol

E. coli ..... *Escherichia coli*

ED ..... Entner-Doudoroff

Edd ..... Phosphogluconate Dehydratase

EDTA ..... Ethylenediaminetetraacetic acid

EPR ..... Electron Paramagnetic Resonance

Fd ..... Ferre

Fe.....Iron

Fec.....Ferric Citrate

Fe-S.....Iron-Sulfur

fes.....Ferric-Enterobactin Esterase

FF.....Fast Flow

FPLC.....Fast Protein Liquid Chromatography

Fur.....Ferric Uptake Regulator

Grx.....Glutaredoxin

HCl.....Hydrochloric acid

Hsc.....Heat Shock Cognate

ICP-MS.....Inductively Coupled Plasma Mass Spectrometry

IPTG.....Isopropyl ß-D-1-thiogalactopyranoside

Isc or ISA.....Iron Sulfur Cluster

LB.....Lennox Broth

LC-MS.....Liquid Chromatography-Mass Spectrometry

MQ.....MilliQ

NaCl.....Sodium Chloride

NaOH.....Sodium Hydroxide

NH_4SO_4.....Ammonium Sulfate

$NiCl_2$.....Nickel Chloride

Nif.....Nitrogen Fixation

OD.....Optical Density

OxyR.....Oxygen Regulator

PCH.....Pyochelin

PFA.....Perfluoroalkoxy

PLP.....Pyridoxal Phosphate

PMSF.....Phenylmethylsulfonyl Fluoride

PPP.....Pentose Phosphate Pathway

PVD.....Pyoverdine

RT-qPCR.....Quantitative Reverse Transcription Polymerase Chain Reaction

SDS.....Sodium Dodecyl Sulfate

Suf.....Sulfur Formation

TFA.....Trifluoroacetic Acid

UV-VIS.....Ultraviolet-Visible Spectroscopy

CHAPTER 1

INTRODUCTION

Iron

Iron is an essential trace metal that can be found in virtually all organisms from bacteria to humans. In humans, iron is required for heme biosynthesis and oxygen transport (Abbaspour et al., 2014). Bacteria use iron for DNA biosynthesis (Ratledge and Dover, 2000; Brown et al., 1969; Ehrenberg and Reichard, 1972; Messenger and Barclay, 1983; Andrews et al., 2003) and amino acid biosynthesis (Ratledge and Dover, 2000; McCandliss and Herrmann, 1978; McCandliss et al., 1978; Ray and Bauerle, 1991; Stephens and Bauerle, 1991). The struggle of maintaining iron homeostasis between humans and bacteria can lead to pathogenesis (Skaar, 2010).

Iron is a first-row transition metal that can be found in the Earth's crust. The incompletely filled *d* orbitals of iron allows its oxidation states to range from Fe^{2-} to Fe^{7+} (Ilbert and Bonnefov, 2013; Lu et al., 2016). At physiological pH, ferrous and ferric iron are most common and biologically relevant. Atmospheric oxygen levels started to increase about 2.5 billion years ago changing iron bioavailability from the soluble ferrous (Fe^{2+}) state to the oxidized and less soluble ferric (Fe^{3+}) state (Boyd et al., 2014; Anbar et al., 2007; Anbar, 2008) causing microorganisms to evolve and develop new ways to metabolize iron and oxygen. Intracellular redox cycling of enzymes produces hydrogen

peroxide and superoxide (Imlay, 2015). Ferrous iron (Fe^{2+}) and hydrogen peroxide (H_2O_2) react to form a free hydroxyl radical ($OH^{\bullet}$) which can cause oxidative damage. This process is referred to as the Fenton reaction (Koppenol, 2001; Koppenol, 1993; Fenton, 1876; Fenton, 1894; Fenton, 1896). Hydrogen peroxide can further react with the hydroxyl radical to form superoxide ($O_2^{\bullet-}$). Superoxide will then react with hydrogen peroxide to form a hydroxyl radical: Haber – Weiss reaction (Haber and Weiss, 1932). This chain reaction is terminated by ferrous iron and the hydroxyl radical generating ferric iron and water (Figure 1.1). In order to address the deleterious effects of superoxide and hydrogen peroxide, bacterial cells employ superoxide dismutases to degrade superoxide and peroxidases or catalases to degrade hydrogen peroxide. In *Escherichia coli* (*E. coli*), this process is partly regulated by OxyR (Pomposiello and Demple, 2001). The abundance and redox potential of iron allows its incorporation into many enzymes. Iron is required for bacterial cell survival and growth due to its essentiality in catalytic and electron transport processing such as oxidative phosphorylation (Kashket and Brodie, 1963), cellular respiration (Rainnie and Bragg, 1973), DNA synthesis, aromatic biosynthesis (McCandliss and Herrmann, 1978; McCandliss et al., 1978; Ray and Bauerle, 1991; Stephens and Bauerle, 1991), and DNA biosynthesis (Brown et al., 1969; Ehrenberg and Reichard, 1972; Messenger and Barclay, 1983; Andrews et al., 2003). The essentiality and potential toxicity of iron is addressed by tight intracellular regulation of iron. Iron also plays an auto-regulatory role in maintaining iron homeostasis. When iron is limiting in *E. coli*, the homodimeric protein Fur or ferric uptake regulator protein cannot bind to its own promoter region of DNA and repress transcription of iron acquisition genes. However, when iron is in excess, iron-bound Fur is active and can bind to its own promoter region and repress

$$Fe^{2+} + H_2O_2 \rightarrow Fe^{3+} + HO^- + HO^{\bullet} \quad (1)$$

$$HO^{\bullet} + H_2O_2 \rightarrow H_2O + O_2^{\bullet-} + H^+ \quad (2)$$

$$O_2^{\bullet-} + H^+ + H_2O_2 \rightarrow O_2 + HO^{\bullet} + H_2O \quad (3)$$

$$Fe^{2+} + HO^{\bullet} + H^+ \rightarrow Fe^{3+} + H_2O \quad (4)$$

Figure 1.1. Fenton and Haber – Weiss reaction.

expression of at least 80 iron acquisition genes (Figure 1.2; Andrews et al., 2003; Seo et al., 2014; Keseler et al., 2011; McHugh et al., 2003; Semsey et al., 2006).

Iron Acquisition Pathways

Escherichia coli K-12 can acquire iron using several pathways: FecA, FhuA, Feo, and FepA. When iron is limiting, ferric citrate can be used as a sole iron source using the ferric citrate transport system. This system can be regulated by an outer membrane protein FecA (Welz and Braun, 1998; Harle et al., 1995), a cytoplasmic membrane protein FecR (Ochs et al., 1995; Van Hove et al., 1990), and FecI which is located in the cytoplasm (Angerer et al., 1995; Crosa, 1997; Enz et al., 1995; Ochs et al., 1996). FecA is an outer membrane transport protein that binds ferric citrate (Braun et al., 2003; Wagegg and Braun, 1981) and transports it to the periplasmic binding protein, FecB. FecC, FecD, and FecE further transports ferric citrate in the cytoplasmic membrane (Pressler et al., 1988; Staudenmaier et al., 1989). FhuA transports ferrichrome (Schultz-Hauser et al., 1992; Ferguson et al., 1998; Locher et al., 1998) and Feo transports ferrous iron (Kammler et al., 1993). In general, FepA is responsible for the majority of iron uptake when iron is limiting. Enterobactin is a siderophore or high affinity iron-binding small molecule that binds to the outer membrane protein FepA. Ferric-enterobactin is further transported from FepA to FepB in the periplasm, and FepCDG in the inner membrane space (Larsen et al., 1997; Braun, 1995). The backbone of intracellular Fe^{3+}–enterobactin is then hydrolyzed by the esterase Fes to release ferric iron for its utilization (Brickman and McIntosh, 1992; Greenwood and Luke 1978; Bryce and Brot, 1972; Langman et al., 1972).

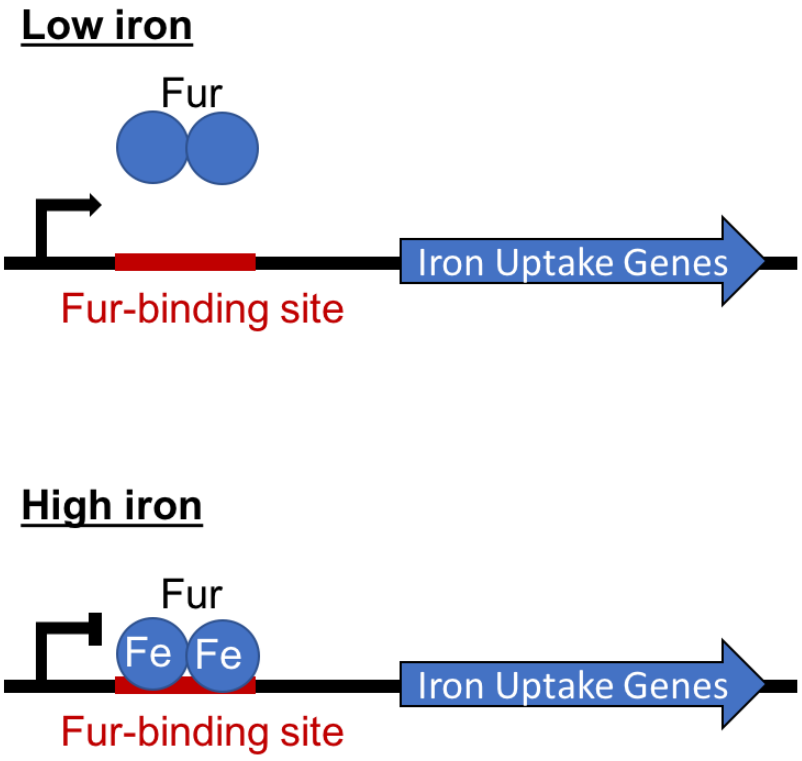

Figure 1.2. Regulation of the Ferric uptake regulator (Fur). Modified figure from Simon Andrews, 2003.

Iron-Sulfur Clusters

Inorganic sulfide and nonheme iron form iron-sulfur (Fe-S) clusters in various oxidation states including [2Fe-2S], [3Fe-4S], [4Fe-4S], [8Fe-8S], and [8Fe-7S] (Johnson et al., 2005). However, the most common types of clusters are [2Fe-2S], [3Fe-4S], and [4Fe-4S] (Figure 1.3; Fontecave, 2006). Fe-S clusters are involved in gene regulation (Kiley and Beinert, 2003; Demple, 2002), electron transfer (Hunsicker-Wang et al., 2003), and carbon metabolism via aconitase (Robbins and Stout, 1989 a, b; Lauble et al., 1992) and fumarase A (Flint et al., 1992; Flint, 1993). Gluconate metabolism can also require an Fe-S cluster enzyme. The enzyme 6-phosphogluconate dehydratase (Edd) allows 6-phosphogluconate to enter the Pentose Phosphate Pathway (PPP). Alternatively, the Entner-Doudoroff (ED) pathway can be used (Entner and Doudoroff, 1952; Peekhaus and Conway, 1998).

Iron Sulfur Cluster Biogenesis

Sulfur is an essential iron cofactor that can be used to synthesize methionine and cysteine (Bolton et al., 1951). Despite iron and sulfur essentiality both can be toxic in excess (Johnson et al., 2005). Therefore, the *in vivo* formation and trafficking of iron-sulfur (Fe-S) clusters are highly regulated. In *E. coli*, Fe-S clusters can be synthesized upon expression of the *isc* and *suf* pathway. The isc pathway is induced under normal conditions expressing these genes: *iscR, iscS, iscU, iscA, hscB, hscA, fdx,* and *IscX* (Figure 1.4). Whereas the suf pathway is induced under oxidative stress and iron-limiting conditions and express the following genes: *sufA, sufB, sufC, sufD, sufS,* and *sufE* (Figure 1.4, Mettert and Kiley, 2015; Blanc et al., 2015; Boyd et al., 2014; Outten, 2015; Py and Barras, 2010;

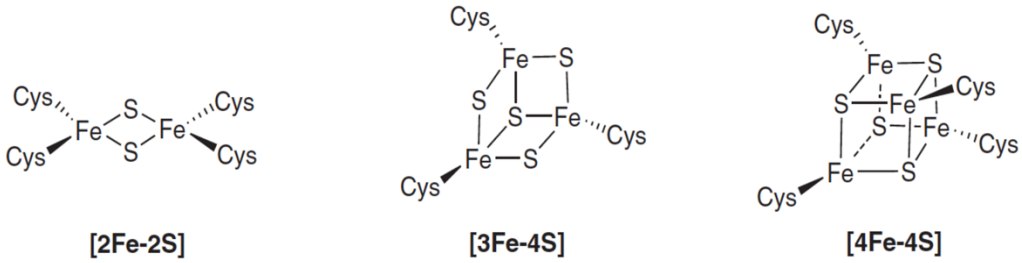

Figure 1.3. Biologically relevant Fe-S cluster types.

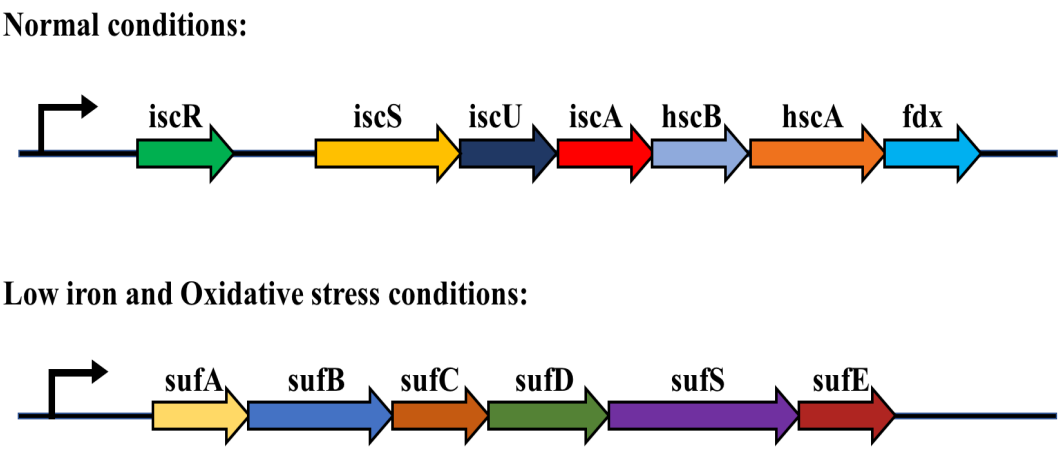

Figure 1.4. Fe-S cluster biogenesis operons in *E. coli.*

Roche et al., 2013; Outten et al., 2004). When Fe-S clusters are in excess, Holo- or iron-bound IscR can represses *iscRSUA*. Contrarily, when Fe-S clusters are limiting, ApoIscR cannot repress the *isc* operon (Schwartz et al., 2001; Yeo et al., 2006). IscR, Apo-Fur, and oxidative stress via OxyR can induce the *suf* operon (Mettert and Kiley, 2014; Yeo et al., 2006; Outten et al., 2004; Zheng et al., 2001).

Iron-sulfur cluster biogenesis requires that L-cysteine be converted to L-alanine and sulfane sulfur by a cysteine desulfurase enzyme such as IscS and SufS (Kambampati and Lauhon, 1999; Outten et al., 2003; Layer et al., 2007). Pyridoxal phosphate (PLP) and SufE bind to SufS enhancing its cysteine desulfurase activity (Outten et al., 2003). The persulfide intermediate assembled at cysteine position 364 on the dimeric SufS is transferred as a sulfur atom to SufE at cysteine position 51 (Singh et al., 2013; Ollagnier-de-Choudens et al., 2003). SufE then transfers to SufB of the scaffold protein $SufBC_2D$. The Fe-S cluster is assembled onto $SufBC_2D$; however, the iron source is unknown (Layer et al., 2007). The presence of $SufBC_2D$ enhances cysteine desulfurase activity of the SufS and SufE complex (Outten et al., 2003; Layer et al., 2007). Finally, $SufBC_2D$ can transfer its (Fe-S) cluster to SufA, an A-Type carrier protein (Chahal et al., 2009). A-Type carrier proteins are thought to transfer clusters to and from scaffold and apo targets (Vinella et al., 2009). IscS generates sulfur from L-cysteine (Schwartz et al., 2000). The persulfide intermediate assembled at cysteine position 328 of IscS is transferred to the IscU scaffold protein (Smith, 2001; Urbina, 2001; Smith, 2005; Cupp-Vickery, 2003). IscU can transfer its cluster to the A-Type carrier protein IscA (Ollagnier-de-Choudens et al., 2004). HscA and HscB can assist in the Fe-S cluster release from IscU (Hoff et al., 2000). The role of ferredoxin (*fdx*) in the *isc* pathway is unclear. However, ferredoxin can accept Fe-S clusters

from a scaffold protein (Chahal et al., 2012; Wu et al., 2002; Mansy et al., 2002) and A-Type carrier proteins (Ollagnier-de-Choudens et al., 2001; Ollagnier-de-Choudens et al., 2003; Wu et al, 2003; Nishio and Nakai, 2000).

Iron-Sulfur Cluster Trafficking

The crystal structure of dimeric SufA reveals three conserved cysteine residues at position number 50, 114, and 116 (Wada et al., 2005; Figure 2). It is believed that SufA can coordinate a [2Fe-2S] cluster at its dimeric interface. Modeling and biochemical studies suggest that SufA can bind an Fe atom alone, a [2Fe-2S] cluster, and/or a [4Fe-4S] cluster (Gupta et al., 2009; Wada et al., 2005; Ollagnier-de Choudens et al., 2003; Ollagnier-de Choudens et al., 2004). However, the coordination chemistry has not been elucidated. SufA has also been shown to transfer its cluster to apoproteins including $SufBC_2D$, a scaffold protein as proposed in the previously mentioned phylogenomic studies (Chahal et al., 2009). IscA shares a 48% sequence identity with SufA (Wada et al., 2005) and is similarly predicted to bind iron and iron-sulfur clusters. The crystal structure and modeling data suggest that IscA may coordinate two [2Fe-2S] clusters per homodimer using cysteine residues at position number 35, 99, and 101 (Cupp-Vickery et al., 2004). Biochemical studies show that tetrameric IscA can bind iron (Ding and Clark, 2004; Ding et al., 2004) as well as a [2Fe-2S] cluster. This cluster can be transferred to the IscU scaffold protein (Ollagnier-de Choudens et al., 2004). (Nif) IscA can also bind a [4Fe-4S] cluster and transfer it to the NifU scaffold protein in *Azotobacter vinelandii* (Mapolelo et al., 2012). Despite the lack of a crystal structure of ErpA, it is known that ErpA possesses conserved cysteine residues similarly to IscA and SufA. ErpA can also bind iron-sulfur

clusters including a [2Fe-2S] and a [4Fe-4S] cluster. Holo-ErpA can transfer its cluster to the apo-protein apo-IspG (Loiseau et al., 2007).

Glutaredoxins (Grx) are generally known as redox proteins that use glutathione as a cofactor. These proteins have been classified into two main groups: monothiol and dithiol glutaredoxins (Yeung et al., 2011). Dithiol glutaredoxins contain two cysteine residues in its active site and monothiol glutaredoxins contain only one cysteine in its active site (Lillig et al., 2008). Additionally, glutaredoxins can be dived into subclasses depending on its number of grx domains. Bacterial glutaredoxins have a single grx domain while eukaryotic glutaredoxins can have up to three grx domains (Mapolelo et al., 2013). In *E. coli,* there are four known glutaredoxins referred to as Grx1, Grx2, Grx3, and Grx4 (Lillig et al., 2008). *E. coli* Grx1 and Grx3 are classical dithiol glutaredoxins that contain a CXXC motif in the active site (Lillig et al., 2008; Fernandes and Holmgren, 2004). Grx2 contains the conserved CPYC motif in its thioredoxin/glutaredoxin fold; however, the second domain containing an alpha helix is unusual (Ye et al., 2014). Grx4 is the only monothiol glutaredoxin found in *E. coli* and has been associated with Fe-S cluster metabolism.

Significance

Bacterial infections begin with an overgrowth of cells in the human body. In order to combat bacterial infections, the host employs 'nutritional immunity' which is designed to starve bacterial cells of iron and nutrients. Bacteria secrete siderophores that bind and sequester iron. This iron is then transported back into the bacterial cells and this process can lead to the development of pathogenic bacteria (Skaar, 2010; Figure 1.5). The disruption to bacterial iron homeostasis can also lead to antibiotic resistance (Mehi et al.,

2014). The aim of this work is to provide insight into understanding bacterial iron homeostasis which may contribute to the development of novel drug for the treatment of resistant and pathogenic bacteria.

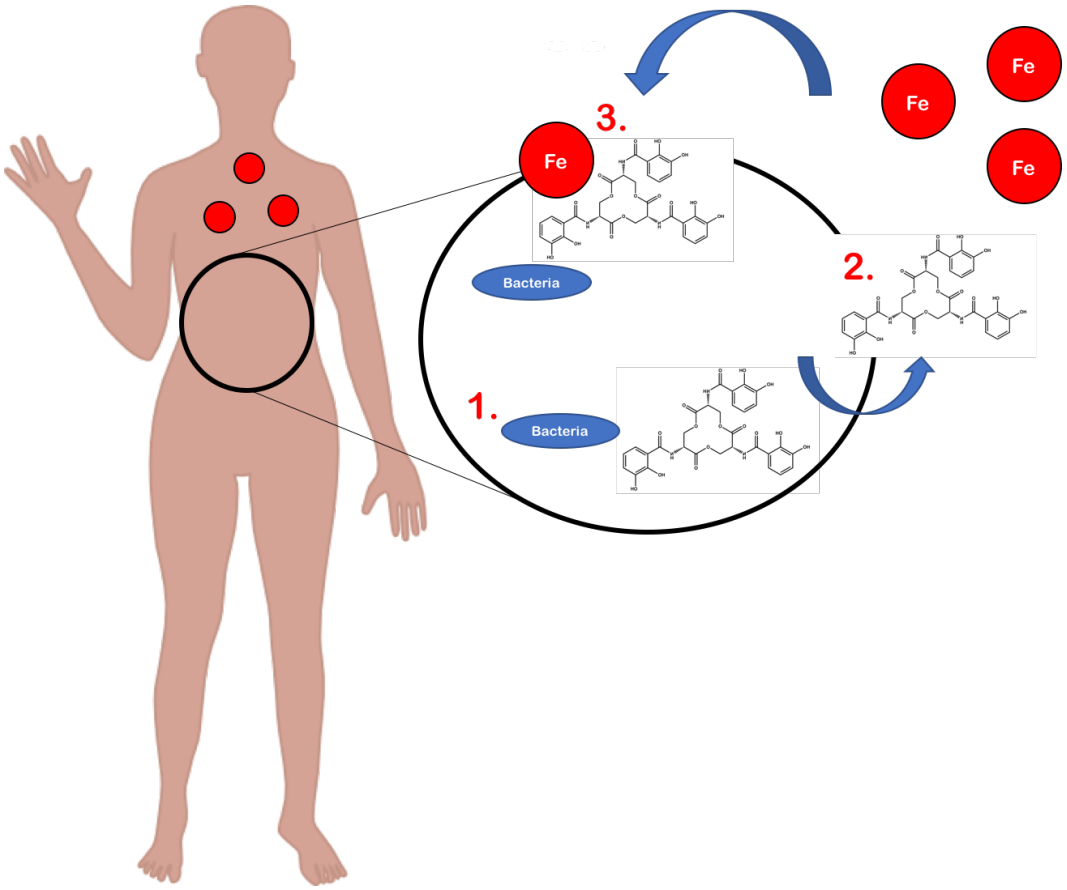

Figure 1.5. Schematic of innate immune response to bacterial infection.

REFERENCES

1. Abbaspour, N., Hurrell, R., and Kelishadi, R. (2014) Review on iron and its importance for human health. *J Res Med Sci* **19:** 164-174.

2. Anbar, A. D. (2008) Oceans, Elements, and Evolution. *Science* **322**: 1481-1483.

3. Anbar, A. D., Duan, Y., Lyons, T. W., Arnold, G. L., Kendall, B., Creaser, R. A., Kaufman, A. J., Gordon, G. W., Scott, C., Garvin, J., and Buick, R. (2007) A whiff of oxygen before the Great Oxidation Event? Science **317:** 1903-1906.

4. Andrews, S.C., Robinson, A.K., and Rodriguez-Quinones, F. (2003) Bacterial iron homeostasis. *FEMS Microbiol Rev* **27:** 215-237.

5. Angerer, A., Enz, S., Ochs, M., and Braun, V. (1995) Transcriptional regulation of ferric citrate transport in *Escherichia coli* K-12. FecI belongs to a new sub-family of sigma 70–type factors that respond to extracytoplasmic stimuli. *Mol Microbiol* **19:** 163-174.

6. Blanc, B., Gerez, C., and Ollagnier de Choudens, S. (2015) Assembly of Fe/S proteins in bacterial systems: biochemistry of the bacterial ISC system. *Biochim Biophys Acta* **1853:** 1436-1447.

7. Bolton, E.T., Cowie, D.B., and Sands, M.K. (1951) Sulfur metabolism in *Escherichia coli. J Bacteriol* **63:** 309-318.

8. Boyd, E.S., Thomas, K.M., Dai, Y., Boyd, J.M., and Outten, F.W. (2014) Interplay between oxygen and Fe-S cluster biogenesis: insights from the Suf pathway. *Biochemistry* **53:** 5834-5847.

9. Braun, V. (1995) Energy-coupled transport and signal transduction through the gram-negative outer membrane via TonB-ExbB-ExbD-dependent receptor proteins. *FEMS Microbiol Rev* **16:** 295–307.

10. Braun, V., Mahren, S., and Ogierman, M. (2003) Regulation of the FecI-type ECF sigma factor by transmembrane signaling. *Curr Opin Microbiol* **6:** 173-180.

11. Brickman, T.J., and McIntosh, M.A. (1992) Overexpression and purification of ferric enterobactin esterase from *Escherichia coli.* Demonstration of enzymatic hydrolysis of enterobactin and its iron complex. *J Biol Chem* **267***:* 12350-12355.

12. Brown, N.C., Eliasson, R., Reichard, P., and Thelander, L. (1969) Spectrum and iron content of protein B2 from ribonucleoside diphosphate reductase. *European J Biochem* **9:** 512-518.

13. Bryce, G.F. and Brot, N. (1972) Enzymic synthesis of the cyclic trimer of 2,3-dihydroxy-N-benzoyl-L-serine in *Escherichia coli. Biochemistry* **11:** 1708-1715.

14. Chahal, H. K., Dai, Y., Saini, A., Ayala-Castro, C., and Outten F. W. (2009) The $SufBC_2D$ Fe-S scaffold complex interacts with SufA for Fe-S cluster transfer. *Biochemistry* **48:** 10644-10653.

15. Chahal, H.K. and Outten, F.W. (2012) Separate Fe-S scaffold and carrier functions for $SufB_2C_2$ and SufA during *in vitro* maturation of [2Fe-2S] Fdx. *J Inorg Biochem* **116C:** 126-134.

16. Crosa, J. H. (1997) Signal transduction and transcriptional and posttranscriptional control of iron-regulated genes in bacteria. *Microbiol Mol Biol Rev* **61:** 319-336.

17. Cupp-Vickery, J.R., Silberg, J.J., Ta, D.T., and Vickery, L.E. (2004) Crystal structure of IscA, an iron-sulfur cluster assembly protein from *Escherichia coli. J Mol Biol* **338:** 127-137.

18. Cupp-Vickery, J.R., Urbina, H., and Vickery, L.E. (2003) Crystal structure of IscS, a cysteine desulfurase from *Escherichia coli*. *J Mol Biol* **330:** 1049-1059.

19. Demple, B. (2002) Signal transduction by nitric oxide in cellular stress responses. *Mol Cell Biochem* **37:** 11-18.

20. Ding, H. and Clark, R.J. (2004) Characterization of iron binding in IscA, an ancient iron-sulphur cluster assembly protein. *Biochem J* **379:** 433-440.

21. Ding, H., Clark, R.J., and Ding, B. (2004) IscA mediates iron delivery for assembly of iron-sulfur clusters in IscU under the limited accessible free iron conditions. *J Biol Chem* **279:** 37499-37504.

22. Ehrenberg, A., and Reichard, P. (1972) Electron spin resonance of the iron-containing protein B2 from ribonucleotide reductase. *J Biol Chem* **247:** 3485-3488.

23. Entner, N. and Doudoroff, M. (1952) Glucose and gluconic acid oxidation of *Pseudomonas saccharophila*. *J Biol Chem* **196:** 853-862.

24. Enz, S., Braun, V., and Crosa, J. (1995) Transcription of the region encoding the ferric dicitrate-transport system in *Escherichia coli*: similarity between promoters for *fecA* and for extracytoplasmic function sigma factors. *Gene* **163:** 13-19.

25. Fenton, H.J.H. (1896) Constitution of a new dibasic acid, resulting from the oxidation of tartaric acid. *J Chem Soc Trans* **69:** 546-562.

26. Fenton, H.J.H. (1876) On a new reaction of tartaric acid. *Chem News* **33:** 190.

27. Fenton, H.J.H. (1894) The oxidation of tartaric acid in presence of iron. *J Chem Soc Proc* **10:** 157-158.

28. Fernandes A.P. and Holmgren, A. (2004) Glutaredoxins: glutathione-dependent redox enzymes with functions far beyond a simple thioredoxin backup system. *Antioxidants Redox Signaling* **6:** 63-74.

29. Ferguson, A.D., Hofmann, E., Coulton, J.W., Diederichs, K., and Welte, W. (1998) Siderophore-mediated iron transport: crystal structure of FhuA with bound lipopolysaccharide. *Science* **282:** 2215-2220.

30. Flint, D.H. (1993) *Escherichia coli* Fumarase A catalyzes the isomerization of enol and keto oxalacetic acid. *Biochemistry* **32:** 799-805.

31. Flint, D.H., Emptage, M.H., and Guest, J.R. (1992) Fumarase A from *Escherichia coli:* purification and characterization as an iron-sulfur cluster containing enzyme. *Biochemistry* **31:** 10331-10337.

32. Fontecave, M. (2006) Iron-sulfur clusters: ever-expanding roles. *Nat Chem Biol* **2:** 171-174.

33. Greenwood, K.T., and Luke, R.K. (1978) Enzymatic hydrolysis of enterochelin and its iron complex in *Escherichia coli* K-12. Properties of enterochelin esterase. *Biochim Biophys Acta.* **525:** 209-218.

34. Gupta, V., Sendra, M., Naik, S.G., Chahal, H.K., Huynh, B.H., Outten, F.W., Fontecave, M., and Ollagnier-de-Choudens, S. (2009) Native *Escherichia coli* SufA, coexpressed with $SufBC_2D$, purifies as a [2Fe-2S] protein and acts as an Fe-S transporter to Fe-S target enzymes. *J Am Chem Soc* **131:** 6149-6153.

35. Haber, F. and Weiss, (1932) J. Über die Katalyse des Hydroperoxydes. *Naturwiss* **51:** 948-950.

36. Harle, C., Kim, I., Angerer, A., and Braun, V. (1995) Signal transfer through three compartments: transcription initiation of *Escherichia coli* ferric dicitrate transport system from the cell surface. *EMBO J.* **14:** 1430-1438.

37. Hoff, K.G., Silberg, J.J., Vickery, L.E. (2000) Interaction of the iron-sulfur cluster assembly protein IscU with the Hsc66/Hsc20 molecular chaperone system of *Escherichia coli. Proc Natl Acad Sci USA* **97:** 7790-7795.

38. Hunsicker-Wang, L.M., Heine, A., Chen, Y., Luna, E.P., Todaro, T., Zhang, Y.M., Williams, P.A. McRee, D.E., Hirst, J., Stout, C.D., and Fee, J.A. (2003) High-resolution structure of the soluble, respiratory-type Rieske protein from *Thermus thermophiles:* analysis and comparison. *Biochemisry* **42:** 7303-7317.

39. Ilbert, M. and Bonnefov, V. (2013) Insight into the evolution of the iron oxidation pathways. *Biochim Biophys Acta* **1827:** 161-175.

40. Imlay, J. (2015) Diagnosing oxidative stress in bacteria: not as easy as you might think. *Curr Opin Microbiol* **24:** 124-131.

41. Iwema, T., Picciocchi, A., Traore, D.A.K., Ferrer, J., Chauvat, F., and Jacquamet, L. (2009) Structural basis for deleivery of the intact [Fe2S2] cluster by monothiol glutaredoxin. *Biochemistry* **48:** 6041-6043.

42. Johnson, D.C., Dean, D.R., Smith, A.D., and Johnson, M.K. (2005) Structure, function, and formation of biological iron-sulfur clusters. *Annu Rev Biochem* **74:** 247-281.

43. Kambampati, R. and Lauhon, C.T. (1999) IscS is a sulfurtransferase for the in vitro biosynthesis of 4-thiouridine in Escherichia coli tRNA. Biochemistry. **38:** 16561-16568.

44. Kammler, M., Schon, C., and Hantke, K. (1993) Characterization of the ferrous iron uptake system of *Escherichia coli. J Bacteriol* **175:** 6212-6219.

45. Kashket, E.R. and Brodie, A.F. (1963) Oxidative phosphorylation in fractionated bacterial systems. *J Biol Chem* **238:** 2564-2570.

46. Keseler, I.M., Collado-Vides, J., Santos-Zavaleta, A., Peralta-Gil, M., Gama-Castro, S., Muniz-Rascado, L., Bonavides-Martinez, C., Paley, S., Krummenacker M., Altman, T., Kaipa, P., Spaulding, A., Pacheco, J., Latendresse, M., Fulcher, C., Sarker, M., Shearer, A.G., Mackie, A., Paulsen, I., Gunsalus, R.P., and Karp, P.D. (2011) EcoCyc: a comprehensive database of *Escherichia coli* biology. *Nucleic Acids Res* **39:** D583-590.

47. Kiley, P.J. and Beinert, H. (2003) The role of Fe-S proteins in sensing and regulation in bacteria. *Curr Opin Microbiol* **6:** 181-185.

48. Koppenol, W.H. (1993) The centennial of the Fenton reaction. *Free Radic Biol Med* **15:** 645-651.

49. Koppenol, W.H. (2001) The Haber-Weiss cycle — 70 years later, *Redox Rep* **6:** 229-234.

50. Langman, L., Young, I.G., Frost, G.E., Rosenberg, H., and Gibson, F. (1972) Enterochelin system of iron transport in *Escherichia coli:* mutations affecting ferric-enterochelin esterase. *J Bacteriol* **112:** 1142-1149.

51. Larsen, R.A., Foster-Hartnett, D., McIntosh, M.A., and Postle, K. (1997) Regions of *Escherichia coli* TonB and FepA proteins essential for *in vivo* physical interactions. *J Bacteriol* **179:** 3213-3221.

52. Lauble, H., Kennedy, M.C., Beinert, H., and Stout, C.D. (1992) Crystal structures of aconitase with isocitrate and nitroisocitrate bound. *Biochemistry* **31:** 2735-2748.

53. Layer, G., Gaddam, S.A., Ayala-Castro, C.N., Ollagnier-de Choudens, S., Lascoux, D., Fontecave, M., and Outten, F.W. (2007) SufE transfers sulfur from SufS to SufB for iron-sulfur cluster assembly. *J Biol Chem* **282:** 13342-13350.

54. Lillig, C.H., Berndt, C., and Holmgren, A. (2008) Glutaredoxin systems. *Biochim Biophys Acta* **1780:** 1304-1317.

55. Locher, K.P., Rees, B., Koebnik, R., Mitschler, A., Moulinier, L., Rosenbusch, J.P., Moras, D. (1998) Transmembrane signaling across the ligand-gated FhuA receptor: crystal structures of free and ferrichrome-bound states reveal allosteric changes. *Cell* **95:** 771-778.

56. Loiseau, L., Gerez, C., Bekker, M., Ollagnier-de-Choudens, S., Py, B., Sanakis, Y., Teixeira de Mattos, J., Fontecave, M., and Barras, F. (2007) ErpA, an iron-sulfur (Fe-S) protein of the A-type essential for respiratory metabolism in *Escherichia coli. Proc Natl Sci USA* **104:** 13626-13631.

57. Lu, J., Jian, J., Huang, W., Lin, H., Li, J., and Zhou, M. (2016) Experimental and theoretical identification of the Fe(VII) oxidation state in FeO4-. *Phys Chem Chemical Phys* **18:** 31125-31131.

58. Mansy, S.S., Wu, G., Surerus, K.K., and Cowan, J.A. (2002) Iron-sulfur cluster biogenesis *Thermatoga maritima* IscU is a structured iron-sulfur cluster assembly protein. *J Biol Chem* **227:** 21397-21404.

59. Mapolelo, D.T., Zhang, B., Naik, S.G., Huynh, B.H., and Johnson, M.K. (2012) Spectroscopic and functional characterization of iron-sulfur cluster bound forms of *Azotobacter vinelandii* (Nif) IscA. *Biochemistry* **51:** 8071-8084.

60. Mapolelo, D.T., Zhang, B., Randeniya, S., Albetel, A., Li, H., Couturier, J., Outten, C.E., Rouhier, N., and Johnson, M.K. (2013) Monothiol glutaredoxins and A-type proteins: partners in Fe-S cluster trafficking. *Dalton Trans.* **42:** 3107-3115.

61. McCandliss, R.J. and Herrmann, K.M. (1978) Iron, an essential element for biosynthesis of aromatic compounds. *Proc Natl Sci USA* **75:** 4810-4813.

62. McCandliss, R.J., Poling, M.D., and Herrmann, K.M. (1978) 3-deoxy-d-arabino-heptulosonate 7-phosphate synthase. *J Biol Chem* **253:** 4259-4265.

63. McHugh, J.P., Rodriguez-Quinones, F., Abdul-Tehrani, H., Svistunenko, D.A., Poole, R.K., Cooper, C.E., and Andrews, S.C. (2003) Global iron-dependent gene regulation in *Escherichia coli.* A new mechanism for iron homeostasis. *J Biol Chem* **278:** 29478-29486.

64. Mehi, O., Bogos, B., Csorgo, B., Pal, F., Nyerges, A., Papp, B., and Pal, C. (2014) Pertubration of iron homeostasis promotes the evolution of antibiotic resistance. *Mol Biol Evol* **31:** 2793-2804.

65. Messenger, A.J. and Barclay, R. (1983) Bacteria, iron, and pathogenicity. *Biochem Education* **11:** 54-63.

66. Mettert, E.L. and Kiley PJ. (2014) Coordinate regulation of the Suf and Isc Fe-S cluster biogenesis pathways by IscR is essential for viability of *Escherichia coli*. *J Bacteriol* **196:** 4315-4323.

67. Mettert, E.L. and Kiley, P.J. (2015) How is Fe-S cluster formation regulated? *Annu Rev Microbiol* **69:** 505-526.

68. Nishio, K. and Nakai, M. (2000) Transfer of iron-sulfur cluster from NifU to apoferredoxin. *J Biol Chem* **275:** 22615-22618.

69. Ochs, M., Angerer, A., Enz, S., and Braun, V. (1996) Surface signaling in transcription regulation of the ferric citrate transport system of *Escherichia coli*: mutational analysis of the alternative sigma factor FecI supports its essential role in *fec* transport gene transcription. *Mol Gen Genet* **250:** 455-465.

70. Ochs, M., Veitinger, S., Kim, I., Welz, D., Angerer, A., and Braun, V. (1995) Regulation of citrate dependent iron transport system in *Escherichia coli*: FecR is required for transcriptional activation by FecI. *Mol Microbiol* **15:** 119-132.

71. Ollagnier-de-Choudens, S., Lascoux, D., Loiseau, L., Barras, F., Forest, E., and Fontecave, M. (2003) Mechanistic studies of the SufS-SufE cysteine desulfurase: evidence for sulfur transfer from SufS to SufE. *FEBS Lett* **555:** 263-267.

72. Ollagnier-de-Choudens, S., Mattioli, T., Takahashi, Y., and Fontecave, M. (2001) Iron-sulfur cluster assembly characterizaztion of IscA and evidence for a specific and functional complex with ferredoxin. *J Biol Chem* **276:** 22604-22607.

73. Ollagnier-de-Choudens, S., Nachin, L., Sanakis, Y., Loiseau, L., Barras, F., and Fontecave, M. (2003) SufA from *Erwinia chrysanthemi.* Characterization of a scaffold protein required for iron-sulfur cluster assembly. *J Biol Chem* **278:** 17993-18001.

74. Ollagnier-de-Choudens, S., Sanakis, Y., and Fontecave, M. (2004) SufA/IscA: reactivity studies of a class of scaffold proteins involved in [Fe-S] cluster assembly. *J Biol Inorg Chem* **9:** 828-838.

75. Outten. F.W., Djaman, O., and Storz, G. (2004) A *suf* operon requirement for Fe-S cluster assembly during iron starvation in *Escherichia coli*. *Mol Microbiol* **52:** 861-872.

76. Outten, F.W., Wood, M.J., Munoz, F.M., and Storz, G. (2003) The SufE protein and the $SufBC_2D$ complex enhance SufS cysteine desulfurase activity as part of a sulfur transfer pathway for Fe-S cluster assembly in Escherichia coli. *J Biol Chem* **278:** 45713-45719.

77. Outten, F.W. (2015). Recent advances in the Suf Fe-S cluster biogenesis pathway: beyond the *Proteobacteria*. *Biochim. Biophys. Acta* **1853:**1464-1469.

78. Peekhaus, N. and Conway, T. (1998) What's for dinner?: Entner-Doudoroff metabolism in *Escherichia coli. J Bacteriol* **180:** 3495-3502.

79. Pomposiello, P.J. and Demple, B. (2001) Redox-operated genetic switches: the SoxR and OxyR transcription factors. *Trends Biotechnol* **19:** 109-114.

80. Pressler, U., Staudenmaier, H., Zimmermann, L., and Braun, V. (1988) Genetics of the iron dicitrate transport system of *Escherichia coli. J Bacteriol* **170:** 2716-2724.

81. Py, B. and Barras, F. (2010) Building Fe-S proteins: bacterial strategies. *Nat Rev Microbiol* **8:** 436-446.

82. Rainnie, D.J. and Bragg, P.D. (1973) The effect of iron deficiency on respiration and energy-coupling in *Escherichia coli. J Gen Microbiol* **77:** 339-349.

83. Ratledge, C. and Dover, L.G. (2000) Iron metabolism in pathogenic bacteria. *Annu Rev Microbiol* **54:** 881-941.

84. Ray, J.M. and Bauerle, R. (1991) Purification and properties of tryptophan-sensitive 3-deoxy-d-arabino-heptulosonate 7-phosphate synthase from *Escherichia coli. J Bacteriol* **173:** 1894-1901.

85. Robbins, A.H. and Stout, C.D. (1989) Structure of activated aconitase: formation of the [4Fe-4S] cluster in the crystal. *Proc Natl Acad Sci USA* **86:** 3639-3643.

86. Robbins, A.H. and Stout, C.D. (1989) The structure of aconitase. *Proteins* **5:** 289-312.

87. Roche, B., Aussel, L., Ezraty, B., Mandin, P., Py, B., and Barras, F. (2013) Iron/sulfur proteins biogenesis in prokaryotes: formation, regulation and diversity. *Biochim Biophys Acta* **1827:** 455-469.

88. Schultz-Hauser, G., Koster, W., Schwarz, H., and Braun, V. (1992) Iron (III) hydroxamate transport in *Escherichia coli* K-12: FhuB-mediated membrane association of the FhuC protein and negative complementation of fhuC mutants. *J Bacteriol* **174:** 2305-2311.

89. Schwartz, C.J., Djaman, O., Imlay, J.A., and Kiley, P.J. (2000) The cysteine desulfurase, IscS, has a major role in *in vivo* Fe-S cluster formation in *Escherichia coli*. *Proc Natl Acad Sci USA* **97:** 9009-9014.

90. Schwartz, C.J., Giel, J.L., Patschkowski, T., Luther, C., Ruzicka, F.J., Beinert, H., Kiley, and P.J. (2001) IscR, an Fe-S cluster-containing transcription factor, represses expression of *Escherichia coli* genes encoding Fe-S cluster assembly proteins. *Proc Natl Acad Sci USA* **98:** 14895-14900.

91. Semsey, S., Andersson, A.M.C., Krishna, S., Jensen, M.H., Masse, E., and Sneppen, K. (2006) Genetic regulation of fluxes: iron homeostasis of *Escherichia coli. Nucleic Acids Res* **34:** 4960-4967.

92. Seo, S.W., Kim, D., Latif, H., O'Brien, E.J., Szubin, R., and Palsson, B.O. (2014) Deciphering Fur transcriptional regulatory network highlights its complex role beyond iron metabolism in *Escherichia coli. Nat Commun* **5:** 4910.

93. Singh, H., Dai, Y., Outten, F.W., and Busenlehner, L.S. (2013) *Escherichia coli* SufE sulfur transfer protein modulates the SufS cysteine desulfurase through allosteric conformational dynamics. *J Biol Chem* **288:** 36189-36200.

94. Smith, A.D., Agar, J.N., Johnson, K.A., Frazzon, J., Amster, I.J., Dean, D.R., and Johnson, M.K. (2001) Sulfur transfer from IscS to IscU: the first step in iron-sulfur cluster biosynthesis. *J Am Chem Soc* **123:** 11103-11104.

95. Smith, A.D., Frazzon, J., Dean, D.R., and Johnson, M.K. (2005) Role of conserved cysteines in mediating sulfur transfer from IscS to IscU. *FEBS Lett* **579:** 5236-5240.

96. Staudenmaier, H., Van Hove, B., Yaraghi, Z., and Braun, V. (1989) Nucleotide sequences of the fecBCDE genes and locations of the proteins suggest a periplasmic-binding-protein-dependent transport mechanism for iron (III) dicitrate in *Escherichia coli. J Baceteriol* **171:** 2626-2633.

97. Stephens, C.M. and Bauerle, R. (1991) Analysis of the metal requirement of 3-deoxy-d-arabino-heptulosonate 7-phosphate synthase from *Escherichia coli. J Biol Chem* **266:** 20810-20817.

98. Urbina, H.D., Silberg, J.J., Hoff, K.G., and Vickery, L.E. (2001) Transfer of sulfur from IscS to IscU during Fe/S cluster assembly. *J Biol Chem* **276:** 44521-6

99. Van Hove, B., Staudenmaier, H., and Braun, V. (1990) Novel two-component transmembrane transcription control: regulation of iron dicitrate transport in *Escherichia coli* K-12. *J Bacteriol* **172:** 6749-6758.

100. Vinella, D., Brochier-Armanet, C., Loiseau, L., Talla, E., and Barras, F. (2009) Iron-sulfur (Fe/S) protein biogenesis: phylogenomic and genetic studies of A-type carriers. *PLOS Genet* **5:** e1000497.

101. Wada, K., Hasegawa, Y., Gong, Z., Minami, Y., Fukuyama, K., Takahashi, Y. (2005) Crystal structure of *Escherichia coli* SufA involved in biosynthesis of iron-sulfur clusters: implications for a functional dimer. *FEBS Lett* **579:** 6543-8.

102. Wagegg, W. and Braun, V. (1981) Ferric citrate transport in *Escherichia coli* requires outer membrane receptor protein fecA. *J Bacteriol* **145:** 156-163.

103. Welz, D. and Braun, V. (1998) Ferric citrate transport of *Escherichia coli:* functional regions of the FecR transmembrane regulatory protein. *J Bacteriol* **180:** 2387-2394.

104. Wu, S. and Cowan, J.A. (2003) Iron-sulfur cluster biosynthesis. A comparative kinetic analysis of native and cys-substituted ISA-mediated $[2Fe\text{-}2S]^{2+}$ cluster transfer to an apoferredoxin target. *Biochemistry* **42:** 5784-5791.

105. Wu, S., Wu, G., Surerus, K.K., and Cowan, J.A. (2002) Iron-sulfur cluster biosynthesis. Kinetic analysis of [2Fe-2S] cluster transfer from holo IscU to apo Fd: role of redox chemistry and a conserved aspartate. *Biochemistry* **41:** 8876-8885.

106. Ye, J., Nadar, S.V., Li, J., and Rosen, B.P. (2014) Structure of *Escherichia coli* Grx2 in complex with glutathione: a dual-function hybrid of glutaredoxin and glutathione S-transferase. *Acta Crystallogr C Biol Crystallogr* **70:** 1907-1913.

107. Yeo, W.S., Lee, J.H., Lee, K.C., Roe, J.H. (2006) IscR acts as an activator in response to oxidative stress for the *suf* operon encoding Fe-S assembly proteins. *Mol Microbiol* **61:** 206-218.

108. Yeung, N., Gold, B., Liu, N.L., Prathapam, R., Sterling, H.J., Williams, E.R., and Butland, G. (2011) The *E. coli* monothiol glutaredoxin GrxD forms homodimeric and heterodimeric FeS cluster containing complexes. *Biochemistry* **50:** 8957-8969.

109. Zheng, M., Wang, X., Templeton, L.J., Smulskim D.R., LaRossam, R.A., and Storz, G. (2001) DNA microarray-mediated transcriptional profiling of the *Escherichia coli* response to hydrogen peroxide. *J Bacteriol* **183:** 4562-4570.

CHAPTER 2

NICKEL EXPOSURE REDUCES ENTEROBACTIN PRODUCTION IN *E. COLI*

ABSTRACT

Escherichia coli is a well-studied bacterium that can be found in many niches, such as industrial wastewater, where the concentration of nickel can rise to low millimolar levels. Recent studies show that nickel exposure can repress pyochelin or induce pyoverdine siderophore production in *Pseudomonas aeruginosa* (Braud et al., 2010). Understanding the molecular crosstalk between siderophore production, metal homeostasis, and metal toxicity in microorganisms is critical for designing bioremediation strategies for metal-contaminated sites. Here we show that high nickel exposure prolongs lag phase duration as a result of low intracellular iron levels in *E. coli*. Although *E. coli* cells respond to low intracellular iron during nickel stress by maintaining high expression of iron uptake systems such as *fepA*, the demand for iron is not met due to a lack of siderophores in the extracellular medium during nickel stress. Taken together, these results indicate that nickel inhibits iron accumulation in *E. coli* by reducing the presence of enterobactin in the extracellular medium.

INTRODUCTION

Nickel exposure can cause allergies and lung cancer in humans (Macomber and Hausinger, 2011; Denkhaus and Salnikow, 2002; Kasprzak et al., 2003; Das et al., 2008).

It can also be found in the environment due to industrial pollution which can also affect microorganisms such as *Escherichia coli* (Nriagu, 1980). Waste water near industrial sites can contain up to millimolar quantities of nickel (Ansari and Malik, 2010). In *E. coli,* lower levels of nickel exposure affect RcnR, a nickel metalloregulator, that is released from RcnA repressing nickel efflux (Iwig et al., 2006). Inversely, nickel can also bind and repress NikR which regulates nickel transport of NikABCDE (De Pina et al., 1999). Nickel is structurally similar to cobalt and copper which have been shown to disrupt iron homeostasis by damaging iron-containing dehydratase enzymes in *E. coli* (Irving and Williams, 1953; Ranquet et al., 2007; Macomber and Imlay, 2009). Nickel disrupts zinc binding to FbaA, the fructose bisphosphate aldolase A (Macomber et al., 2011).

Nickel can also affect siderophore production in *Pseudomonas aeruginosa* by repressing pyochelin (PCH) synthesis and promoting pyoverdine (PVD) production under iron-limiting conditions (Braud et al., 2009). Other metals have similarly been shown to affect siderophore metabolism. Siderophore production is de-regulated by excess molybdenum in *Azotobacter vinelandii* (Duhme et al., 1998) and by aluminum in *Bacillus megaterium* (Hu and Boyer, 1996). Copper and nickel can affect siderophore production in the presence of iron in *Pseudomonas aeruginosa* (Braud et al., 2010; Visca et al., 1992). Therefore, understanding the molecular crosstalk between siderophore production, metal homeostasis, and metal toxicity in microorganisms is critical for designing bioremediation strategies for metal-contaminated sites (Dixit et al., 2015). For example, Actinobacteria can be used to de-toxify metal-contaminated sites and break-down complex organic matter (Alvarez et al., 2017; Polti et al., 2011). Despite its robust metabolic profile and the

emergence of new actinobacteria species, the molecular details of siderophore production is unclear (Wang et al., 2014).

MATERIALS AND METHODS

Bacterial strains and culture conditions

Strains used in this study are derivatives of the parent wild-type strain *E. coli* MG1655. An individual colony was transferred from fresh Lennox broth (LB) agar plates into a 4 mL volume of LB and grown for 4 – 5hrs at 37 °C with shaking at 200 rpm. Cells from this culture were pelleted and washed twice in sterile 1X M9 minimal media salts; then the OD_{600nm} was normalized to 1.0. Normalized cells were diluted 1:200 into M9 glucose minimal media containing 1X M9 minimal salts (BD Difco), 0.2% (w/v) glucose (Acros Organics), 0.2% (w/v) magnesium sulfate, 0.1 mM calcium chloride, and 0.5 g/mL Thiamine HCl (Sigma-Aldrich). Prepared M9 media typically contained ~300 nM iron and ~70 nM nickel as measured by ICP-MS. Cultures were incubated overnight for 18 – 20 hr, at 37 °C and 200 rpm, then washed and pelleted twice in sterile 1X M9 salts as described above. The resulting cell suspensions were normalized to an OD_{600} of 2.0 and diluted 1:50 into M9 gluconate minimal media with 0.2 % (w/v) potassium gluconate (Alfa Aesar) to give an initial OD_{600} of 0.04. Nickel chloride (Sigma-Aldrich) was added to described final concentrations in the M9 gluconate minimal media, from 0 µM up to 50 µM.

Cell growth was monitored as optical density at 600nm (OD_{600}) and plotted versus time (in hours). Lag phase duration was determined using the online fitting program,

DMFit (www.ifr.ac.uk/safety/DMfit), applying the no-asymptote fitted model and parameters (Baranyi and Roberts, 1994). Stationary phase OD_{600} measurements were omitted for best fit of the model. Doubling time of the cells during the exponential phase of growth, where the steepest linear fit line could be applied, was determined using the Online Doubling Calculator (http://www.doubling-time.com/compute.php) (Roth, 2006).

Inductively – Coupled Plasma Mass Spectrometry (ICP-MS)

Preparatory cell growth in LB and glucose minimal media was conducted as described above**.** Cell cultures were then grown in 2 L M9 gluconate minimal media with or without 50 µM nickel chloride in a 4 L culture flask at 37 °C and 200 rpm. Samples of 150 mL were centrifuged at 3,000 x g for 20min and then pelleted three times at 16,000 x g with intermediate washing in 1mL sterile, ice-cold wash solution consisting of 50 mM EDTA tetrasodium salt, 100 mM oxalic acid, 100 mM NaCl, and 10 mM KCl, to remove any cell surface-associated metal ions. Washed cell pellets were re-suspended in a 1 mL volume of ice-cold, sterile 1X M9 salts. A small portion of each sample was then diluted 40-fold to record the final OD_{600}. Cell re-suspensions were transferred to an acid-washed, Perfluoroalkoxy (PFA) microcentrifuge tube (Savillex Corporation) and centrifuged at 16,000 x g. After centrifugation, the supernatant was discarded and the cell pellets were frozen in liquid nitrogen. Cell pellets were stored at -80 °C until ready for digestion and ICP-MS analysis.

Samples for ICP-MS were thawed for 15 min on ice followed by drying at 80 °C for 30 min. A 400 µL volume of trace-metal grade HNO_3 (distilled on site at the Center

for Elemental Mass Spectrometry (CEMS), University of South Carolina) was added to each sample tube and digested at 80 °C for 4 hrs. After digestion, each sample tube was centrifuged for 1 min at 16,000 x g and the supernatant was diluted 1:20 into MQ H_2O, giving a final acid matrix of 3.5 %. Blanks consisting of 3.5 % trace-metal grade HNO_3 only in MQ H_2O (18MΩ) were made and prepared in the same manner as the cell samples. Standard element solutions (Inorganic Ventures) were also prepared in the same final acid matrix of 3.5 % to establish a limit of detection and a calibration curve for determining the concentrations of each metal analyzed. The isotopes of biologically relevant transition metals with masses of ^{56}Fe, ^{58}Ni, ^{64}Zn, ^{55}Mn, and ^{63}Cu were selected for analysis based on natural abundances. Samples were analyzed under medium resolution to resolve polyatomic interferences (e.g. $^{40}Ar^{16}O$ for ^{56}Fe) on a Thermo Element 2 High Resolution ICP-MS instrument operated by CEMS at the University of South Carolina. A cyclonic spray chamber (Elemental Scientific) was used for delivery of sample into the instrument.

β-Galactosidase assays for promoter-lacZ fusion strains

Wild-type *E. coli* MG1655 strains containing Φ*fepAp-LacZ* (PK9849), Φ*iscRp-lacZ* (PK7571), and Φ*sufAp-lacZ* (PK7722) were kindly provided by Patricia Kiley (University of Wisconsin – Madison) (Giel et al., 2006). All cells were initially plated on LB with 30 g/mL kanamycin overnight at 37 °C. One colony was transferred to M9 glucose minimal media for approximately 18 hours at 37 °C at 200 rpm. The cell culture was then diluted 1:50 to a final OD_{600} of 0.04 in 100 mL of M9 gluconate minimal media with or without 50 μM $NiCl_2$ and grown for 5 hours at 37 °C at 200 rpm. At various time

points cells were collected by centrifugation at 3,000 x g and re-suspended in Z-buffer (0.06 M sodium diphosphate, 0.04 M monosodium phosphate, 0.01 M potassium chloride, 0.001 M magnesium sulfate, and 0.05 M β-mercaptoethanol). β-Galactosidase activity was measured after addition of 200 µL of 4 mg/mL ortho-nitrophenyl-ß-galactoside per mL of cells permeabilized with chloroform and SDS according to published protocols (Miller, 1972). β-Galactosidase activity was calculated and reported in Miller Units; see Equation 1 below where *t* = time of reaction and v= volume of cells added in mL. Absorbance at 420 nm, 550 nm, and 600 nm were measured using a Beckman-Coulter DU800 UV-Vis Spectrophotometer. Miller units normalize β -galactosidase activity to total cell number via optical density at 600 nm (OD_{600}) measurement.

Equation 1: Miller Unit = $1000 * [Abs_{420} – (1.75 * Abs_{550})] / [t * v * Abs_{600}]$

Arnow assay for catechol determination

Methods from Arnow and Ma were adapted for the quantification of catecholate siderophore production (to include any enterobactin breakdown products) by *E. coli* under nickel stress (Ma and Payne, 2012; Arnow, 1937). Wild-type MG1655 and *fepA* deletion strains were cultured as described above. Cells were cultured in 0.2 % gluconate M9 minimal media with or without 50 µM nickel chloride. Every two hours 1 mL was collected from each growth, the OD at 650 nm was measured and recorded, and then each volume was cleared of cells via centrifugation at 16,000 x g for 1 min. A 500 µL volume of cleared supernatant was transferred to a clean, 4.0mL polypropylene cuvette. 500 µL 0.5 N HCl, 500 µL of a 10 % sodium nitrate / 10 % sodium molybdate mixture (Sigma-

Aldrich), and 500 µL 1 N NaOH were added to the cuvette. All assay samples were measured against a blank mixture of fresh gluconate M9 minimal media with the above reagents listed for the assay. The absorbance at 515 nm was measured and recorded immediately after mixing. Arnow units were calculated using Equation 2:

Equation 2: Arnow Unit = 1000 * [Abs_{515}/Abs_{650}]

Enterobactin purification and quantification using FPLC

E. coli MG1655 wild-type and Δ*fepA* were plated onto LB and incubated overnight at 37 °C. A single colony was cultured according as described above. Cultured cells were washed, normalized, and diluted to a final optical density of 0.04 in M9 gluconate minimal media, with or without 50 µM nickel chloride. Cultures were incubated for 2 hours at 37 °C at 200rpm. The cells were centrifuged for 20 min at 4 °C and 8,000 x g. The supernatant was sterile filtered twice using a fresh 0.22 µm filter (Millipore) each time and a total of 1 L spent media was collected. Enterobactin and its hydrolysis products were purified using a modified form of a previously published protocol (O'Brien and Gibson, 1970). Briefly, the sterile, filtered supernatant was loaded onto a DEAE-Sepharose Fast Flow column equilibrated with 10 mM sodium phosphate buffer, pH 7.0. Fractions (5 mL) were collected by eluting at 4 °C using a step gradient of 0.0 M, 0.05 M, 0.15 M, 1.0 M, and 2.0 M ammonium chloride. Enterobactin and its hydrolysis products were identified based on the concentration of ammonium chloride at which they eluted and further confirmed by ESI-MS (data not shown).

Quantification of enterobactin and its hydroylsis products by LC-MS

Wild-type MG1655 *E. coli* cells were diluted from an overnight culture in 120 mL fresh M9 gluconate minimal media and cultured for 2 hours with or without 50 µM nickel chloride at 37 °C. At 2 hours, culture media was collected after removing cells via centrifugation. Culture media was twice extracted using a 1:1 ratio of 100 % ethyl acetate to culture medium. The ethyl acetate layer was collected and evaporated by rotovap. The residue was resuspended in 10 % acetonitrile and 0.1 % trifluoroacetic acid (TFA) and analyzed by LC-MS (Winkelmann et al., 1994). LC-MS samples were analyzed on a Waters Q-Tof API US, quadrupole time-of-flight mass spectrometer and Dionex Ultimate 3000 UPLC. A 30 µL injection volume was loaded onto a Chromegabond WR C18, 2.1 mm x 150 mm, 3 um particle (ES Industries) column using a binary gradient at a flow rate of 200 uL / min. Solvent A: water with 0.1 % formic acid and solvent B: acetonitrile with 0.1 % formic acid. The run was set to 10 % B for 2 minutes, 95 % over 20 mins, and finally held at 95 % for 15 mins.

Total RNA isolation and quantitative RT-PCR

Cells were cultured in gluconate for 2 hours with or without 50 µM nickel chloride. After centrifugation, cell pellets were harvested by centrifugation and stored at -80 °C. RNA was extracted using an acid phenol-chloroform method (Kawano et al., 2002) and stored at -80 °C. A total RNA (1 µg) was used to generate gene-specific cDNA using iScript (BioRad) according to manufacturer's instructions and gene-specific primers. Copy number of cDNA was measured by PCR using SSoAdvanced Universal SYBR Green

Supermix (BioRad). ΔCq expression was calculated using the average Cq values of both the experimental gene (*fepA, entC*) and the control gene (*ihfB*). mRNA fold change is representative of $2^{(-\Delta\Delta Cq)}$.

RESULTS

Wild-type E. coli cells are sensitive to nickel stress during lag phase

E. coli cells have three primary stages of growth: lag phase, exponential phase, and stationary phase (Wade, 1952). Nickel is toxic at low micromolar levels (8 μM) to bacterial cells in exponential phase and nickel was shown to disrupt the zinc-dependent metalloenzyme Class 2 Fructose-bisphosphate aldolase, FbaA (Macomber et al., 2011). Nickel exposure in exponential phase *E. coli* was also shown to induce DNA relaxation and damage, possibly by inhibiting DNA replication and RecBCD-mediated DNA repair (Gault et al., 2016; Kumar et al., 2017). However, Rolfe et al., have shown that bacterial cells accumulate essential trace metals during *lag phase* in preparation for the transition into exponential phase (Rolfe et al., 2012). Iron uptake genes are upregulated and intracellular iron levels are increased during lag phase. During exponential phase, these genes are downregulated and intracellular iron levels decrease as the iron is progressively divided amongst daughter cells. To determine the effects of nickel during lag phase of *E. coli*, growth was monitored after exposure of freshly diluted lag phase cells to 0 μM – 50 μM nickel chloride (Figure 2.1 A). Lag phase duration (Figure 2.1 B) was quantified using the Baranyi and Roberts model (Baranyi and Roberts, 1994) while the exponential phase (doubling time) duration (Figure 2.1 C) was quantified using a formula developed by Roth

(Roth, 2006). Lag phase duration is not significantly affected at the lower nickel toxicity range (below 10 μM). However, as the concentration of nickel increases above 10 μM, lag phase duration also increases. The doubling time does not significantly change when the nickel-treated cells exit lag phase and enter exponential phase. Similarly, the final cell density reached in stationary phase also does not significantly change after nickel exposure in lag phase (Fig. 2.1 A).

Intracellular iron levels are lower in nickel-treated E. coli cells

Soft metals have been shown to disrupt iron metabolism in *E. coli* (Xu and Imlay, 2012; Macomber and Imlay, 2009; Ranquet et al., 2007). Recent studies link nickel stress to disruption of iron metabolism in exponential phase, possibly by inducing Fur-dependent repression of iron uptake systems (Gault et al., 2016). To better understand the phenotypic effects of nickel toxicity, intracellular metal concentrations during lag phase nickel stress were measured using inductively coupled plasma mass spectrometry (ICP-MS). Cells that were not exposed to nickel showed an increasing amount of iron over time during lag phase (Figure 2.2 A). In contrast, cells exposed to a toxic level of nickel (50 μM) showed no increase in intracellular iron throughout lag phase. Manganese and copper levels were not significantly affected but zinc levels were elevated in response to nickel. The increased zinc accumulation in response to nickel is consistent with disruption of zinc metalloproteins by nickel as previously reported (Macomber et al., 2011).

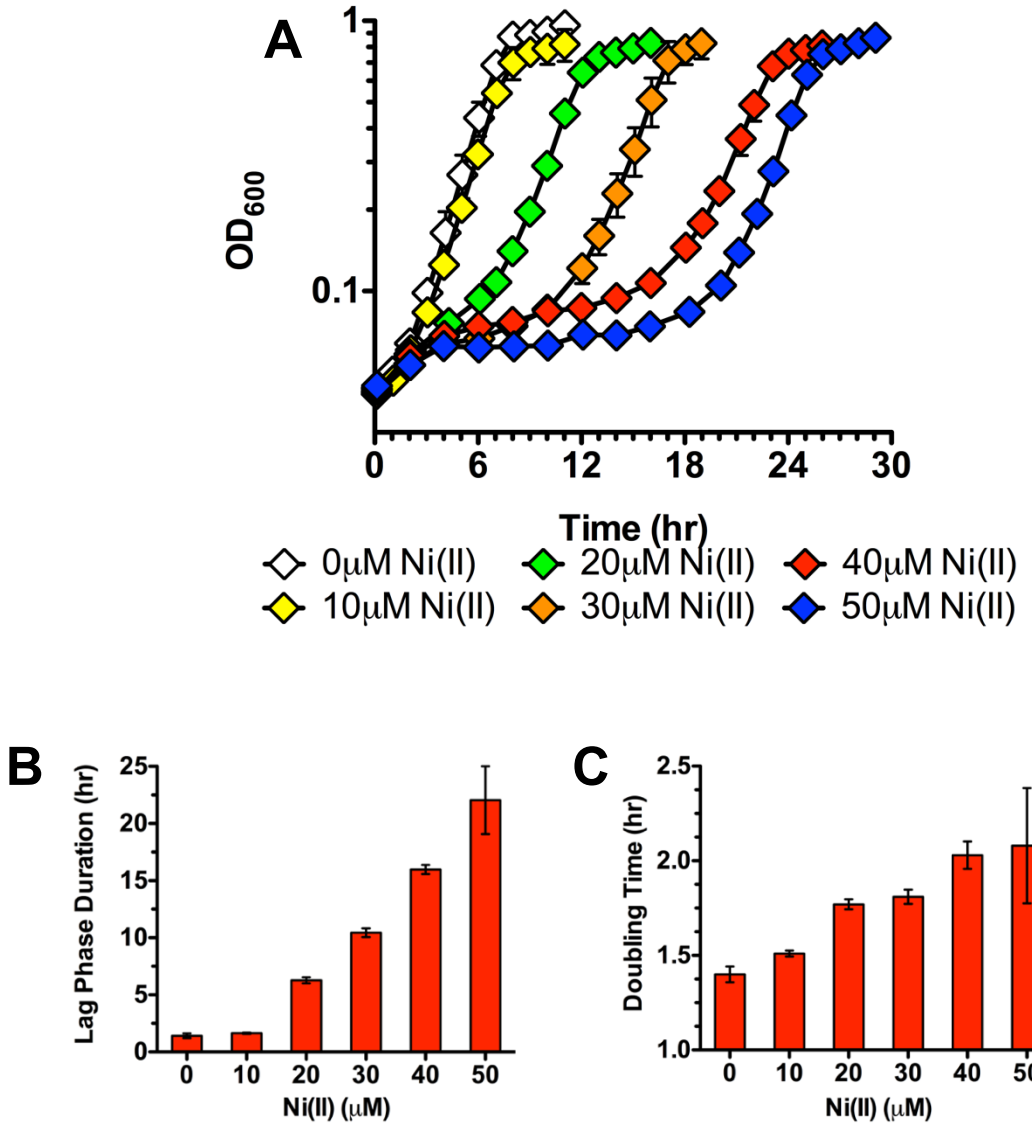

Figure 2.1. Nickel exposure extends lag phase duration. (A) Growth curves of wild type MG1655 *E. coli* cells exposed to 0 μM, 10 μM, 20 μM, 30 μM, 40 μM, or 50 μM nickel chloride. (B) Lag phase duration calculated from the growth curve data shown in Figure 1A. (C) Doubling times calculated from the growth curve data shown in Figure 2.1A. All growths were repeated in triplicate (n = 3) and error bars indicate one standard deviation from the mean value.

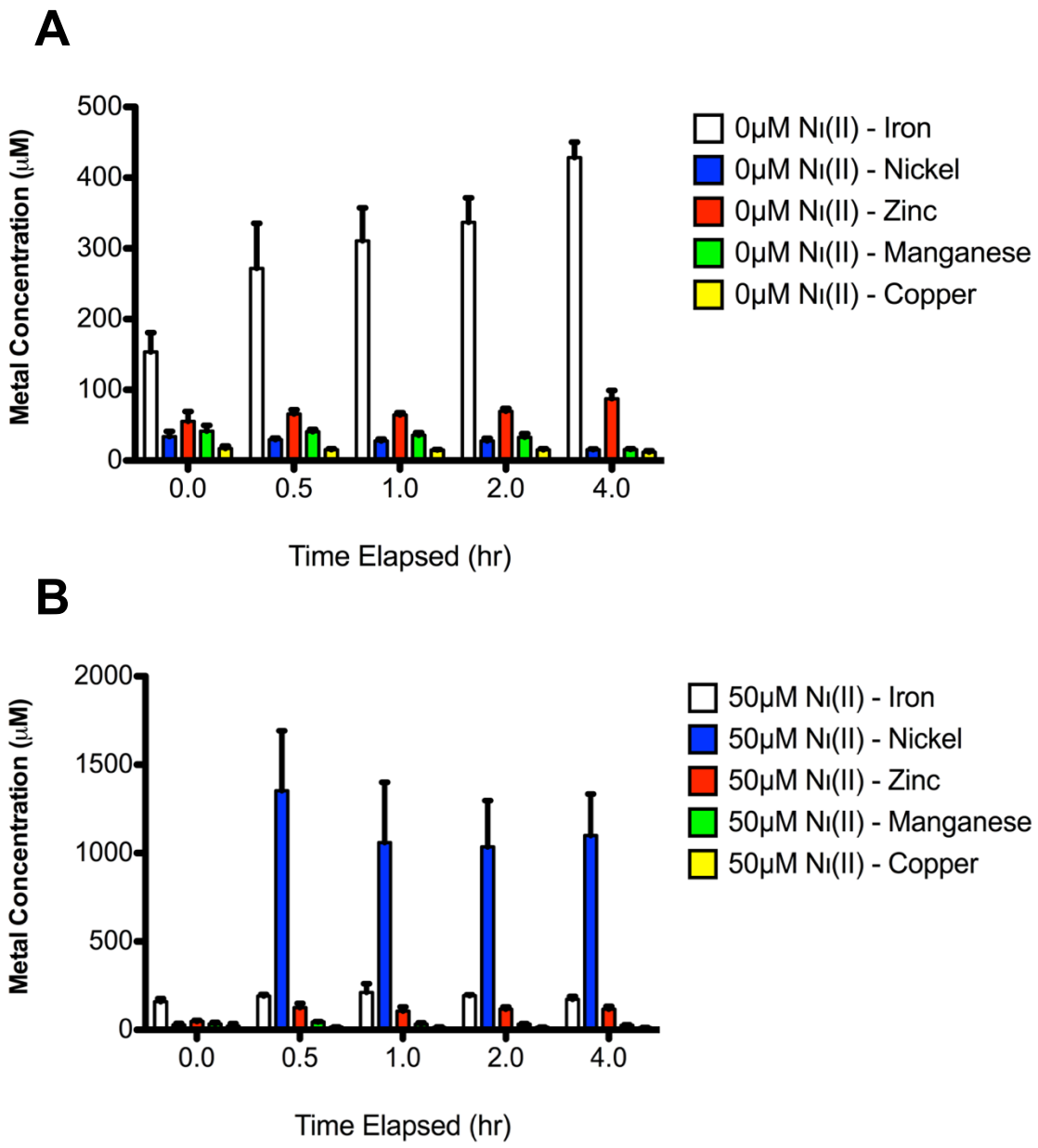

Figure 2.2. Intracellular iron levels are decreased upon exposure to nickel during the lag phase. (A) Intracellular metal concentrations were measured in wild type MG1655 *E. coli* cells that were exposed to 0 μM nickel chloride using ICP-MS. (B) Intracellular metal concentrations were measured in wild type MG1655 *E. coli* cells that was exposed to 50 μM nickel chloride using ICP-MS. All measurements were repeated in triplicate (n = 3) and error bars indicate one standard deviation from the mean value.

High nickel exposure triggers an 'iron starvation' response in lag phase E. coli cells

In order to determine the effects of nickel exposure on intracellular iron homeostasis, expression of genes involved in iron homeostasis were monitored using a series of promoter-*lacZ* fusion constructs in vivo. Iron uptake (*fepA*) and iron-sulfur (Fe-S) cluster biogenesis (*iscR, sufA*) genes are upregulated during lag phase and their expression progressively declines over time in exponential phase (Rolfe et al., 2012). The ferric uptake regulator, Fur, regulates iron homeostasis by repressing the transcription of iron uptake genes under iron replete conditions (Escolar L, et al., 1998; Hunt et al., 1994). However, when cellular demand for iron is high, Fur repression of genes like *fepA* and *sufA* that are involved in adaptation to iron starvation is reversed leading to their induction. Under normal growth conditions (in the absence of nickel), we observed that *fepA* and *sufA* gene expression levels gradually decreased over time throughout lag phase (Figure 2.3 A and Figure 2.3 B). In contrast, nickel exposure (50 μM) results in a consistently high level of *fepA* and *sufA* expression throughout lag phase when compared to cells that were not exposed to nickel (Figure 2.3 A and Figure 2.3 B). The nickel-dependent upregulation of *fepA* was also independently confirmed by RT–qPCR (Figure 2.4). The expression of *iscR* is auto-regulated in response to demand for Fe-S cluster biogenesis and is influenced indirectly by intracellular iron availability. Therefore, *iscR* expression can also be used as an indicator of intracellular iron status. Similar to what was observed for *fepA* and *sufA*, *iscR* expression gradually decreased throughout lag phase in control cells but remained high throughout lag phase in nickel-treated cells (Figure 2.3 C). These results are

consistent with other studies and clearly support the hypothesis that nickel disrupts iron metabolism in multiple growth phases in *E. coli* (Gault et al., 2016).

The presence of siderophores decreases in nickel-treated E. coli cells

When iron is limiting, cells export siderophores into the extracellular environment in order to chelate ferric iron for transport into the cell. The primary siderophore in the strain of *E. coli* used for these studies is the catechol enterobactin. In order to assess the effects of nickel on siderophore production, catechol levels were monitored in the culture medium using the Arnow assay (Ma and Payne, 2012; Arnow, 1937). Siderophore production is reported in Arnow units, which are normalized for bacterial cell density. Since they are all catechols, this assay should detect enterobactin and its hydrolysis products if they are present in the extracellular medium. The presence of catechols in the culture medium gradually increases over time throughout lag and exponential phase in control cells not exposed to nickel (Figure 2.5 A). In contrast, high nickel stress reduces the catechol accumulation in the culture medium (Figure 2.5 A). The decrease in extracellular siderophore levels was proportional to increasing media nickel concentrations (Figure 2.6). The siderophore enterobactin is imported by FepA after it chelates extracellular ferric iron. In order to test if the decrease in extracellular siderophore levels during nickel stress was due to an increased rate of clearance of enterobactin by active import via FepA, catechol production also was measured in a *fepA* deletion mutant strain (Δ*fepA*). Siderophore levels were also lower in Δ*fepA* cells exposed to nickel in comparison to untreated cells (Figure 2.5 B). The Arnow assay cannot differentiate enterobactin from its four hydrolysis products, which can also be secreted into the media

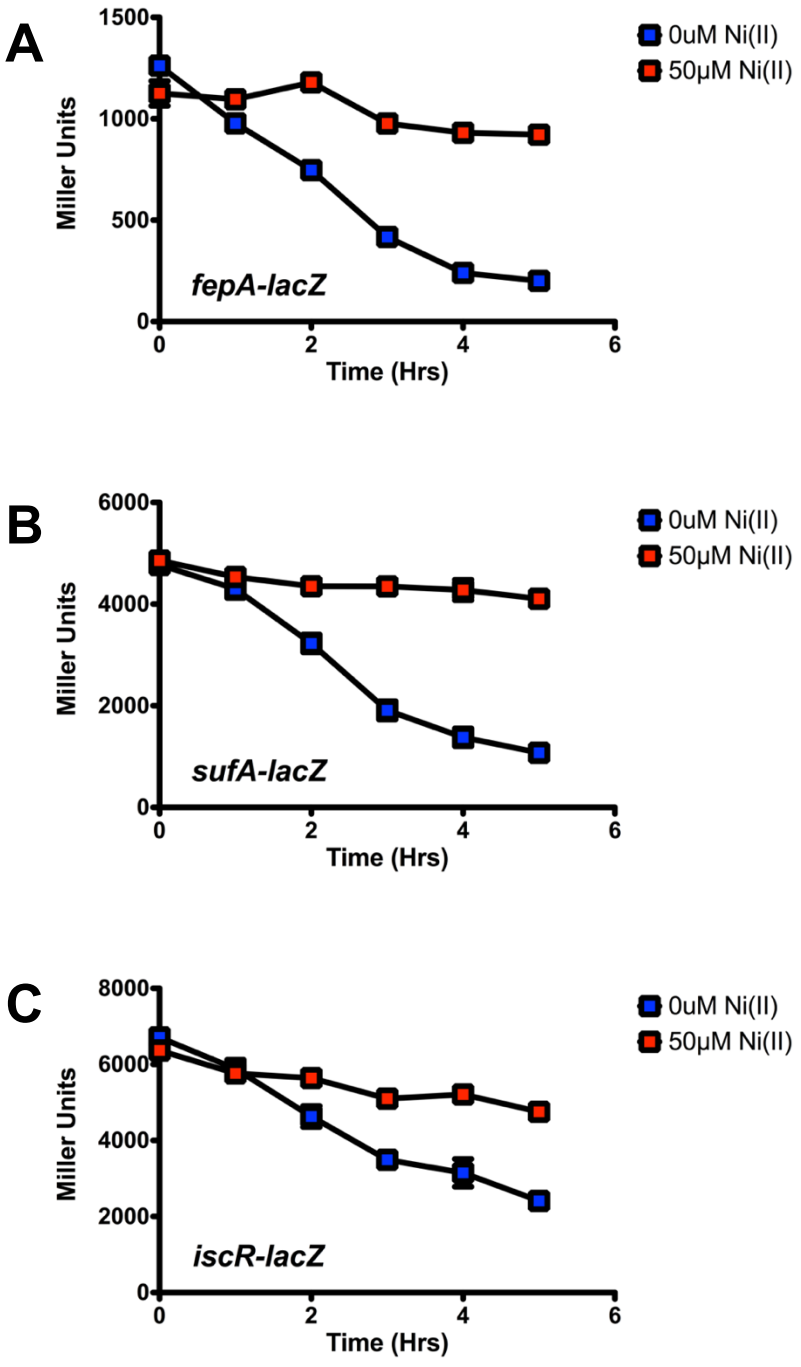

Figure 2.3. Nickel induces the *Fur* and *IscR* regulons. Relative gene expression levels are shown in Miller Units which accounts for any observed differences in bacterial cell growth or optical density at 600nm. (A) *fepA-lacZ* gene expression levels. (B) *sufA-lacZ* gene expression levels. (C) *iscR-lacZ* gene expression levels. All measurements were repeated in triplicate (n = 3) and error bars indicate one standard deviation from the mean value.

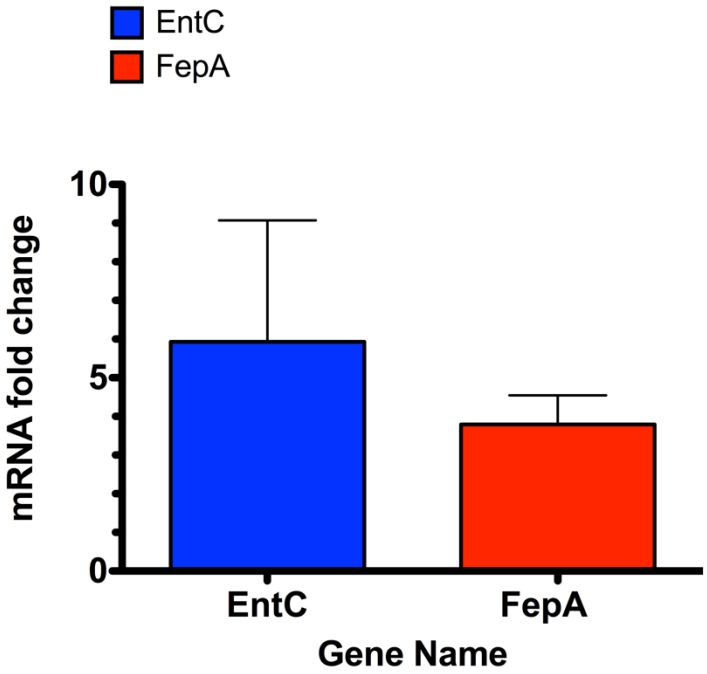

Figure 2.4. Nickel induces *entC* and *fepA* mRNA expression. $2^{(-\Delta\Delta Cq)}$ values are reported as mRNA fold change of nickel-treated cells in comparison to untreated control cells after 2 hours in M9 gluconate minimal media. All measurements were repeated in triplicate (n=3) and error bars indicate one standard deviation from the mean value.

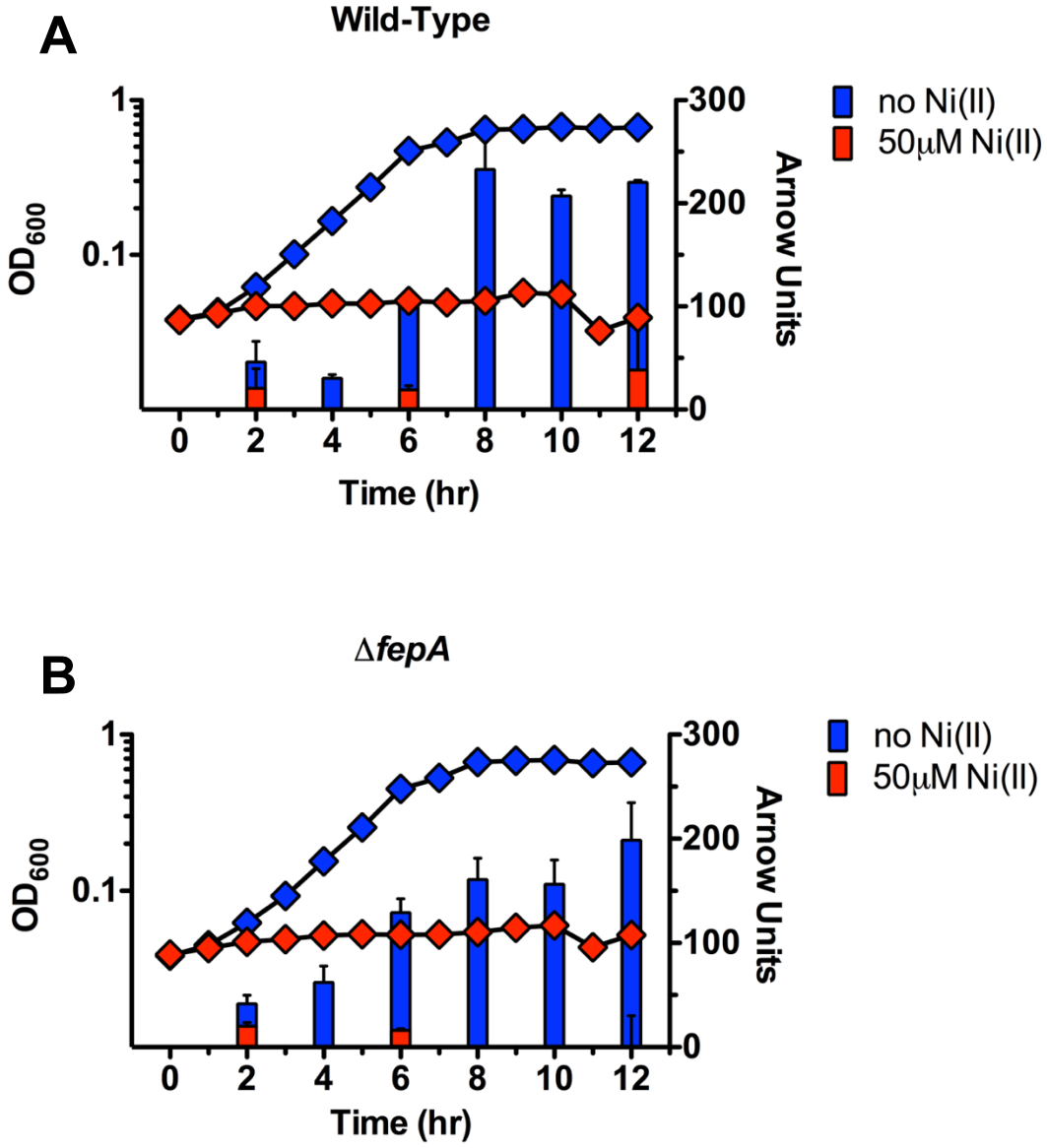

Figure 2.5. Nickel decreases levels of extracellular catecholate siderophores during lag phase. Total catecholate production is expressed in Arnow units (right axis, bars). Relative growth is expressed by optical density at 600 nm (left axis, diamonds). (A) Wild-type and (B) Δ*fepA* MG1655 *E. coli* cells measurements are overlaid with growth data from the same cultures (left axis, diamonds). All growths were repeated in triplicate (n = 3) and error bars indicate one standard deviation from the mean value.

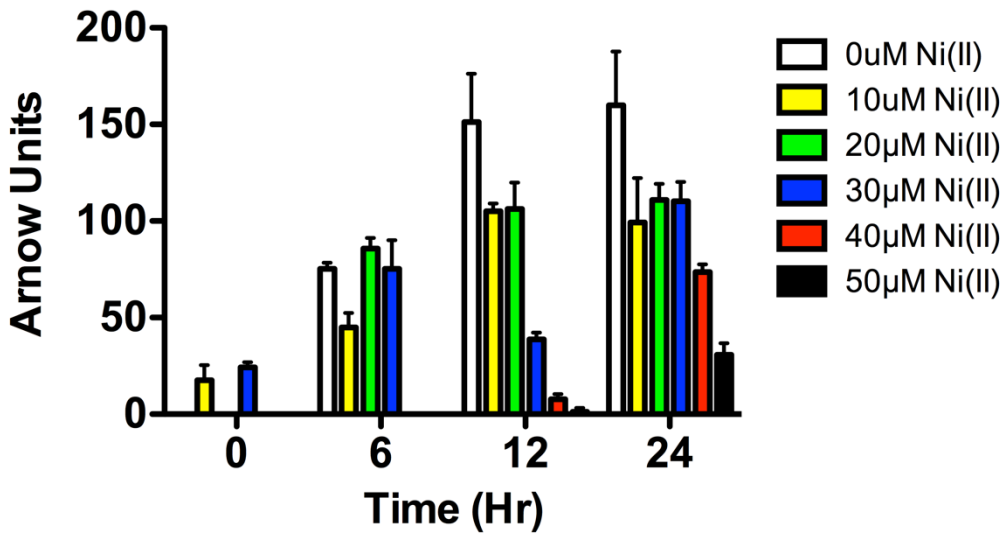

Figure 2.6. Nickel concentration proportionally affects catechol production over time. Arnow units are used to measure catechol production and one Arnow unit equals 1000 x OD_{515nm} / OD_{650nm}. Wild-type *E. coli* cells were cultured in M9 gluconate minimal media containing either 0 μM, 10 μM, 20 μM, 30 μM, 40 μM, or 50 μM nickel chloride for 24 hours. All growths were repeated in triplicate (n=3) and error bars indicate one standard deviation from the mean value.

as low affinity iron chelators (Hantke, 1990). In order to assess the effects of nickel exposure on extracellular enterobactin and its hydrolysis products, fast protein liquid chromatography (FPLC) was used to separate and quantify enterobactin products from the extracellular medium. In both wild-type and Δ*fepA* strains the presence of enterobactin and all of its hydrolysis products are lower during nickel exposure (Figure 2.7 A and Figure 2.7 B). Liquid chromatography – mass spectrometry (LC-MS) also showed that in the wild-type strain nickel exposure resulted in a reduction of enterobactin and its hydrolysis products (Figure 2.8).

DISCUSSION

The amount of nickel exposure can proportionally affect the relative growth of *Escherichia coli* cells over time in iron-limited media. The first stage of growth known as lag phase shows a significant impact from nickel exposure (Fig. 2.2 A). The lag phase duration of cells exposed to 50μM nickel chloride is approximately 10-fold longer than cells that were not exposed to nickel stress (Fig 2.2 B). According to Rolfe et al, lag phase is the stage of growth where bacterial cells accumulate iron (Rolfe et al., 2012). Nickel exposure in lag phase results in lower iron accumulation (Fig.2.2 A) and a cellular iron starvation response where genes required for adaptation to iron starvation are constitutively expressed at high levels during lag phase nickel exposure (Fig. 2.2 B). Therefore, the disruption of iron homeostasis by lag phase nickel exposure stress (Fig 2.2 B).

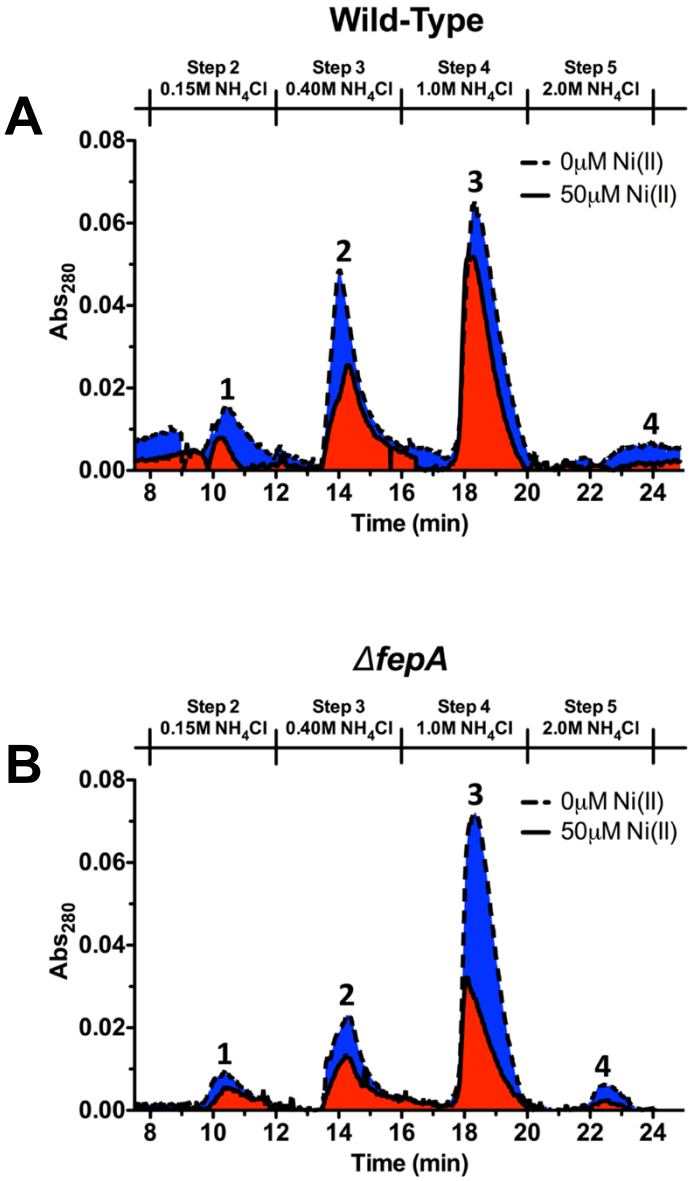

Figure 2.7. Nickel decreases levels of extracellular enterobactin and its hydrolysis products during lag phase (A) Spent media from Wild-type MG1655 culture with 0 μM nickel or 50μM $NiCl_2$ was filtered and enterobactin-related metabolites were separated by FPLC (B) Spent media from Δ*fepA* cultures with no added nickel or 50 μM $NiCl_2$ was filtered and enterobactin-related metabolites were separated by FPLC. Elution times are shown across the bottom axis. The elution peak annotated '1' refers to the linear dimer, '2' refers to the hydrolytically cleaved linear trimer, '3' refers to the non-hydrolytically cleaved linear trimer, and '4' refers to cyclized enterobactin.

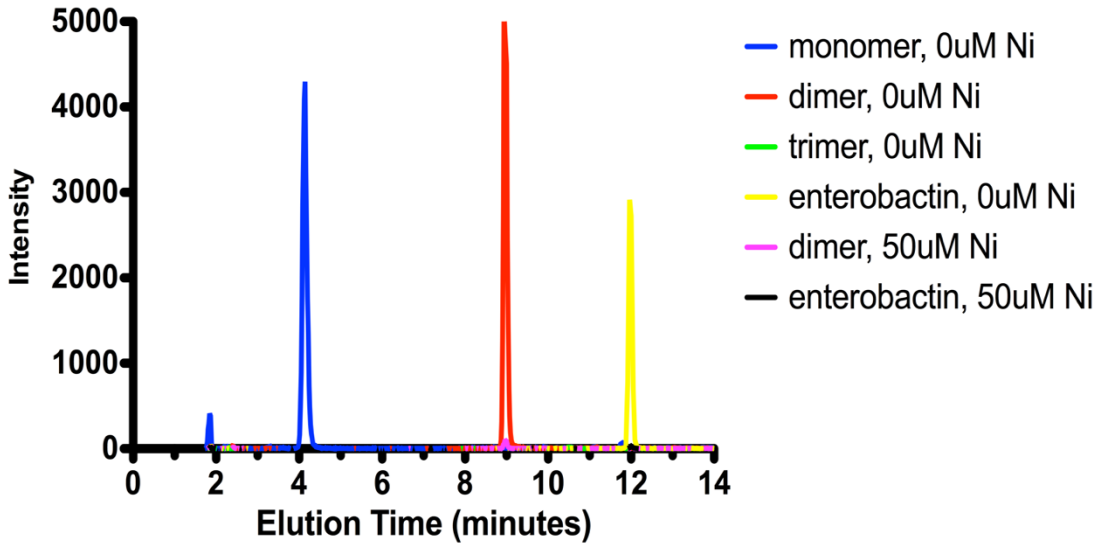

Figure 2.8. Nickel decreases extracellular enterobactin and its hydrolysis products during lag phase. Spent media from Wild-type MG1655 culure with 0 µM and 50 µM nickel chloride was sterile filtered and enterobactin-related metabolites were twice extracted using a 1:1 ratio of 100% ethyl acetate to culture media. Ethyl acetate was removed using rotovap and the residue was resuspended in 10% acetonitrile and 0.1 % trifluoroacetic acid. Sample was analyzed by liquid chromatography – mass spectrometry.

Therefore, the disruption of iron homeostasis by lag phase nickel exposure is in good agreement with other recent studies on iron homeostasis and nickel toxicity (Gault et al., 2016; Rolfe et al., 2012). Interestingly, once nickel-exposed cells exit lag phase, the exponential phase duration (doubling time) shows a much milder 2-fold increase even at the highest nickel concentration tested. Furthermore, the final cell density reached in stationary phase does not seem to be significantly altered by lag phase nickel exposure (Fig. 2.2 A). This result may be partially explained by the selection for a nickel-resistant mutant population during lag phase, which then grows nearly at wild-type rates once they accumulate or exit lag phase. In fact, preliminary studies in our laboratory indicate that a nickel-resistant population is selected for after high nickel exposure in lag phase (at concentrations above 30 μM $NiCl_2$, data not shown).

Despite the demand for iron and the transcriptional upregulation of iron uptake genes, the level of the siderophore enterobactin and all its hydrolysis products are lower in nickel-treated cells as compared to untreated control cells. Previously it was shown that nickel exposure in exponential phase of growth causes repression of iron uptake pathways, including *fepA* and the *entCEBA* operon used for enterobactin synthesis (Gault et al., 2016). The exact mechanism for this inappropriate repression is not clear but may involve a nickel-dependent increase in intracellular labile iron, perhaps from damaged or mis-metallated iron proteins, which then triggers inappropriate Fur-dependent repression of target genes. Using the *lacZ* promoter fusion construct for *fepA* we also observed similar reduced expression during *exponential* phase nickel exposure (data not shown). However, expression of both *fepA* and *entC* is constitutively high during *lag* phase nickel exposure, as measured by *lacZ* promoter fusions and RT-qPCR (Figure 2.4). Therefore,

transcriptional repression of the *entCEBA* system does not explain the observed reduction of enterobactin in the media during lag phase nickel exposure.

Taken together, these findings support the notion that high nickel exposure can disrupt siderophore production in *E. coli* as was previously reported in *Pseudomonas aeruginosa* under iron-limiting conditions (Visca et al., 1992). These results may provide an additional mechanism to help explain the observed drop in iron accumulation under nickel stress seen in *E. coli* grown under aerobic conditions in minimal media (Gault et al., 2016). Under those growth conditions where ferric iron predominates, the enterobactin uptake pathway would be the main route for iron entry into the cell. However, the results we obtained in lag phase also point to some distinct differences in nickel-mediated disruption of iron homeostasis between lag and exponential growth phases. In lag phase the reduction in iron accumulation is much more severe and the *Fur* and *IscR* regulons are responding appropriately to the resulting iron starvation. Despite the transcriptional upregulation of the enterobactin synthesis and transport systems, the siderophore is failing to accumulate in the media and is not mediating iron uptake into the cell. The results also indicate that siderophore-mediated bioremediation may be perturbed if the toxic metal, in this case nickel, also disrupts siderophore production or metabolism.

REFERENCES

1. Alvarez, A., Saez, J.M., Davila Costa, J.S., Colin, V.L., Fuentes, M.S., Cuozzo, S.A., Benimelli, C.S., Polti, M.A., and Amoroso, M.J. (2017) Actinobacteria: current research and perspectives for bioremediation of pesticides and heavy metals. *Chemosphere.* **166:** 41-62.

2. Ansari, M. and Malik, A. (2010) Seasonal variation of different microorganisms with nickel and cadmium in the industrial wastewater and agricultural soils. *Environ Monit Assess* **167:** 151-163.

3. Arnow, L.E. (1937) Colorimetric determination of the components of 3,4-dihydroxyphenylalanine-tyrosine mixtures. *J Biol Chem* **118:** 531-537.

4. Baranyi, J. and Roberts, T.A. (1994). A dynamic approach to predicting bacterial growth in food. *Int J Food Microbiol* **23:** 277-294.

5. Braud, A., Geoffroy, V., Hoegy, F., Mislin, G.L., and Schalk, I.J. (2010) Presence of the siderophores pyoverdine and pyochelin in the extracellular medium reduces toxic metal accumulation in *Psuedomonas aeruginosa* and increases bacterial metal tolerance. *Environ Microbiol Rep* **2:** 419-425.

6. Braud, A., Hoegy, F., Jezequel, K., Lebeau, T., and Schalk IJ. (2009) New insights into the metal specificity of the Pseudomonas aeruginosa pyoverdine-iron uptake pathway. *Environ Microbiol* **11**: 1079-1091.

7. Das, K.K., Das, S.N., and Dhundasi, S.A. (2008) Nickel, its adverse health effects and oxidative stress. *Ind J Med Res* **128:** 412-425.

8. De Pina, K., Desjardin, V., Mandrand-Berthelot, M., Giordano, G., and Wu, L. (1999) *J Bacteriol* **181:** 670-674.

9. Denkhaus, E. and Salnikow, K. (2002) Nickel essentiality, toxicity, and carcinogenicity. *Critical Rev Oncology Hematology* **42:** 35-56.

10. Dixit, R., Wasiullah, Malaviya, D., Pandiyan, K., Sing, U.B., Sahu, A., Shukla, R., Singh, B.P., Rai, J.P., Sharma, P.K., Lade, H., and Paul, D. (2015) Bioremediation of heavy metals from soil and aquatic environment: an overview of principles and criteria of fundamental processes. *Sustainability.* **7:** 2189-2212.

11. Duhme, A.K., Hider, R.C., Naldrett, M.J., and Pau, R.N. (1998) The stability of the molybdenum-azotochelin complex and its effect on siderophore production in *Azotobacter vinelandii. J Biol Inorganic Chem.* **3:** 520-552.

12. Escolar, L., Perez-Martin, J., and de Lorenzo, V. (1998) Coordinated repression in vitro of the divergent *fepA-fes* promoters of *Escherichia coli* by the iron uptake regulation (Fur) protein. *J Bacteriol* **180:** 2579-2582.

13. Gault, M., Effantin G., and Rodrigue, A. (2016) Ni exposure impacts the pool of free fe and modifies DNA supercoiling via metal-induced oxidative stress in *Escherichia coli* K-12. *Free Radic Biol Med* **97:** 351-361.

14. Giel, J.L., Rodionov, D., Liu, M., Blattner, F.R., and Kiley, P.J. (2006) IscR-dependent gene expression links iron-sulphur cluster assembly to the control of O_2-regulated genes in *Escherichia coli*. *Mol Microbiol* **60:** 1058–1075.

15. Hantke, K. (1990) Dihydroxybenzolyserine—a siderophore for *E. coli. FEMS Microbiol Lett* **67:** 5-8.

16. Hu, X. and Boyer, G.L. (1996) Siderophore-mediated aluminum uptake by *Bacillus magaterium* ATCC 19213. *Appl Environ Microbiol.* **62:** 4044-4048.

17. Hunt, M.D., Pettis, G.S., and McIntosh, M.A. (1994) Promoter and operator determinants for fur-mediated iron regulation in the bidirectional *fepA-fes* control region of the *Escherichia coli* enterobactin gene system. *J Bacteriol* **176:** 3944-3955.

18. Irving, H. and Williams, R.J.P. (1953) The stability of transition-metal complexes. *J Chem Soc* **0:** 3192-3210.

19. Iwig, J.S., Rowe, J.L., and Chivers, P.T. (2006) Nickel homeostasis in *Escherichia coli* – the RcnR-RcnA efflux pathway and its linkage to NikR function. *Mol Microbiol* **62:** 252-262.

20. Kasprzak, K.S., Sunderman, F.W., Jr., and Salnikow, K. (2003) Nickel carcinogenesis. *Mutat Res.* **533:** 67-97.

21. Kawano, M., Oshima, T., Kasai, H., and Mori, H. (2002) Molecular characterization of long direct repeat (LDR) sequences expressing a stable mRNA encoding for a 35-amino-acid cell-killing peptide and a *cis*-encoded small antisense RNA in *Escherichia coli*. *Mol Microbiol* **45:** 333-349.

22. Kumar, V., Mishra, R.K., Kaur, G., and Dutta, D. (2017) Cobalt and nickel impair DNA metabolism by the oxidative stress independent pathway. *Metallomics* **9:** 1596-1609.

23. Ma, L. and Payne, S.M. (2012) AhpC is required for optimal production of enterobactin by *Escherichia coli.* *J Bacteriol* **194:** 6748-6757.

24. Macomber, L. and Hausinger, R.P. (2011) Mechanisms of nickel toxicity in microorganisms. *Metallomics* **3:** 1153-1162.

25. Macomber, L., Elsey, S.P., Hausinger, R.P. (2011) Fructose-1, 6-bisphosphate aldolase (class II) is the primary site of nickel toxicity in *Escherichia coli*. *Mol Microbiol* **82:** 1291-1300.

26. Macomber, L., and Imlay, J.A. (2009) The iron-sulfur clusters of dehydratases are primary intracellular targets of copper toxicity. *Proc Natl Acad Sci USA* **20:** 8344-8349.

27. Miller, J.H. (1972). Experiments in molecular genetics. Cold Spring Harbor Laboratory, Cold Spring Harbory, NY.

28. Nriagu, J.O. (1980) A silent epidemic of environmental metal poisoning? *Environ Pollution* **50:** 139-161.

29. O'Brien, I.G. and Gibson, F. (1970) The structure of enterochelin and related 2,3-dihydroxy-n-benzoylserine conjugates from *Escherichia coli*. *Biochim Biophys Acta* **215:** 393-402.

30. Polti, M.A., Atjian, M.C., Amoroso, M.J., and Abate, C.M. (2011) Soil chromium bioremediation: synergic activity of actinobactera and plants. *International Biodeterior Biodegrad* **65:** 1175-1181.

31. Ranquet, C., Ollagnier-de-Choudens S., Loiseau L., Barras F., and Fontecave M. (2007) Cobalt stress in *Escherichia coli*: The effect on the iron-sulfur proteins. *J Biol Chem* **282:** 30442-30451.

32. Rolfe, M.D., Rice, C.J., Lucchini, S., Pin, C., Thompson, A., Cameron, A.D., Alston, M., Stringer, M.F., Betts, R.P., Baranyi, J., Peck, M.W., and Hinton, J.C. (2012) Lag phase is a distinct growth phase that prepares bacteria for exponential growth and involves transient metal accumulation. *J Bacteriol* **194:** 686-701.

33. Roth, V. (2006). Doubling Time. (http://www.doubling-time.com/compute.php

34. Visca, P., Colotti, G., Serino, L., Verzili, D., Orsi, N., and Chiancone, E. (1992) Metal regulation of siderophore synthesis in *Pseudomonas aeruginosa* and functional effects of siderophore-metal complexes. *Appl Environ Microbiol* **58:** 2886-2893.

35. Wade, H.E. (1952) Observations on the growth phases of *Escherichia coli*, American Type 'B'. *J Gen Microbiol* **7:** 18-23.

36. Wang, W., Qiu, Z., Tan, H., Cao, L. (2014) Siderophore production by actinobacteria. *Biometals* **27:** 623-631.

37. Winkelmann, G., Cansier, A., Beck, W., and Jung, G. (1994) HPLC separation of enterobactin amd linear 2,3-dihydroxybenzoylserine derivatives: a study on mutants of *Escherichia coli* defective in regulation (*fur*), esterase (*fes*) and transport (*fepA*). *Biometals* **7:** 149-154.

38. Xu, F.F. and Imlay, J.A. (2012) Silver(I), mercury(II), cadmium(II), and zinc(I) target exposed enzymic iron-sulfur clusters when they toxify *Escherichia coli*. *Appl Environ Microbiol* **78:** 3614-3621.

CHAPTER 3

ENTEROBACTIN BIOSYNTHESIS PROMOTES NICKEL RESISTANCE IN *E. COLI*

ABSTRACT

Siderophore production can protect against metal toxicity by reducing metal accumulation by sequestration. However, it has not been shown to affect whether constitutive expression of siderophore biosynthesis genes can also promote metal resistance. Herein, we characterize the phenotypic effects of *E. coli* cells constitutively expressing the *ent* operon which is responsible for enterobactin biosynthesis. Our data shows that cells deficient in enterobactin secretion can partially overcome nickel toxicity when enterobactin accumulates inside the cell. It is evident that enterobactin hydrolysis products are secreted into the extracellular space. These hydrolysis products can bind and sequester nickel when iron is limiting.

INTRODUCTION

Enterobactin is the predominant siderophore secreted by *E. coli* under iron-limiting conditions. Niches where those conditions exist include soil (Solomon et al., 2002), plants (Itoh et al., 1998), and mammalian intestinal systems or pathogenesis sites (Van Elsas et al., 2011). In *E. coli,* enterobactin is synthesized by the concerted action of the gene products encoded by the *entCEBA* operon (Ma and Payne, 2012; Crosa et al., 2002; Walsh

et al., 1990). It is then exported from the cytoplasm by the inner membrane transporter protein EntS (Miethke et al., 2007; Bleuel et al., 2005; Furrer et al., 2002). Extracellular ferric iron binds to apo-enterobactin forming Fe^{3+}–enterobactin. Fe^{3+}–enterobactin is preferentially imported back into the cell by binding to the outer membrane transporter protein FepA, then to FepB in the periplasm, and through the FepCDG transporter in the inner membrane (Larsen et al., 1997; Braun et al., 1995). Enterobactin is the cyclized form of three N-(2, 3-dihydroxybenzoyl)-L-serine monomeric units (Ehmann, et al., 2000; Shaw-Reid, et al., 1999; Gehring et al., 1998; Gehring et al., 1997). The backbone of intracellular Fe^{3+}–enterobactin must be hydrolyzed by the esterase Fes releasing ferric iron from its tightly chelated complex (Brickman and McIntosh 1992; Greenwood and Luke 1978; Bryce and Brot, 1972; Langman et al., 1972). The cleavage of intracellular enterobactin (cyclo-tris(2,3-dihydroxy-N-benzoylseryl) by Fes results in the production of four linear hydrolysis products including: the non-hydrolytically cleaved trimer (N, N', N''-tris(2,3-dihydroxybenzoyl)-O-(a-aminoacrylyl)-O-seryl serine), the hydrolytically cleaved trimer (N, N', N'''-tris(2,3-dihydroxybenzoyl)-O-seryl-O-seryl serine), a linear dimer (N, N'-bis(2,3-dihydroxybenzoyl)-O-(a-aminoacrylyl)-O-seryl serine), and a linear monomer (2,3-dihydroxy-N-benzoylserine) (Lin et al., 2005; Brickman et al., 1992; O'Brien and Gibson, 1970).

Siderophores like enterobactin have been shown to impact metabolism of other essential or toxic metals. For example, enterobactin can facilitate the reduction of Cu^{2+} to Cu^{1+} and increase copper cytotoxicity in uropathogenic *E. coli* (Chaturvedi et al., 2012). Siderophores have been shown to protect against metal toxicity perhaps by chelating other metals (Koh et al., 2015). The presence of the *Pseudomonas aeruginosa* siderophores

pyochelin (PCH) and pyoverdine (PVD) have been shown to decrease intracellular nickel accumulation (Braud et al., 2009; Braud et al., 2009; Braud et al., 2010). Additionally, media supplementation with PCH and PVD reduced nickel toxicity in iron-limited and iron-supplemented media (Braud et al., 2010). Despite this, little is known about how siderophore gene expression might affect how bacterial cells respond to nickel stress. Our goal in this work is to test if enterobactin biosynthesis gene expression and siderophore production can alter the effects of nickel toxicity under iron-limiting conditions in *Escherichia coli.*

MATERIALS AND METHODS

Bacterial strains and culture conditions

Strains used in this study are derivatives of the parent wild-type strain *E. coli* MG1655. An individual colony was transferred from fresh Lennox broth (LB) agar plates into a 4 mL volume of LB and grown for 4 – 5 hrs at 37 °C with shaking at 200 rpm. Cells from this culture were pelleted and washed twice in sterile 1X M9 minimal media salts; then the OD_{600nm} was normalized to 1.0. Normalized cells were diluted 1:200 into M9 glucose minimal media containing 1X M9 minimal salts (BD Difco), 0.2% (w/v) glucose (Acros Organics), 0.2 % (w/v) magnesium sulfate, 0.1 mM calcium chloride, and 0.5 g/mL Thiamine HCl (Sigma-Aldrich). Prepared M9 media typically contained ~300 nM iron and ~70 nM nickel as measured by ICP-MS. Cultures were incubated overnight for 18 – 20 hr, at 37 °C and 200 rpm, then washed and pelleted twice in sterile 1X M9 salts as described above. The resulting cell suspensions were normalized to an OD 600 nm of 2.0

and diluted 1:50 into M9 gluconate minimal media with 0.2 % (w/v) potassium gluconate (Alfa Aesar) to give an initial OD 600 nm of 0.04. Nickel chloride (Sigma-Aldrich) was added to described final concentrations in the M9 gluconate minimal media, from 0 µM up to 50 µM. No ampicillin was added to gluconate minimal medium during nickel exposure due to the potential for complexation of nickel and ampicillin (Mukherjee and Ghosh, 1995; Bravo and Anacona, 1998).

Cell growth was monitored as optical density at 600nm (OD_{600}) and plotted versus time (in hours). Lag phase duration was determined using the online fitting program, DMFit (www.ifr.ac.uk/safety/DMfit), applying the no-asymptote fitted model and parameters (Baranyi and Roberts, 1994). Stationary phase OD_{600} measurements were omitted for best fit of the model.

Arnow assay for catechol determination

Methods from Arnow and Ma were adapted for the quantification of catecholate siderophore production (to include any enterobactin breakdown products) by *E. coli* under nickel stress (Ma and Payne, 2012; Arnow, 1937). Cells were cultured in 0.2 % gluconate M9 minimal media with or without 50 µM nickel chloride. After 21 hours, 1 mL was collected from each growth, the OD at 650 nm was measured and recorded, and then each volume was cleared of cells via centrifugation at 16,000 x g for 1 min. A 500 µL volume of cleared supernatant was transferred to a clean, 4.0 mL polypropylene cuvette. 500 µL 0.5 N HCl, 500 µL of a 10% sodium nitrate / 10% sodium molybdate mixture (Sigma-Aldrich), and 500 µL 1 N NaOH were added to the cuvette. All assay samples were

measured against a blank mixture of fresh gluconate M9 minimal media with the above reagents listed for the assay. The absorbance at 515 nm was measured and recorded immediately after mixing. Arnow units were calculated using Equation 2:

Equation 2: Arnow Unit = 1000 * [Abs_{515} / Abs_{650}]

Enterobactin purification and quantification using FPLC

Strains were plated onto LB and incubated overnight at 37 °C. A single colony was cultured according as described above. Cultured cells were washed, normalized, and diluted to a final optical density of 0.04 in M9 gluconate minimal media, with 50 µM nickel chloride. Cultures were incubated for 12 hours at 37 °C at 200 rpm. The cells were centrifuged for 20 min at 4 °C and 8,000 x g. The supernatant was sterile filtered twice using a fresh 0.22 µm filter (Millipore) each time and a total of 1 L spent media was collected. Enterobactin and its hydrolysis products were purified using a modified form of a previously published protocol (O'Brien and Gibson, 1970). Briefly, the sterile, filtered supernatant was loaded onto a DEAE-Sepharose Fast Flow column equilibrated with 10 mM sodium phosphate buffer, pH 7.0 and 5 mL fractions were collected by eluting at 4 °C using a step gradient of 0.0 M, 0.05 M, 0.15 M, 1.0 M, and 2.0 M ammonium chloride. The UV-Visible absorption spectroscopy spectra were obtained by scanning monomer, dimer, trimer #1, trimer #2, and enterobactin from elution fraction #8, #11, #15, #19, and #23, respectively at 280 nm.

Quantification of enterobactin and its hydroylsis products by extraction

Strains were diluted from an overnight culture into fresh M9 gluconate minimal media and cultured for 12 hours with 50 μM nickel chloride at 37 °C. Culture media was twice extracted using a 1:1 ratio of 100 % ethyl acetate to culture medium (Winkelmann et al., 1994). The ethyl acetate layer was collected and scanned using UV-Visible absorption spectroscopy.

Catechol metal binding studies using Atomic Absorption Spectroscopy (AAS)

Preparatory cell growth in LB and glucose minimal media was conducted as previously described**.** Cell cultures were then grown in M9 gluconate minimal media to OD_{600nm} = 0.1 then treated with 50 μM nickel chloride for 3 hours in a culture flask at 37 °C and 200 rpm. Cells were centrifuged at 4,000 x g for 20 min and then the supernatant was sterile filtered using a 0.22 μm filter (Millipore). Enterobactin and its hydrolysis products were purified using a modified form of a previously published protocol (O'Brien and Gibson, 1970). Briefly, the sterile, filtered supernatant was loaded onto a DEAE-Sepharose Fast Flow column equilibrated with 10 mM sodium phosphate buffer, pH 7.0 and 5 mL fractions were collected by eluting at 4 °C using a step gradient of 0.0 M, 0.05 M, 0.15 M, 1.0 M, and 2.0 M ammonium chloride. The metal content of monomer, dimer, trimer #1, trimer #2, and enterobactin from elution fraction #8, 11, 15, 19, and 23, respectively was measured using AAS. Otherwise, the supernatant was twice extracted with 100% ethyl acetate, evaporated by rotovap, re-suspended in water, and analyzed by AAS.

RESULTS

The entS deletion strain containing pEntCEBA is less sensitive to nickel stress

In order to test the effects of enterobactin biosynthesis on nickel toxicity in *E. coli.* We generated control strains containing an empty plasmid, pWSK29 and strains that contained a plasmid constitutively expressing the *ent* operon. The pWSK29 low-copy number plasmid has an ampicillin resistance cassette for selection (Ma and Payne, 2012). The pEntCEBA plasmid is a pWSK29 derivative that contains the *ent* operon and constitutively expresses these enterobactin biosynthesis genes. Wild-type, Δ*entS* and Δ*fepA* strains that only contain pWSK29 are all sensitive to nickel exposure (Figure 3.1 A). Strains only containing pWSK29 have a lag phase duration time of approximately 18 hours in the presence of high nickel (Figure 3.1 B) and also show reduced siderophore production under nickel stress. The level of siderophores produced by pWSK29 expressing cells are below the limit of detection. Similarly, wild-type and *fepA* deletion strains containing pEntCEBA are sensitive to nickel exposure. However, a slight rescue of nickel toxicity is observed in the *entS* deletion strain that contains the pEntCEBA vector (Figure 3.2 A). Lag phase duration is also shorter (Figure 3.2 B). in comparison to cells containing pWSK29 (Figure 3.1 B). Siderophore levels in the media were also significantly higher in pEntCEBA containing strains in comparison to cells containing pWSK29 (Figure 3.2 C).

Siderophore production in the media was further analyzed by FPLC and UV-Visible absorption spectroscopy. Results showed all strains containing pWSK29 (wild-type, Δ*entS*, and Δ*fepA*) produced similar levels of monomer, dimer (peak 1), and trimer #1 (peak 2, Figure 3.3 A). Wild-type and Δ*entS* strains containing pWSK29 also showed similar amounts of extracellular trimer #2 (peak 3) and enterobactin (peak 4, Figure 3.3 A).

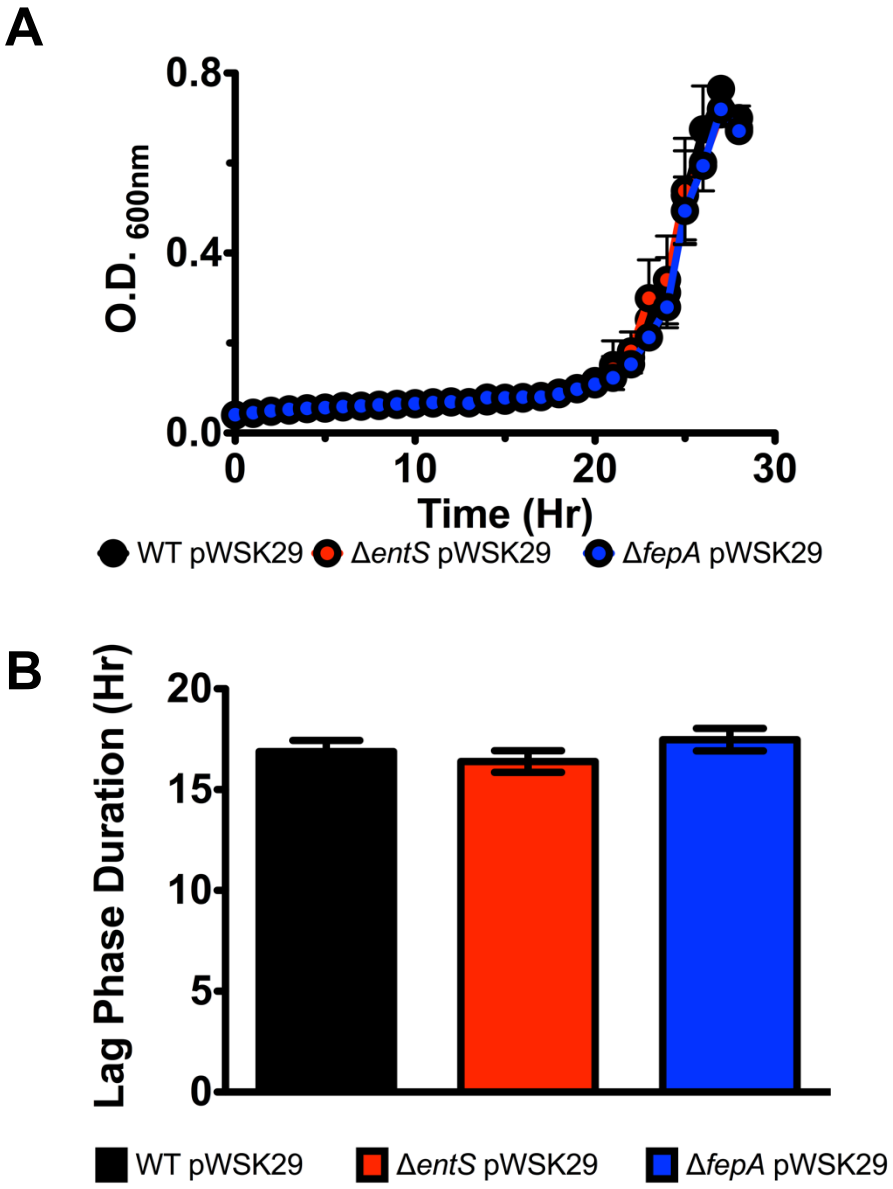

Figure 3.1. Nickel exposure extends lag phase duration in cells containing pWSK29. (A) Growth curves of wild type MG1655 *E. coli* cells in M9 gluconate media exposed to 50 μM nickel chloride. (B) Lag phase duration calculated from the growth curve data shown in Figure 3.1 A. All growths were repeated in triplicate (n=3) and error bars indicate one standard deviation from the mean value.

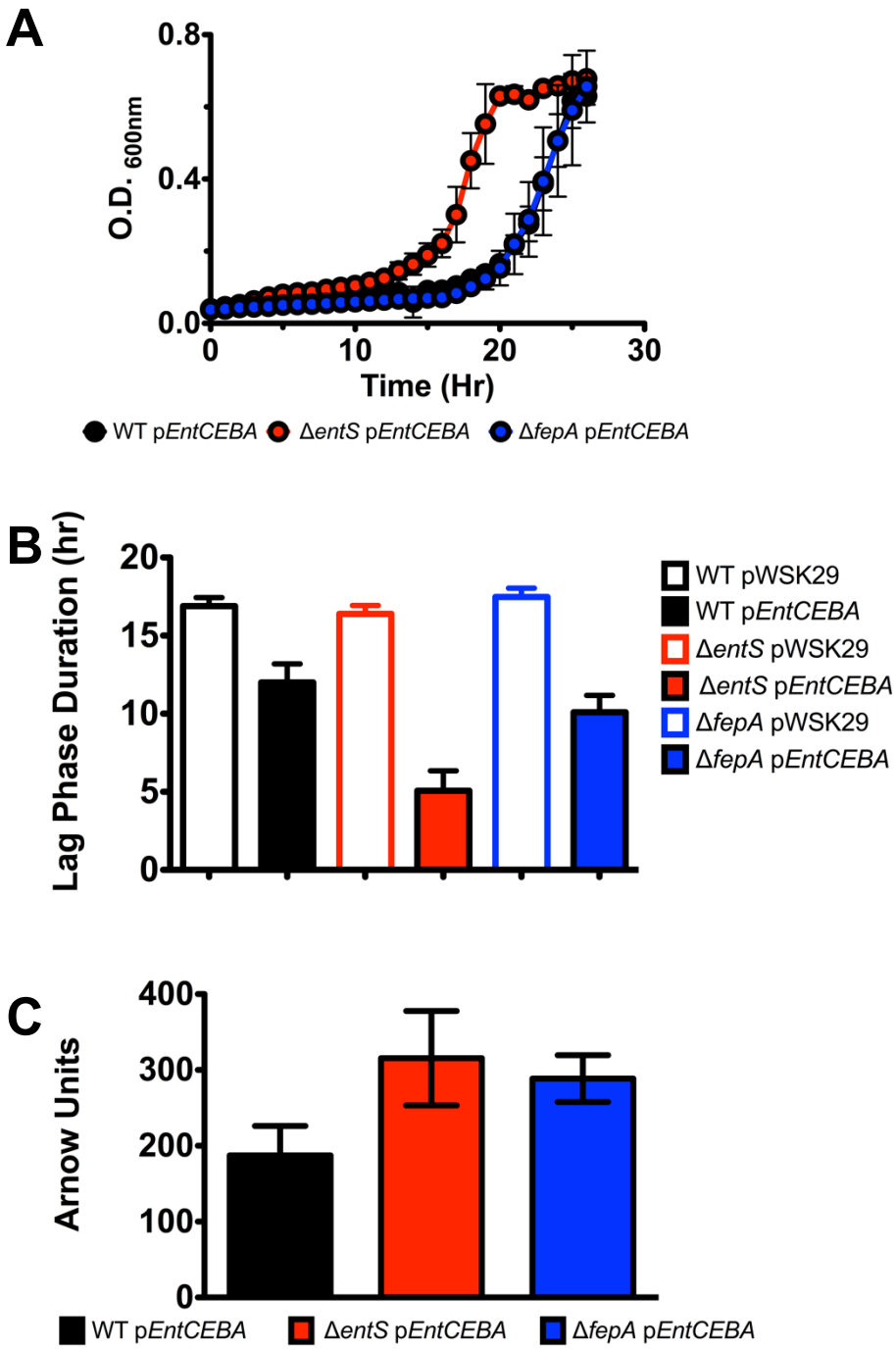

Figure 3.2. Nickel exposure extends lag phase duration in cells containing p*EntCEBA*. (A) Growth curves, (B) lag phase duration, and (C) Arnow units at 21 hours of wild-type, Δ*entS,* and Δ*fepA* strains. All growths were repeated in triplicate (n=3) and error bars indicate one standard deviation from the mean value.

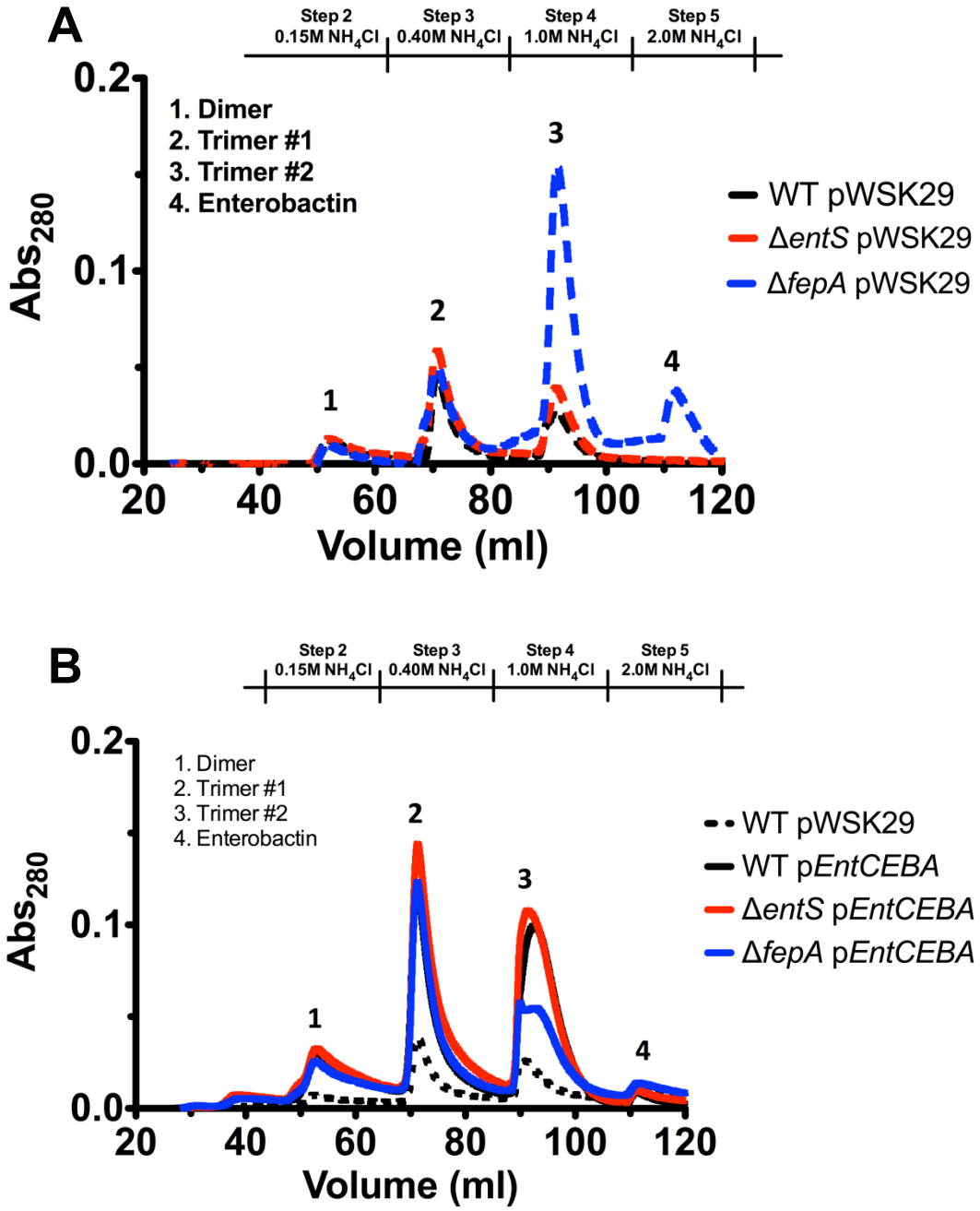

Figure 3.3. FPLC siderophore profile of cells containing pWSK29 (A) or p*EntCEBA* (B) Spent media with 50μM $NiCl_2$ was filtered and enterobactin-related metabolites were separated by FPLC. Elution volumes are shown across the bottom axis. The elution peak annotated '1' refers to the linear dimer, '2' refers to the hydrolytically cleaved linear trimer, '3' refers to the non-hydrolytically cleaved linear trimer, and '4' refers to cyclized enterobactin.

Wild-type and Δ*entS* strains containing pWSK29 also showed similar amounts of extracellular trimer #2 (peak 3) and enterobactin (peak 4, Figure 3.3 A). The Δ*fepA* strain containing pWSK29 showed increased levels of trimer #2 (peak 3) and enterobactin (peak 4, Figure 3.3 A). Wild-type, Δ*entS*, and Δ*fepA* strains containing pEntCEBA showed similar amounts of monomer, dimer (peak 1), and trimer #1 (peak 2, Figure 3.3 B), and enterobactin (peak 4, Figure 3.3 B). While, Δ*fepA* (pEntCEBA) showed less extracellular trimer #2 (peak 3, Figure 3.3 B). A full wavelength scan confirmed that pEntCEBA expressing strains produce more monomer, dimer, and trimer #1 (Figure 3.4). Again, Δ*fepA* pEntCEBA produces the most enterobactin and trimer #2 (Figure 3.5) likely because enterobactin is not efficiently transported back into the cell and accumulates even further in the media.

Due to varying polarity, enterobactin and its hydrolysis products can also be isolated and quantified by ethyl acetate extraction (O'Brien and Gibson, 1970). Therefore, supernatants were twice extracted using 100 % ethyl acetate (Winkelmann et al., 1994) and the purified samples scanned by UV-Visible absorption spectroscopy. The appropriate extinction coefficient was used to measure extracellular enterobactin and its hydrolysis products (Table 3.1).

Enterobactin and its hydrolysis products bind iron and nickel

In order to assess the metal-binding properties of enterobactin and its hydrolysis products, further characterization was required. Siderophores were purified using fast protein liquid chromatography (Figure 3.6) or ethyl acetate extraction (Figure 3.7) and then

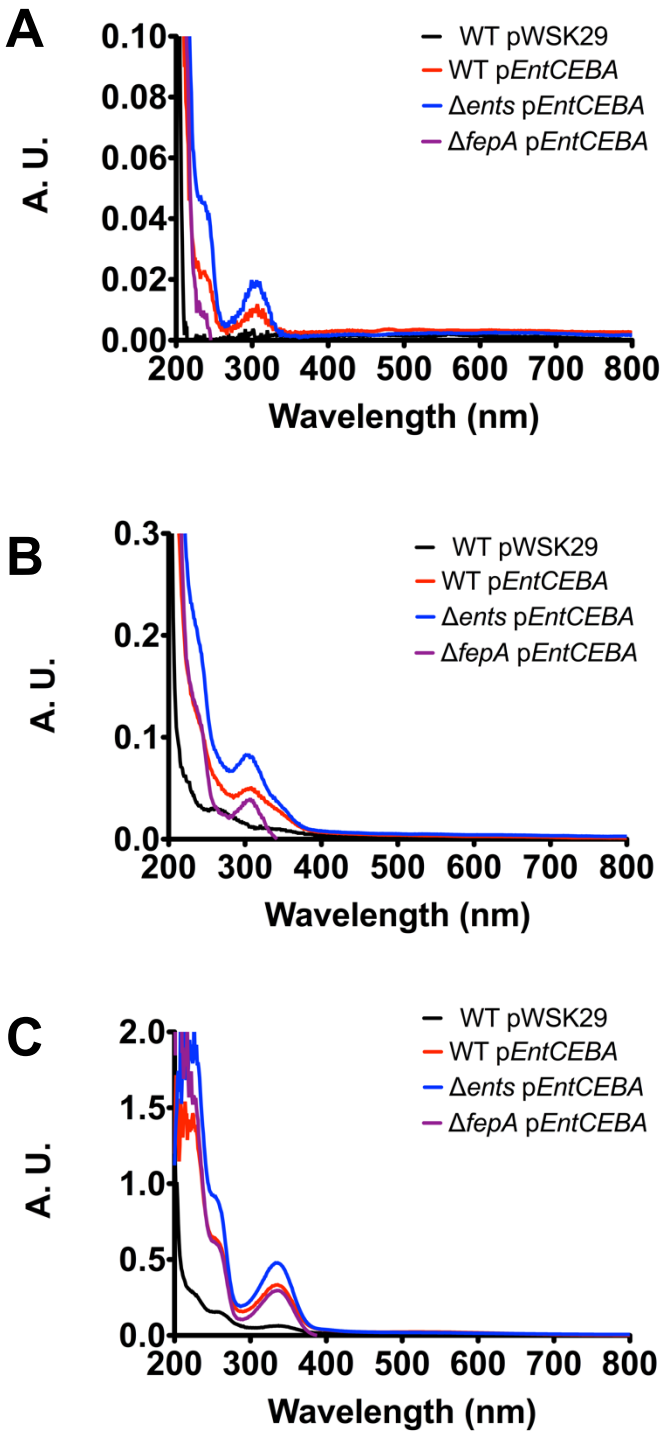

Figure 3.4. UV-visible spectra of monomer (A), dimer (B), and trimer #1 (C). Spent media with 50 μM $NiCl_2$ was filtered and enterobactin-related metabolites were separated by FPLC. Monomer (fraction #8), dimer (fraction #11), trimer #1 (fraction #15), were assessed by UV-visible absorption spectroscopy.

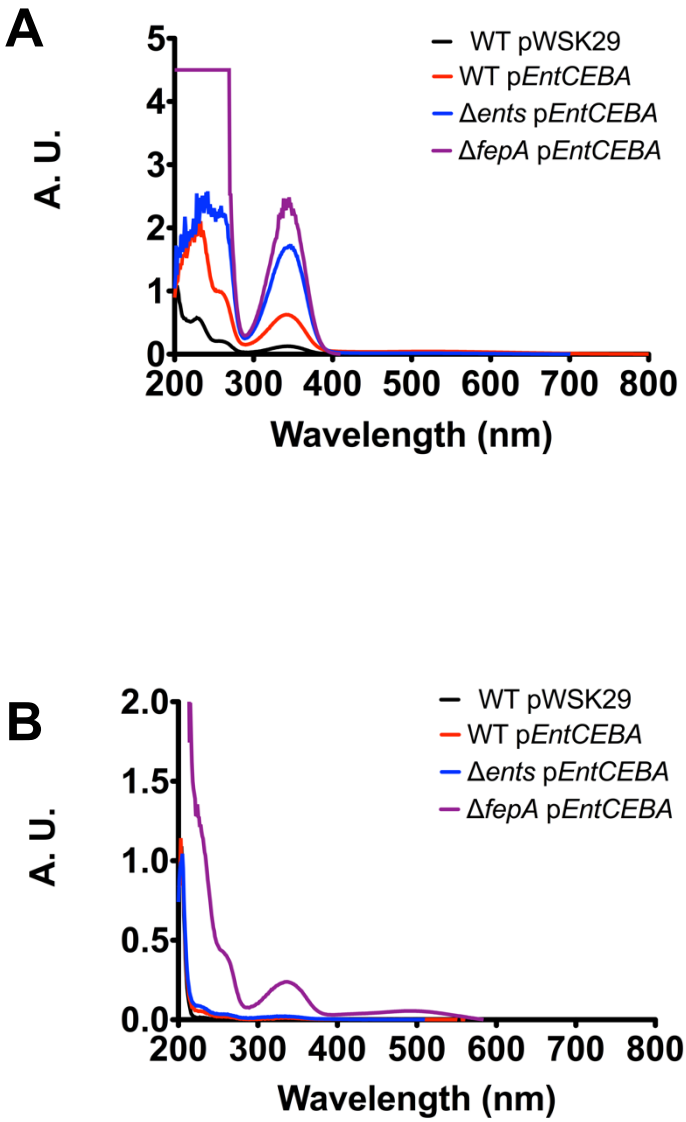

Figure 3.5. UV-visible spectra of trimer #2 (A) and enterobactin (B). Spent media with 50 μM $NiCl_2$ was filtered and enterobactin-related metabolites were separated by FPLC. Trimer #2 (fraction #19), and enterobactin (fraction #23) were assessed by UV-visible absorption spectroscopy.

Table 3.1. Quantification of siderophores extracted by ethyl acetate.

	monomer	dimer	trimer #1	trimer #2	enterobactin
Ethyl Acetate	0	0	0	0	0
WT pWSK29	39	20	13	13	13
△*fepA* pWSK29	72	36	24	24	24
△*entS* pWSK29	104	52	34	34	34
WT p*EntCEBA*	78	39	26	25	25
△*fepA* p*EntCEBA*	94	47	31	31	31
△*entS* p*EntCEBA*	96	49	32	32	32

Enterobactin and its hydrolysis products in A 1:1 100 % ethyl acetate is reported in μM using the appropriate extinction coefficient (O'Brien and Gibson, 1970). In ethyl acetate, the extinction coefficient of monomer (314nm) 3100 $M^{-1}{\cdot}cm^{-1}$, dimer (315nm) 6200 $M^{-1}{\cdot}cm^{-1}$, trimer #1 (315nm) 9360 $M^{-1}{\cdot}cm^{-1}$, trimer #2 (316nm) 9400 $M^{-1}{\cdot}cm^{-1}$, and enterobactin (316nm) 9390 $M^{-1}{\cdot}cm^{-1}$.

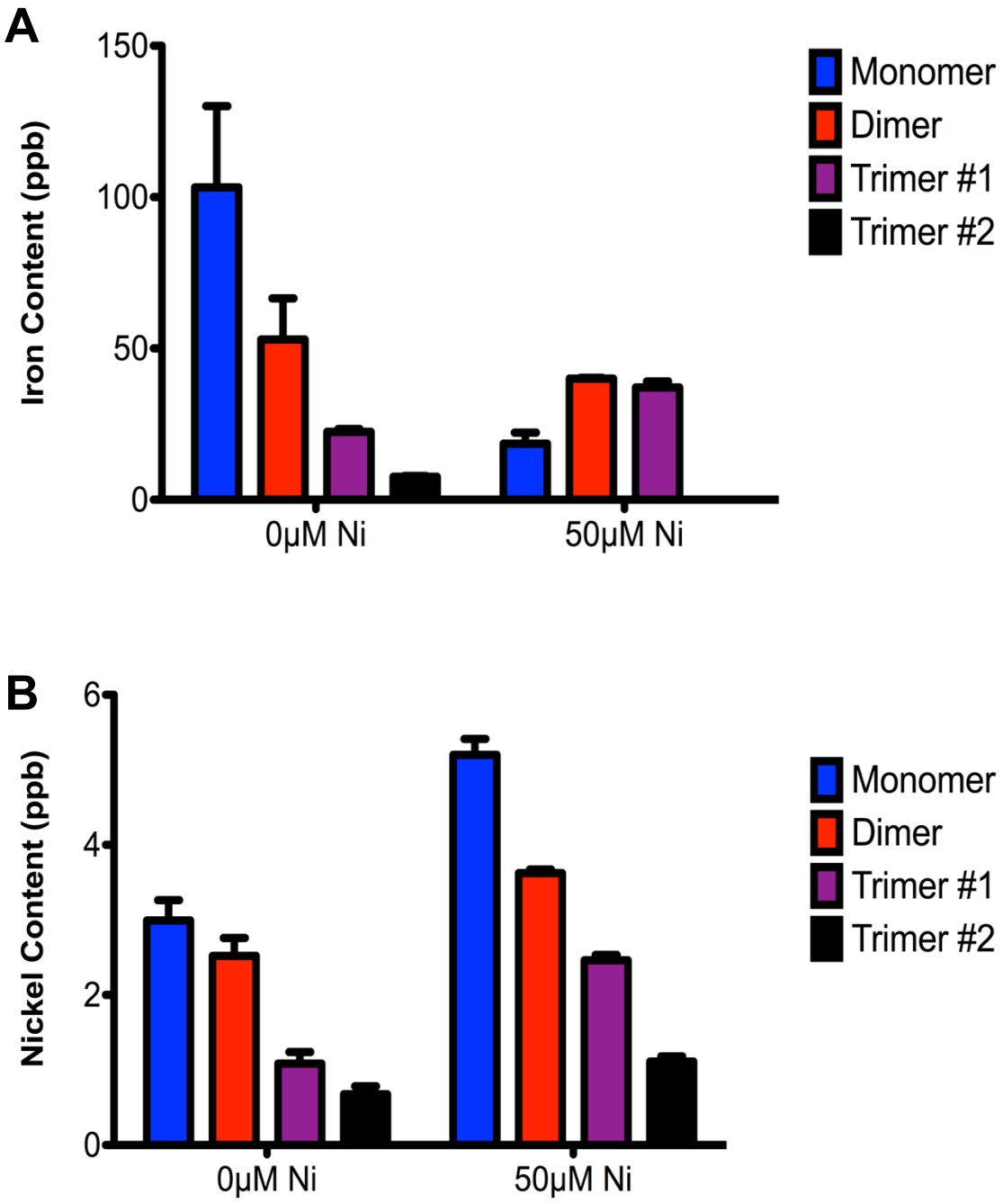

Figure 3.6. Nickel exposure affects metal binding of extracellular siderophores purified by FPLC. Spent media with 50 μM $NiCl_2$ was filtered and enterobactin-related metabolites were separated by FPLC. Monomer (fraction #8), dimer (fraction #11), trimer #1 (fraction #15), and Trimer #2 (fraction #19) were assessed for iron (A) and nickel (B) content using AAS.

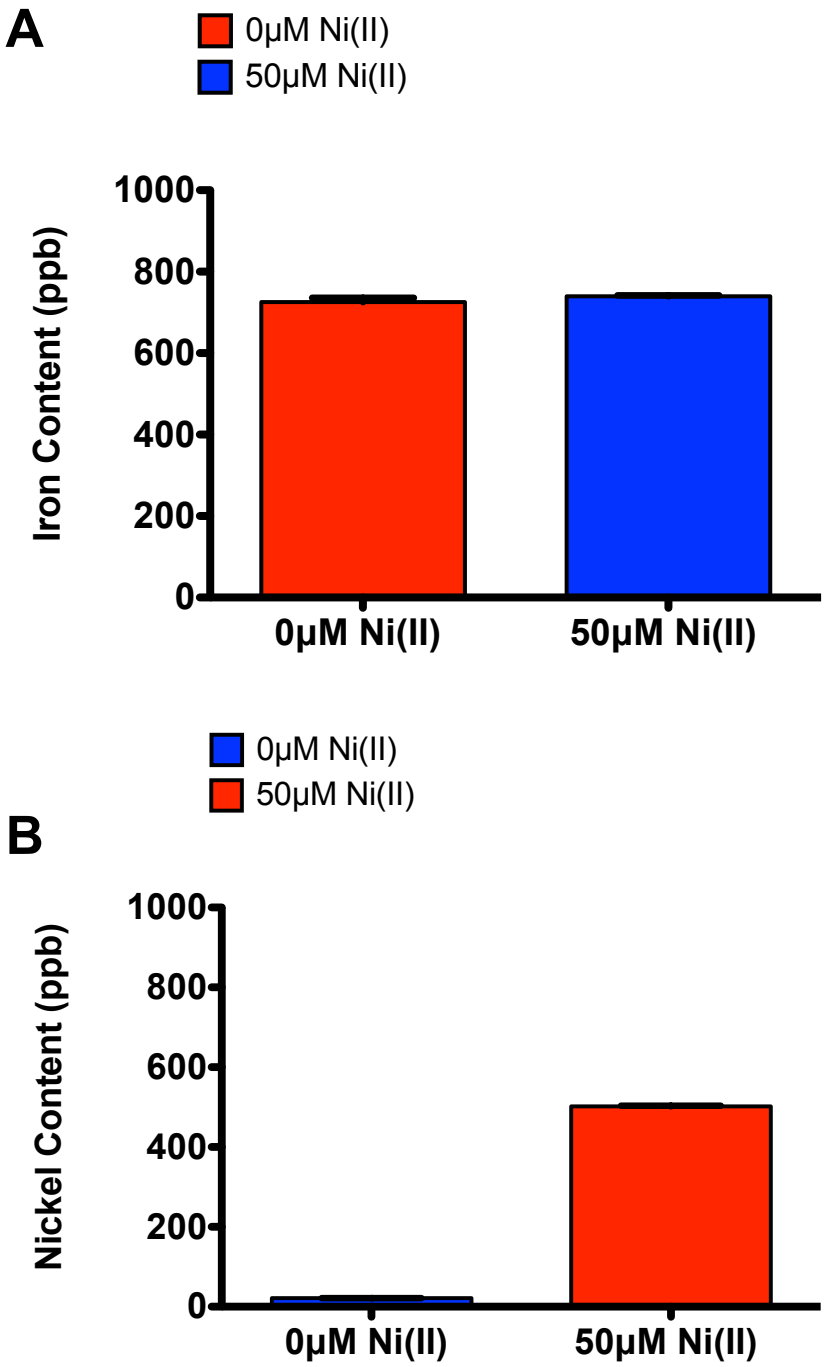

Figure 3.7. Nickel exposure affects metal binding of extracellular siderophores purified by ethyl acetate extraction. Spent media with 50 μM $NiCl_2$ was filtered and enterobactin-related metabolites were separated by ethyl acetate extraction and analyzed for iron (A) or nickel (B) using AAS.

analyzed using atomic absorption spectroscopy (AAS). Upon nickel exposure, enterobactin hydrolysis products bind less iron and more nickel (Figure 3.6). In contrast, when enterobactin is considered, the overall amount of extracellular iron-bound siderophores are not changed in the presence of nickel but the amount of nickel-bound siderophores are still increased (Figure 3.7).

DISCUSSION

Wild-Type MG1655 cells containing the control pWSK29 vector show similar sensitivity to nickel exposure with and without enterobactin export (*entS*) and import (*fepA*) genes (Figure 3.1 A). This is evident by the lag phase duration time and the production of siderophores (Figure 3.1 B, C). In contrast, constitutive expression of enterobactin biosynthesis genes (*entCEBA*) can affect bacterial cell response to nickel exposure (Figure 3.2 A). Deletion of enterobactin exporter gene, *entS*, in combination with constitutive expression of the *ent* operon (*entCEBA*) promotes nickel resistance. Whereas, constitutive expression alone or in combination with Δ*fepA* is not sufficient for a significant amount of rescue. This is supported by a lag phase duration time and extracellular siderophore production (Figure 3.2 B, C). The presence of extracellular enterobactin and trimer #2 is elevated in Δ*fepA* pWSK29 expressing cells (Figure 3.3 A). Similarly, enterobactin and trimer #2 are elevated in pEntCEBA expressing cells (Figure 3.4 B). There are differences observed in the production of monomer, dimer, and trimer #1 (Figure 3.3 and Figure 3.4). The amount of monomer, dimer, and trimer #1 are increased in pEntCEBA expressing cells which may contribute to the partial rescue of the Δ*entS* pEntCEBA strain (Figure 3.3 and Figure 3.4). It is known that 2, 3-dihydroxybenzoic acid is similar to the chemical structure

of monomer and can chelate nickel (Aletras et al., 2001). In general, siderophores have been shown to protect against metal toxicity by chelating the metal (Koh and Henderson, 2015; Braud et al., 2009; Braud et al., 2009; Braud et al., 2010; Chen et al., 1994). In order to address this possibility, siderophores were isolated using two methods and analyzed for metal-binding by AAS. In both cases, it is clear that enterobactin and its hydrolysis products bind iron. However, enterobactin hydrolysis products can also bind nickel (Figure 3.6 and Figure 3.7). Taken together, these findings support the notion that siderophore production promote nickel resistance in *Escherichia coli.*

EntS is the only known exporter for enterobactin; however, it has been previously shown that Δ*ents* bacterial strains can secrete low levels of enterobactin (Caza et al., 2011). Herein, we show that Δ*ents* p*EntCEBA* expressing cells have the highest level of monomer, dimer, and trimer #1 which are most soluble in aqueous solutions (Figure, 3.4) in comparison to organic solvent (Table 3.1). Additionally, the presence of trimer #2 and enterobactin do not assist in rescue. It is also apparent that the monomer, dimer, and trimer #1 preferentially bind and chelate nickel preventing its uptake and providing a protective effect (Figure 3.6). Δ*ents* p*EntCEBA* containing cells are expected to synthesis enterobactin inside the cell without secreting it. Therefore, it is also likely that an accumulation of intracellular enterobactin may play a protective role against nickel toxicity. It is proposed that intracellular siderophores may bind to protein preventing damage from metals (Rasha, 2017; Anahida et al., 2011). Also, siderophores have been shown to promote biofilm formation (Harrison and Bucking, 2009; Marti et al., 2011) leading to antibiotic resistance (Tseng et al., 2013).

References:

1. Aletras, V., Karaliota, A., Kamariotaki, M., Hatzipanayioti, D., and Hadjiliadis, N. (2001) Interaction of Ni(II) with 2, 3-dihydroxybenzoic acid. *Inorganica Chimica Acta* **312:** 151-162.

2. Anahida, S., Yaghmaei, S., and Ghobadinejad, Z. (2011) Heavy metal tolerance of fungi. *Science Iranica* **C18:** 502-508.

3. Arnow, L.E. (1937) Colorimetric determination of the components of 3,4-dihydroxyphenylalanine-tyrosine mixtures. *J Biol Chem* **118:** 531–537.

4. Baranyi, J. and Roberts, T.A. (1994). A dynamic approach to predicting bacterial growth in food. *Int J Food Microbiol* **23:** 277-294.

5. Bleuel, C., Grosse, C., Taudte, N., Scherer, J., Wesenberg, D., Krauss, G.J., Nies, D.H., and Grass, G. (2005) TolC is involved in enterobactin efflux across the outer membrane of *Escherichia coli*. *J Bacteriol* **187:** 6701-6707.

6. Braud, A., Geoffroy, V., Hoegy, F., Mislin, G.L., and Schalk, I.J. (2010) Presence of the siderophores pyoverdine and pyochelin in the extracellular medium reduces toxic metal accumulation in *Psuedomonas aeruginosa* and increases bacterial metal tolerance. *Environ Microbiol Rep* **2:** 419-425.

7. Braud, A., Hannauer, M., Mislin, G.L., and Schalk, I.J. (2009) The Pseudomonas aeruginosa pyochelin-iron uptake pathway and its metal specificity. *J Bacteriol* **191:** 3517-3525.

8. Braud, A., Hoegy, F., Jezequel, K., Lebeau, T., and Schalk IJ. (2009) New insights into the metal specificity of the Pseudomonas aeruginosa pyoverdine-iron uptake pathway. *Environ Microbiol* **11**: 1079-1091.

9. Braun, V. (1995) Energy-coupled transport and signal transduction through the gram negative outer membrane via TonB-ExbB-ExbD-dependent receptor proteins. *FEMS Microbiol Rev* **16:** 295-307.

10. Bravo, A. and Anacona, J.R. (1998) Synthesis and characterization of metal complexes with ampicillin. *J Coordination Chem* **44:** 173-182.

11. Brickman, T.J. and McIntosh, M.A. (1992) Overexpression and purification of ferric enterobactin esterase from *Escherichia coli*. Demonstration of enzymatic hydrolysis of enterobactin and its iron complex. *J Biol Chem* **267:** 12350-12351.

12. Brickman, T.J. and McIntosh, M.A. (1992) Overexpression and purification of ferric enterobactin esterase from *Escherichia coli*. Demonstration of enzymatic hydrolysis of enterobactin and its iron complex. *J Biol Chem* **267:** 12350-12355.

13. Bryce, G.F. and Brot, N. (1975) Enzymic synthesis of the cyclic trimer of 2,3-dihydroxy-N-benzoyl-L-serine in *Escherichia coli*. *Biochemistry* **11:** 1708-1715.

14. Caza, M., Lepine, F., and Dozois, C.M. (2011) Secretion, but not overall synthesis of catecholate siderophores contributes to virulence of extraintestinal pathogenic *Escherichia coli. Mol Microbiol* **80:** 266-282.

15. Chaturvedi, K.S., Hung, C.S., Crowley, J.R., Stapleton, A.E., and Henderson, J.P. (2012) The siderophore yersiniabactin binds copper to protect pathogens during infection. *Nat Chem Biol* **8:** 731-736.

16. Chen, Y., Jurkevitch, E., Bar-Ness, E., and Hadar, Y. (1993) Stability constants of pseudobactin complexes with transition metals. *Soil Sci Soc Am J* **58:** 390-396.

17. Crosa, J.H. and Walsh, C.T. (2002) Genetics and assembly line enzymology of siderophore biosynthesis in bacteria. *Microbiol Mol Biol Rev* **66:** 223-249.

18. Ehmann, D.E., Shaw-Reid, C.A., Losey, H.C., and Walsh, C.T. (2000) The EntF and EntE adenylation domains of *Escherichia coli* enterobactin synthetase: Sequestration and selectivity in acyl-AMP transfers to thiolation domain cosubstrates. *Proc Natl Acad Sci USA* **97:** 2509-2514.

19. Furrer, J.L., Sanders, D.N., Hook-Barnard, I.G., and McIntosh, M.A. (2002) Export of the siderophore enterobactin in *Escherichia coli*: involvement of a 43 kDa membrane exporter. *Mol Microbiol* **44:** 1225-1234.

20. Gehring, A.M., Bradley, K.A., and Walsh, C.T. (1997) Enterobactin biosynthesis in *Escherichia coli*: isochorismate lyase (EntB) is a bifunctional enzyme that is phosphopantetheinylated by EntD and then acylated by EntE using ATP and 2,3-dihydroxybenzoate. *Biochemistry* **36:** 8495-8503.

21. Gehring, A.M., Mori, I., and Walsh, C.T. (1998) Reconstitution and characterization of the *Escherichia coli* enterobactin synthetase from EntB, EntE, and EntF. *Biochemistry* **37:** 2648- 2659.

22. Greenwood, K.T. and Luke, R.K. (1978) Enzymatic hydrolysis of enterochelin and its iron complex in *Escherichia coli* K-12. Properties of enterochelin esterase. J *Biochim Biophys Acta* **525:** 209- 218.

23. Harrison, F. and Bucking, A. (2009) Siderophore production and biofilm formation as linked traits. *ISME J* **3:** 632-634.

24. Itoh, Y., Sugita-Konishi, Y., Kasuga, F., Iwaki, M., Hara-Kudo, Y., Saito, N., Noguchi, Y., Konuma, H., and Kumagai, S. (1998) Enterohemorrhagic

Escherichia coli O157: H7 present in radish sprouts. *Appl Environ Microbiol* **64:** 1532-1535.

25. Koh, E. and Henderson, J.P. (2015) Microbial copper-binding siderophores at the host-pathogen interface. *J Biol Chem* **290:** 18967-18974.

26. Langman, L., Young, I. G., Frost, G. E., Rosenberg, H., and Gibson, F. (1972) Enterochelin system of iron transport in *Escherichia coli*: mutations affecting ferric-enterochelin esterase. *J Bacteriol* **112:** 1142-1149.

27. Larsen, R.A., Foster-Hartnett, D., McIntosh, M.A., and Postle, K. (1997) Regions of *Escherichia coli* TonB and FepA proteins essential for in vivo physical interactions. *J Bacteriol* **179:** 3213-3221.

28. Lin, H., Fischbach, M.A., Liu, D.R., and Walsh, C.T. (2005) In vitro characterization of salmochelin and enterobactin trilactone hydrolases IroD, IroE, and Fes. *J Am Chem Soc* **10:** 11075-11084.

29. Ma, L., and Payne, S.M. (2012) AhpC is required for optimal production of enterobactin by *Escherichia coli.* *J Bacteriol* **194:** 6748-6757.

30. Marti, S., Chabane, Y.N., Alexandre, S., Coquet, L., Vila, J., Jouenne, T., and De, E. (2011) *PLOS One* 6(10): e26030.

31. Miethke, M. and Marahiel, M.A. (2007) Siderophore-based iron acquisition and pathogen control. *Microbiol Mol Biol Rev* **71:** 413-451.

32. Mukherjee, G. and Ghosh, T. (1995) Metal ion interaction with penicillins – Part VII: Mixed-ligand complex formation of cobalt (II), nickel(II), copper(II), and zinc(II) with ampicillin and nucleic bases. *J Inorg Biochem* **59:** 827-833.

33. O'Brien, I.G. and Gibson, F. (1970) The structure of enterochelin and related 2,3-dihydroxy-n-benzoylserine conjugates from *Escherichia coli*. *Biochim Biophys Acta* **215:** 393-402.

34. Rasha, F.M. (2017) Intracellular siderophore detection in an Egyptian, cobalt-treated *F. solani* isolate using SEM-EDX with reference to its tolerance. *Polish J Microbiol* **66:** 235-243.

35. Shaw-Reid, C.A., Kelleher, N.L., Losey, H.C., Gehring, A.M., Berg, C., and Walsh, C.T. (1999) Assembly line enzymology by multimodular nonribosomal peptide synthetases: the thioesterase domain of *E. coli* EntF catalyzes both elongation and cyclolactonization. *Chem Biol* **6**: 385-400.

36. Solomon, E.B., Yaron, S., and Matthews, K.R. (2002) Transmission of *Escherichia coli* O157:H7 from contaminated manure and irrigation water to lettuce plant tissue and its subsequent internalization. *Appl Environ Microbiol* **68:** 397-400.

37. Tseng, B.S., Zhang, W., Harrison, J.J., Quach, T.P., Song, J.L., Penterman, J., Singh, P.K., Chopp, D.L., Packman, A.I., and Parsek, M.R. (2013) The extracellular matrix protects *Pseudomonas aeruginosa* biofilms by limiting the penetration of tobramycin. *Environ Microbiol* **15:** 2865-2878.

38. Van Elsas, J.D., Semenov, A.V., Costa, R., and Trevors, J.T. (2011) Survival of *Escherichia coli* in the environment: fundamental and public health aspects. *ISME J* **5:** 173-183.

39. Walsh, C.T., Liu, J., Rusnak, F., and Sakaitani, M. (1990) Molecular studies on enzymes in chorismate metabolism and the enterobactin biosynthetic pathway. *Chem Rev* **90:** 1105-1129.

40. Winklemann, G., Cansier, A., Beck, W., and Jung, G. (1994) HPLC separation of enterobactin and linear 2,3-dihydroxybenzoylserine derivatives: a study on mutants of *Escherichia coli* defective in regulation (*fur*), esterase (*fes*), and transport (*fepA*). *Biometals* **7:** 149-154.

CHAPTER 4

IDENTIFYING FUNTIONAL REDUNDANCIES IN A-TYPE CARRIER PROTEINS IN *E. COLI*

ABSTRACT

E. coli A-type carrier proteins have been phylogenomically and genetically characterized. However, the biochemical interactions among ATCs have not been fully studied. Herein, we characterize the as-purified and reconstituted holo *E. coli* A-type carrier proteins, ErpA, IscA, and SufA. Using iron and sulfide analysis, circular dichroism, and EPR it has been confirmed that these proteins can coordinate a [2Fe-2S] cluster. IscA and SufA can transfer their clusters to other A-type carrier proteins or receive a cluster from the scaffold protein $SufBC_2D$. The percentage and rate of transfer support that IscA may transfer its cluster to ErpA *in vivo.* Although, the percentage of transfer from SufA to ErpA is lower, the transfer occurs quickly. ErpA can also transfer its cluster to IscA, but the rate and percentage of this reaction seems unlikely *in vivo.*

INTRODUCTION

A-Type carriers (ATCs) are a class of proteins that have unclear biochemical and cellular functions (Vinella et al., 2009). Phylogenomic studies show that there are three A-type carrier proteins in *E. coli* that have evolved into two subfamilies. The first

subfamily (ATC-I) are thought to transfer Fe-S clusters to apoproteins while the second (ATC-II) receives its clusters from a scaffold protein (Vinella et al., 2009). ErpA is classified as ATC-I. IscA and SufA are designated in the ATC-II subfamily. These three proteins structurally similar and share 30% amino acid sequence identity (Figure 4.1; Cupp-Vickery et al., 2004; Wada et al., 2005) and may have overlapping functions in vivo. Genetic studies show that the deletion of *iscA* and *sufA* genes is synthetically lethal in *E. coli* under aerobic conditions, but that strain is viable under anaerobic conditions. A single deletion of the *erpA* gene also results in lethality under aerobic conditions and viability under anaerobic conditions (Loiseau et al., 2007). ErpA has also been shown to interact with IscA and SufA (Py et al., 2018). These results suggest functional redundancy amongst the ATC-II proteins (Figure 4.2; Vinella et al., 2009). However, there is little to no biochemical evidence supporting this model. Our goal in this work is to biochemically characterize apo and holo forms of the three *E. coli* ATC proteins and determine whether *in vitro* functional redundancies occur.

MATERIALS AND METHODS

Protein expression and purification

ErpA was amplified from MG1655 chromosomal DNA as a template using the forward 5'-TAAACATATGAGTGATGACGTAGCACTGCCGC-3' and reverse 5'-ATAGGGATCCTTAGATACTAAAGGAAGAACCGCAA-3' primers. PCR products were digested with *BamHI* and *NdeI* and cloned into the corresponding sites of pET21a (Novagen). The nucleotide sequence of the plasmid insert was confirmed by DNA

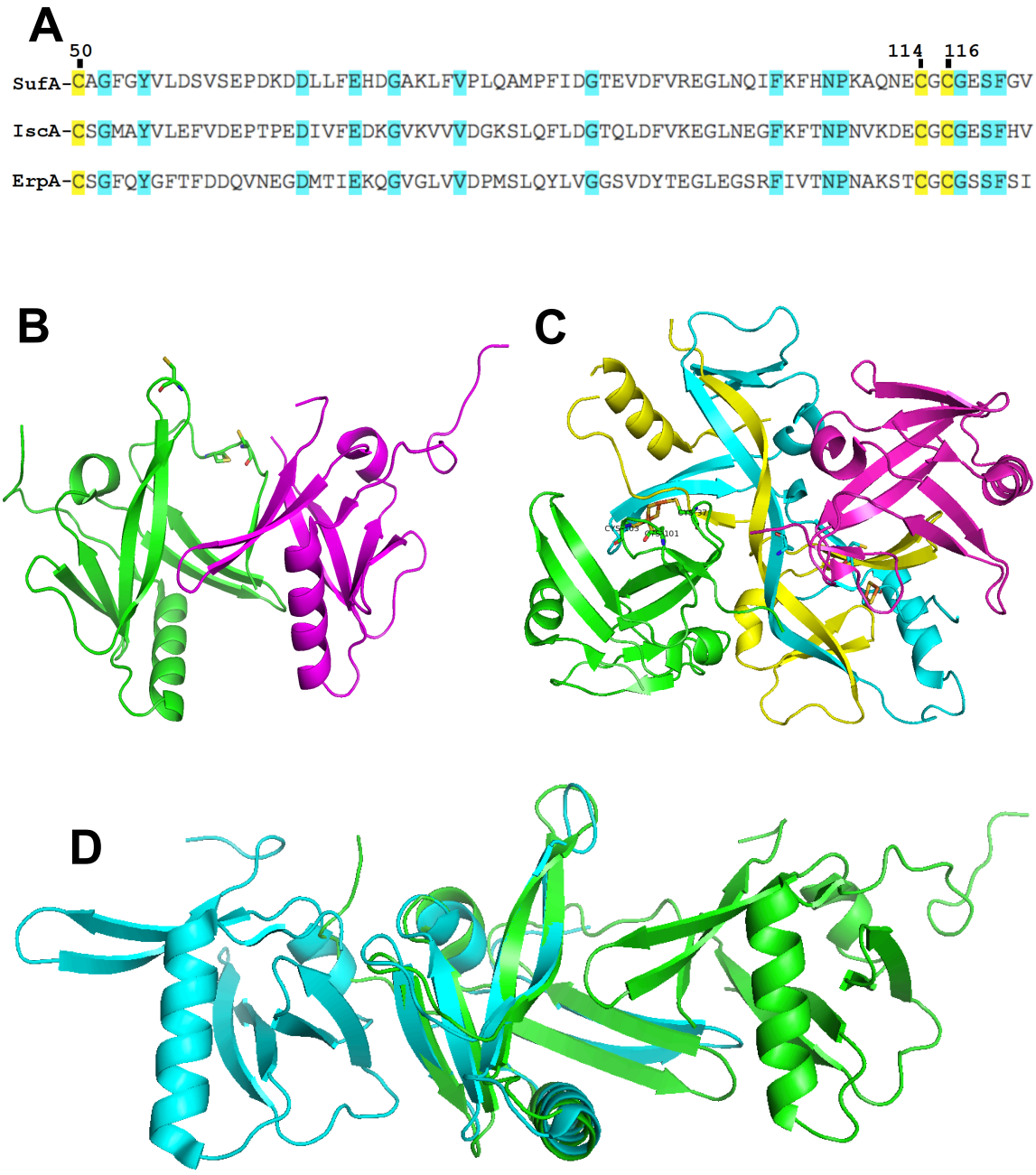

Figure 4.1 *E. coli* A-type carrier amino acid sequences and ribbon diagrams. (A) Sequence alignment of *Escherichia coli* A-type carrier proteins. Conserved cysteines and identical residues are highlighted in yellow and blue, respectively. (B) Ribbon diagram of the *E. coli* SufA dimer. (C) Ribbon diagram of *E. coli* IscA tetramer. (D) Ribbon diagram overlay of *E. coli* SufA (blue) and IscA (green) monomers overlaid.

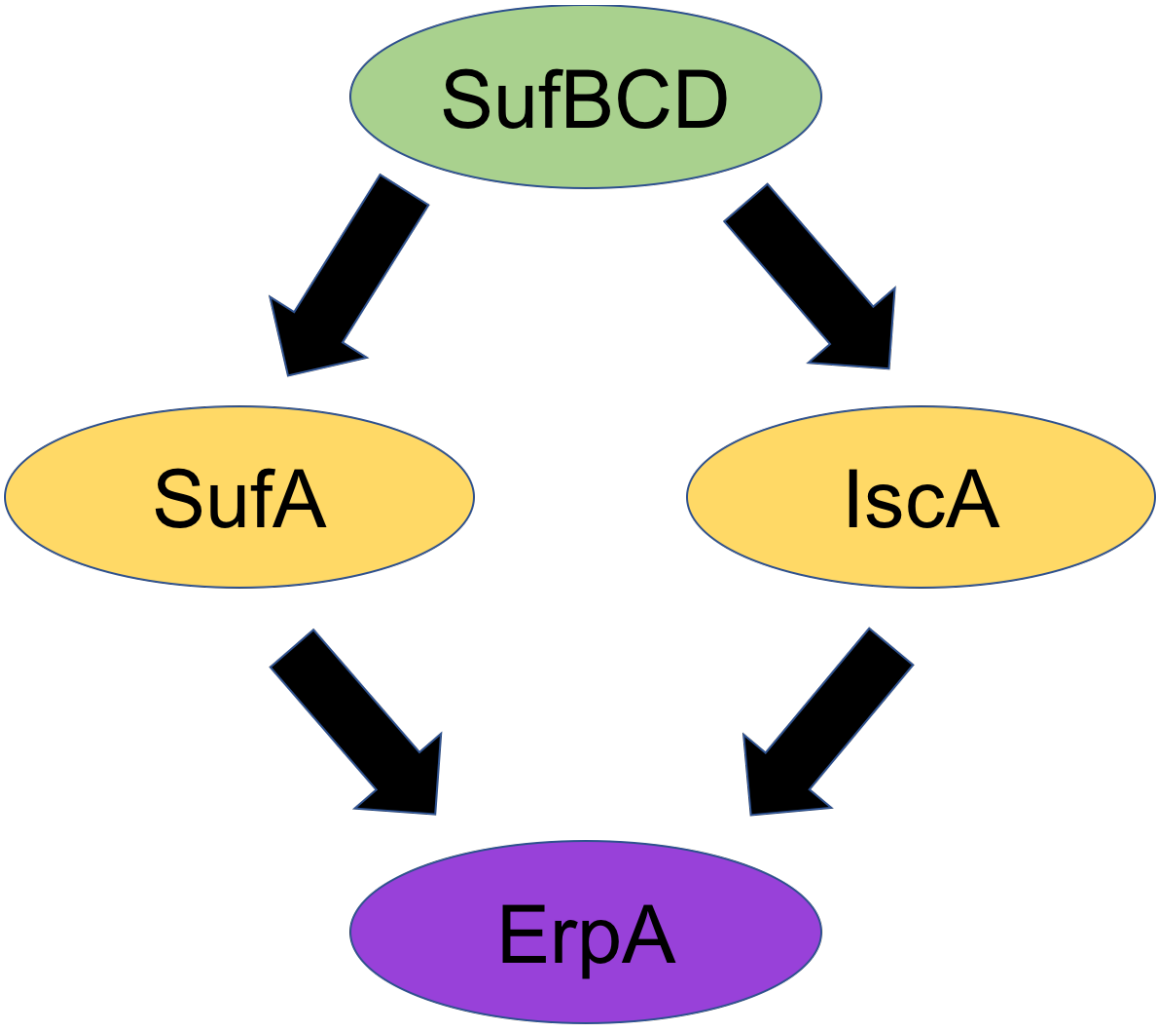

Figure 4.2 Proposed directionality model of Fe-S cluster trafficking amongst $SufBC_2D$ (green: the scaffold protein), SufA, IscA (yellow: Type II A-type protein), and ErpA (purple: Type I A-type protein).

sequencing. The pET21a vector containing the *erpA* gene was induced via an inducible IPTG promoter with 500 μM IPTG in order to over-express ErpA in BL21(DE3) cells. Four liters of cells were cultured at 37 °C to an OD 600 nm of 0.6 to 0.8 before IPTG induction at 18°C overnight. Cells were collected via centrifugation and stored at -80 °C. Cell pellets were re-suspended in 25 mM Tris-HCl, pH 7.5, 10 mM βME, 100 mM NaCl and 1 mM phenylmethanesulfonyl fluoride (PMSF) then lysed via sonication. Cellular debris was mixed with streptomycin sulfate and centrifuged at 16,000 rpm at 4 °C. Cleared cell lysate was loaded onto a Q Sepharose ionic exchange column pre-equilibrated with 25 mM Tris-HCl, pH 7.5, 10 mM βME, and 100 mM sodium chloride (NaCl). ErpA was eluted between 0.35 M to 0.48 M NaCl using a linear gradient starting with Buffer A (25 mM Tris-HCl, pH 7.5, 10 mM βME) to Buffer B (25 mM Tris-HCl, pH 7.5, 10 mM βME, and 1 M NaCl). Eluted protein was loaded onto a Phenyl FF column pre-equilibrated with 25 mM Tris-HCl, pH 7.5, 10 mM βME, and 1 M NH_4SO_4. ErpA was eluted between 0.42 M to 0 M NH_4SO_4 using a linear gradient starting from 1 M NH_4SO_4 to 0 M NH_4SO_4. ErpA eluted at 0.27 M NH_4SO_4 of Buffer B (25 mM Tris-HCl, pH 7.5, 10 mM βME, and 0 M NH_4SO_4). Eluted protein was concentrated using Millipore centrifugal devices and loaded onto the Superdex 75 size exclusion column. Pure protein eluted at 19.0 kDa, was concentrated, and stored at -80 °C.

IscA was amplified from MG1655 chromosomal DNA as a template using the forward 5'-TAAACATATGTCGATTACACTGAGCGACAGTG-3' and reverse 5'-ATAGGGATCCTCAAACGTGGAAGCTTTCGCCGCAA-3' primers. PCR products were digested with *BamHI* and *NdeI* and cloned into the corresponding sites of pET21a (Novagen). The nucleotide sequence of the plasmid insert was confirmed by DNA

sequencing. The pET21a vector containing the *iscA* gene was induced via an inducible IPTG promoter with 500 µM IPTG in order to over-express IscA in BL21(DE3) cells. Four liters of cells were cultured at 37 °C to an OD 600 nm of 0.6 to 0.8 before IPTG induction at 18 °C overnight. Cells were collected via centrifugation and stored at -80 °C. Cell pellets were re-suspended in 25 mM Tris-HCl, pH 7.5, 10 mM βME, 100 mM NaCl and 1 mM phenylmethanesulfonyl fluoride (PMSF) then lysed via sonication. Cellular debris was mixed with streptomycin sulfate and centrifuged at 16,000 rpm at 4 °C. Cleared cell lysate was loaded onto a Q Sepharose ion exchange column pre-equilibrated with 25 mM Tris-HCl, pH 7.5, 10 mM βME, and 100 mM NaCl. IscA eluted at 0.26 M to 0.54 M NaCl using a linear gradient starting with Buffer A (25 mM Tris-HCl, pH 7.5, 10 mM βME) to Buffer B (25 mM Tris-HCl, pH 7.5, 10 mM βME, and 1 M NaCl). Eluted protein was loaded onto a Phenyl FF column pre-equilibrated with 25 mM Tris-HCl, pH 7.5, 10 mM βME, and 1 M NH_4SO_4. IscA eluted at 0.42 M to 0 M NH_4SO_4 using a linear gradient starting from 1 M NaCl to 0 M NH_4SO_4. Eluted protein was concentrated using Millipore centrifugal devices and loaded onto the Superdex 75 size exclusion column. Pure protein eluted at 33.9 kDa, was concentrated, and stored at -80 °C.

SufA was amplified from MG1655 chromosomal DNA as a template using the forward 5'-TAAACATATGGACATGCATTCAGGAACCTTTA-3' and reverse 5'-ATAGGGATCCCTATACCCCAAAGCTTTCGCCACAG-3' primers. PCR products were digested with *BamHI* and *NdeI* and cloned into the corresponding sites of pET21a (Novagen). The nucleotide sequence of the plasmid insert was confirmed by DNA sequencing. The pET21a vector containing the *sufA* gene was induced via an inducible IPTG promoter with 500 µM IPTG in order to over-express SufA in BL21(DE3) cells.

Four liters of cells were cultured at 37 °C to an OD 600 nm of 0.6 to 0.8 before IPTG induction at 18 °C overnight. Cells were collected via centrifugation and stored at -80 °C. Cell pellets were resuspended in 25 mM Tris-HCl, pH 7.5, 10mM βME, 100 mM NaCl and 1 mM phenylmethanesulfonyl fluoride (PMSF) then lysed via sonication. Cellular debris was mixed with streptomycin sulfate and centrifuged at 16,000 rpm at 4 °C. Cleared cell lysate was loaded onto a Q Sepharose ion exchange column pre-equilibrated with 25 mM Tris-HCl, pH 7.5, 10 mM βME, and 100 mM NaCl. SufA eluted between 0.26 M to 0.42 M using a linear gradient starting with Buffer A (25 mM Tris-HCl, pH 7.5, 10 mM βME) to Buffer B (25 mM Tris-HCL, pH 7.5, 10 mM βME, and 1 M NaCl). Eluted protein was loaded onto a Phenyl FF column pre-equilibrated with 25 mM Tris-HCl, pH 7.5, 10 mM βME, and 1 M NH_4SO_4. SufA eluted at 0.42 M to 0 M NH_4SO_4 using a linear gradient starting from 1 M NaCl to 0 M NH_4SO_4. Eluted protein was concentrated using Millipore centrifugal devices and loaded onto the Superdex 75 size exclusion column. Pure protein eluted at 28.2 kDa, was concentrated, and stored at -80 °C.

The pBADmycHisC vector containing the *sufABCDSE* operon (Outten et al., 2003) was induced via an inducible arabinose promoter with 0.2% arabinose in order to over-express $SufBC_2D$ in BL21(DE3) cells and purified as previously described (Layer et al., 2007). Four liters of cells were cultured at 37 °C to an OD 600 nm of 0.6 to 0.8 before arabinose induction at 18 °C overnight. Cells were collected via centrifugation and stored at -80 °C. Cell pellets were re-suspended in 25 mM Tris-HCl, pH 7.5, 10 mM βME, 100 mM NaCl and 1 mM phenylmethanesulfonyl fluoride (PMSF) then lysed via sonication. Cellular debris was mixed with streptomycin sulfate and centrifuged at 16,000 rpm at 4 °C. Cleared cell lysate was loaded onto a Phenyl FF column pre-equilibrated with 25 mM Tris-

HCl, pH 7.5, 10 mM βME, and 1 M (ammonium sulfate) NH_4SO_4. $SufBC_2D$ was eluted using a linear gradient starting from 1 M NH_4SO_4 to 0 M NH_4SO_4. Eluted protein was diluted and then loaded onto a Q Sepharose ion exchange column pre-equilibrated with 25 mM Tris-HCl, pH 7.5, 10 mM βME, and 100 mM NaCl. $SufBC_2D$ was eluted using a linear gradient starting with Buffer A (25 mM Tris-HCl, pH 7.5, 10 mM βME) to Buffer B (25 mM Tris-HCL, pH 7.5, 10 mM βME, and 1 M NaCl). Eluted protein was concentrated and loaded onto a the Superdex 200 size exclusion column with 25mM Tris-HCl, pH 7.5, 10mM βME, 100mM NaCl buffer. Pure protein was concentrated and stored at -80 °C. Protein standards (GE Healthcare) were also re-suspended in 25 mM Tris-HCl, pH 7.5, 10 mM βME, 100 mM NaCl buffer and run using the Superdex 200 size exclusion column.

In vitro Reconstitution of A-Type Carrier Proteins

Apo-proteins or proteins without an Fe-S cluster were treated with a 50-fold molar ratio of EDTA and 20-fold molar ratio of ferricyanide between 10 to 60 minutes on ice followed by desalting (Kennedy and Beinert, 1988). In order to form a holo-protein or a protein that contains an Fe-S cluster, apo-proteins (100 µM) were incubated in the anaerobic chamber in 500 µl (total volume) of reconstitution buffer (25 mM Tris-HCl, pH 7.5, 10 mM βME, and 100 mM NaCl) plus 5 mM DTT (dithiothreitol). Then a catalytic amount of SufS and SufE (4 µM) was added before adding 8-fold molar excess of ferrous ammonium sulfate and a 10-fold molar excess of L-cysteine to protein concentration. Over 30 minutes to an hour, cluster formation was monitored by UV-Visible absorption spectroscopy. The mixture was loaded onto an anaerobic 1 ml Q FF column pre-

equilibrated with 25 mM Tris-HCl, pH 7.5, 10 mM βME, and 0mM to 100 mM NaCl (without DTT). The column was washed with anaerobic reconstitution buffer before elution with 25 mM Tris-HCl, pH 7.5, 10 mM βME, and 500 mM to 1M NaCl (without DTT).

Iron content was determined using the ferrozine assay (Riemer et al., 2004). Size exclusion measurements were calibrated using known molecular weight determination standards and calculated using an equation obtained by the standard curve. UV-visible absorption spectra were recorded using a Beckman DU-800 spectrophotometer. CD spectra were recorded under anaerobic conditions using a Jasco J-815 spectropolarimeter (Jasco, Hachioji, Japan) using a 1cm cuvette.

X-band EPR samples (300 µl total volume) containing 300 to 600 µM total iron were reduced with 5 mM DTT (final concentration) for approximately 10 minutes before storing sample in liquid nitrogen. Spectra were recorded using a Bruker EMX plus spectrometer (~9.4 GHz, Bruker, Billerica, MA) equipped with an ESR900 continuous flow cryostat (Oxford Instruments, Concord, MA) at 4 K, 35 K, and 70 K. The amount of spin for each sample was calculated under non-saturating conditions at 35 K using double integration values of the samples and 1mM Cu EDTA standard.

Fe-S Cluster Transfer Monitored by Circular Dichroism

As a control, the appropriate holo-protein (donor) alone (80 µM iron content, 40 µM cluster) was scanned at 0- and 1-hour at 25 °C in a 1 cm path length anaerobic cuvette using a JASCO J-815 spectrometer. For transfer reactions, 80 µM of apo-protein (acceptor) was added to the holo-protein donor (80 µM iron content, 40 µM cluster) at a total volume

of 300 µl in 25 mM Tris-HCl (final salt concentration between 100 to 200 mM NaCl). The Fe-S cluster transfer was monitored by CD every 10 minutes for 1 hour at 25 °C in a 1 cm path length anaerobic cuvette using a JASCO J-815 spectrometer. These same conditions were used for all combinations of holo-donor and apo-acceptor proteins shown in the Results.

Fe-S Cluster Formation Monitored by Circular Dichroism with and without $SufBC_2D$

As a control, apo-IscA or apo-SufA alone (200 µM protein) was scanned every 5 minutes at 25 °C in a 1 cm path length anaerobic cuvette using a JASCO J-815 spectrometer. $SufBC_2D$ (8 µM protein) was added to either apo-IscA or apo-SufA (200 µM protein) at a total volume of 300 µl in 25 mM Tris-HCl. The formation of Fe-S cluster onto either IscA or SufA reached completion after 10 minutes.

RESULTS

Oligomeric State of Purified A-Type carrier proteins in E. coli

A-Type carrier proteins have Fe-S clusters that are semi-stable in air and partially maintained during aerobic purification. The ATCs also have distinct UV-visible and CD (circular dichroism) spectra in the 300 nm to 600 nm range that represents the Fe-S cluster coordination environment of the individual proteins. Spectra were recorded for all proteins after aerobic purification (Figure 4.3). Iron content of as-purified proteins was determined by the ferrozine assay (Table 4.1). The as-purified CD spectra of ErpA differs from that of IscA and SufA by forming a peak at 345 nm. IscA has less distinct features compared

to ErpA and SufA. However, the 330 nm to 370 nm range shows a pronounced decrease in the CD spectra in comparison to ErpA and SufA (Figure 4.3 B).

The monomeric weight of A-type carrier proteins can be theoretically calculated using the appropriate amino acid sequence. The crystal structure and Fe-S cluster coordination chemistry shows that oligomeric protein states exist in vivo. Size-exclusion chromatography using protein standards of known molecular weight can be used in order to determine the oligomeric state of as-purified ErpA, IscA, and SufA. According to the standard curve ($R^2 = 0.99158$) generated by the calibration standards, ErpA purifies as a 19.0 kilodalton dimeric complex, IscA as a 33.9 trimeric complex, and SufA as a 28.2 kilodalton dimeric complex (Figure 4.4; Table 4.1). The theoretical monomeric mass of ErpA, IscA, and SufA is 12.1, 11.6, and 13.3 kilodaltons (kD).

Real-time reconstitution monitoring of E. coli ATCs

Due to some loss of Fe-S cluster content during aerobic purification, A-type carrier proteins were reconstituted by incubation with ferrous ammonium sulfate, L-cysteine, dithiothreitol, SufS, and SufE under anaerobic conditions. The UV-visible absorption spectra were monitored over time during the reconstitution of ErpA, IscA, and SufA (Figure 4.5). The reconstitution reaction of ErpA shows the formation of thio-ferrate or iron-sulfur chain byproducts. This side reaction can be monitored by an increase in absorption at 600 nm. ErpA reconstitution reaches completion after approximately 30 minutes (Figure 4.5 A). Similarly, IscA and SufA reconstitution reactions reach completion after approximately 30 minutes and then begin to form thioferrate byproducts (Figure 4.5 A). The reactions require purification using an ionic exchange Q-Sepharose

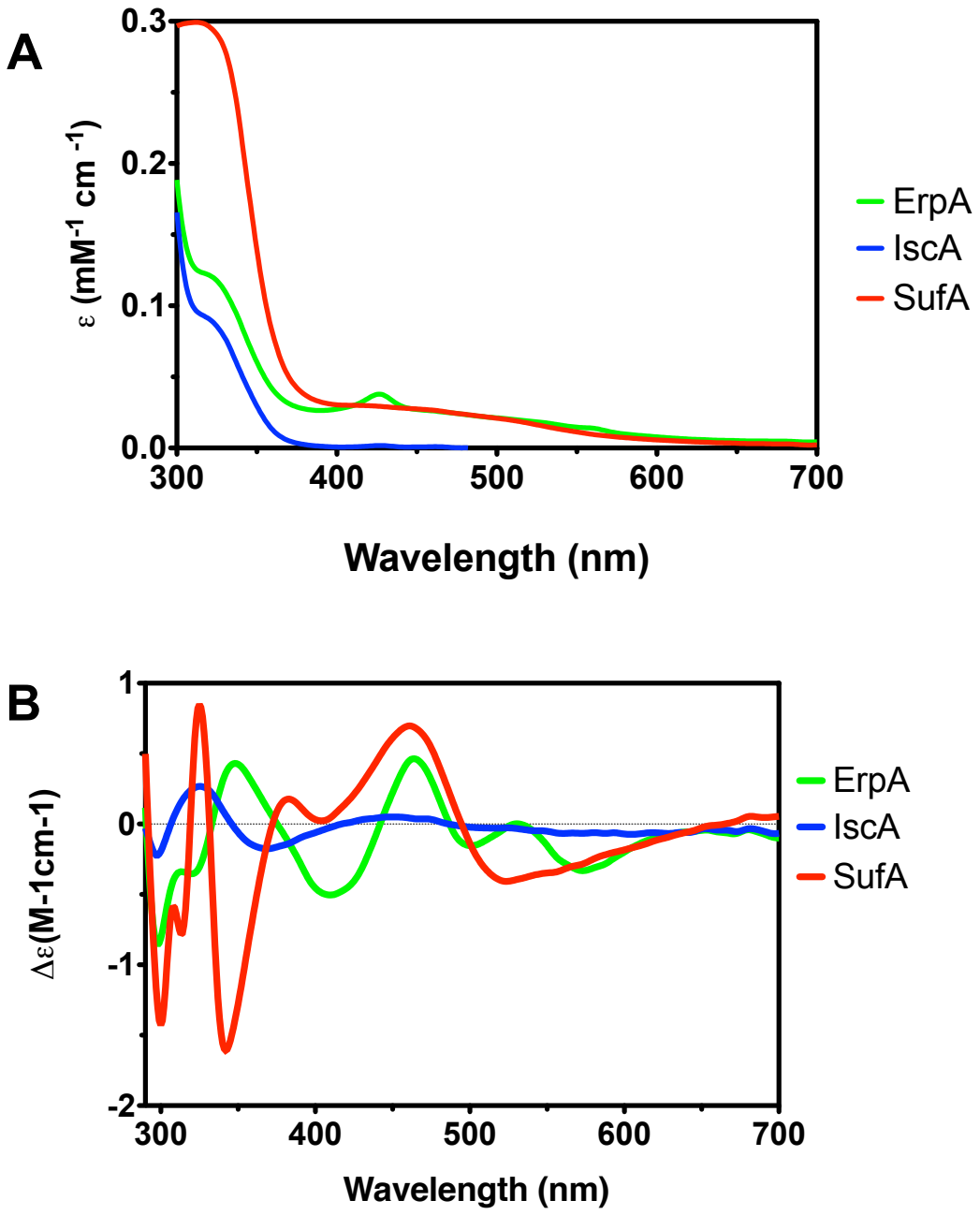

Figure 4.3 (A) Comparison of UV-visible absorption and (B) CD spectra of as-purified ErpA, IscA, and SufA.

Table 4.1 Biochemical properties of ErpA, IscA, and SufA.

	As-purified ErpA	As-purified IscA	As-purified SufA
Fe content	0.4	0.3	0.3
Complex	Dimer	Trimer	Dimer
Theoretical (Da)	12,100	11,556	13,300
Gel filtration (kD)	19.0	33.9	28.2

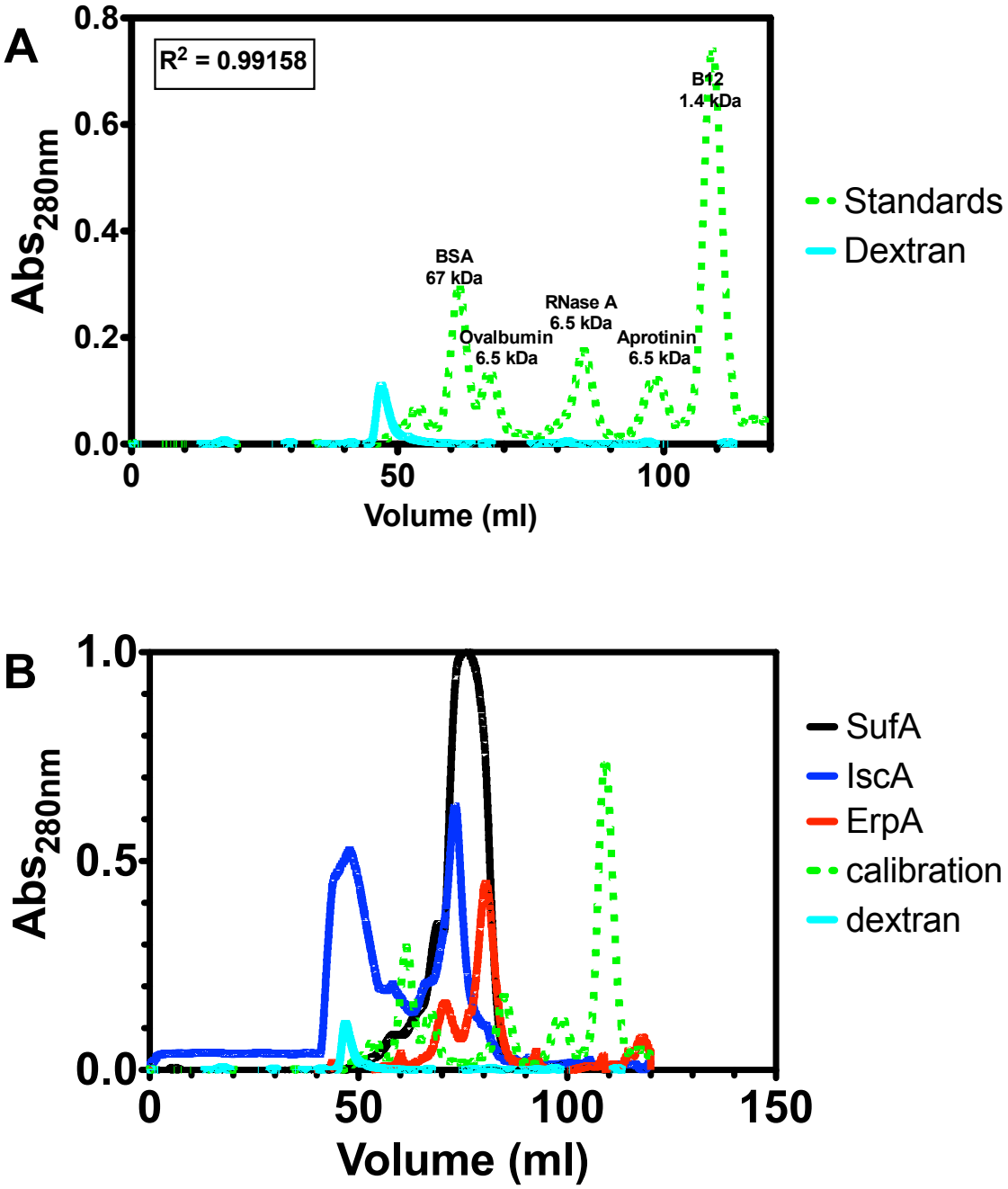

Figure 4.4 Size-exclusion chromatography (SEC) of Superdex 75 (A) calibration standard proteins and (B) A-type carrier proteins with standards.

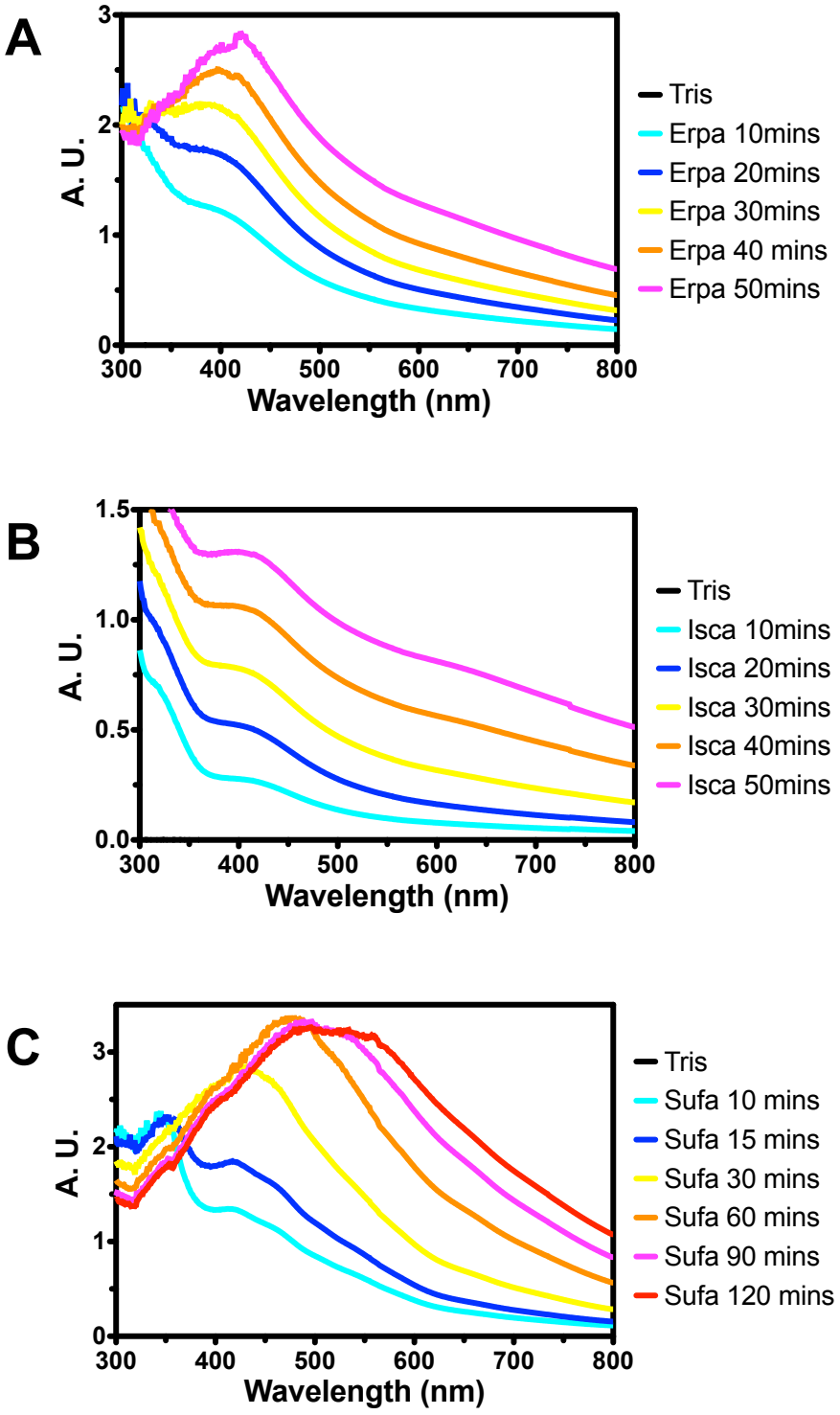

Figure 4.5 UV-visible monitored Fe-S cluster formation of (A) ErpA, (B) IscA, and (C) SufA.

column in order remove byproducts from reconstituted holo-protein.

Characterization of reconstituted A-Type carrier proteins

The UV-visible spectra of purified holo-ErpA and holo-SufA produces an intense shoulder peak at 330 nm and a peak at 420 nm which is indicative of a [2Fe-2S] cluster (Figure 4.6 A). The CD spectra of reconstituted and purified holo-ErpA, holo-IscA, and holo-SufA are more intense than the as-purified samples suggesting that proteins contain a higher amount of iron in comparison (Figure 4.6 B). After removing byproducts, the iron per monomer of holo-ErpA, holo-IscA, and holo-SufA increased to 1.88, 1.40, and 1.32, respectively. The stability of each protein was observed using CD after 1 hour under anaerobic conditions. All of the holo-ATC proteins showed little to no change in their CD spectra indicating the holo-proteins are stable enough at room temperature in order to proceed with further studies (Figure 4.7)

Electron paramagnetic resonance (EPR) can be used to determine the cluster type assembled onto iron-containing proteins such as the holo-form of A-type carrier proteins. At a higher temperature of 70 K, ErpA, IscA, and SufA have more distinct features whereas the EPR spectra is saturated at 4 K. These features are indicative of a $[2Fe\text{-}2S]^{1+}$ reduced cluster which has a slower relaxation time in comparison to a [4Fe-4S] cluster (Figure 4.8; Figure 4.9; Figure 4.10). The g-values of ErpA at 2.02, 2.00, and 1.96 produce an axial shape EPR spectra (Figure 4.8). The EPR spectra of IscA is also axial with g-values at 2.02, 2.00, and 1.97. The g-values produced by the rhombic EPR spectra of SufA are 2.02, 2.00, 1.92 and 2.01, 2.00, 1.96. Using the double integration values of a non-saturated 1

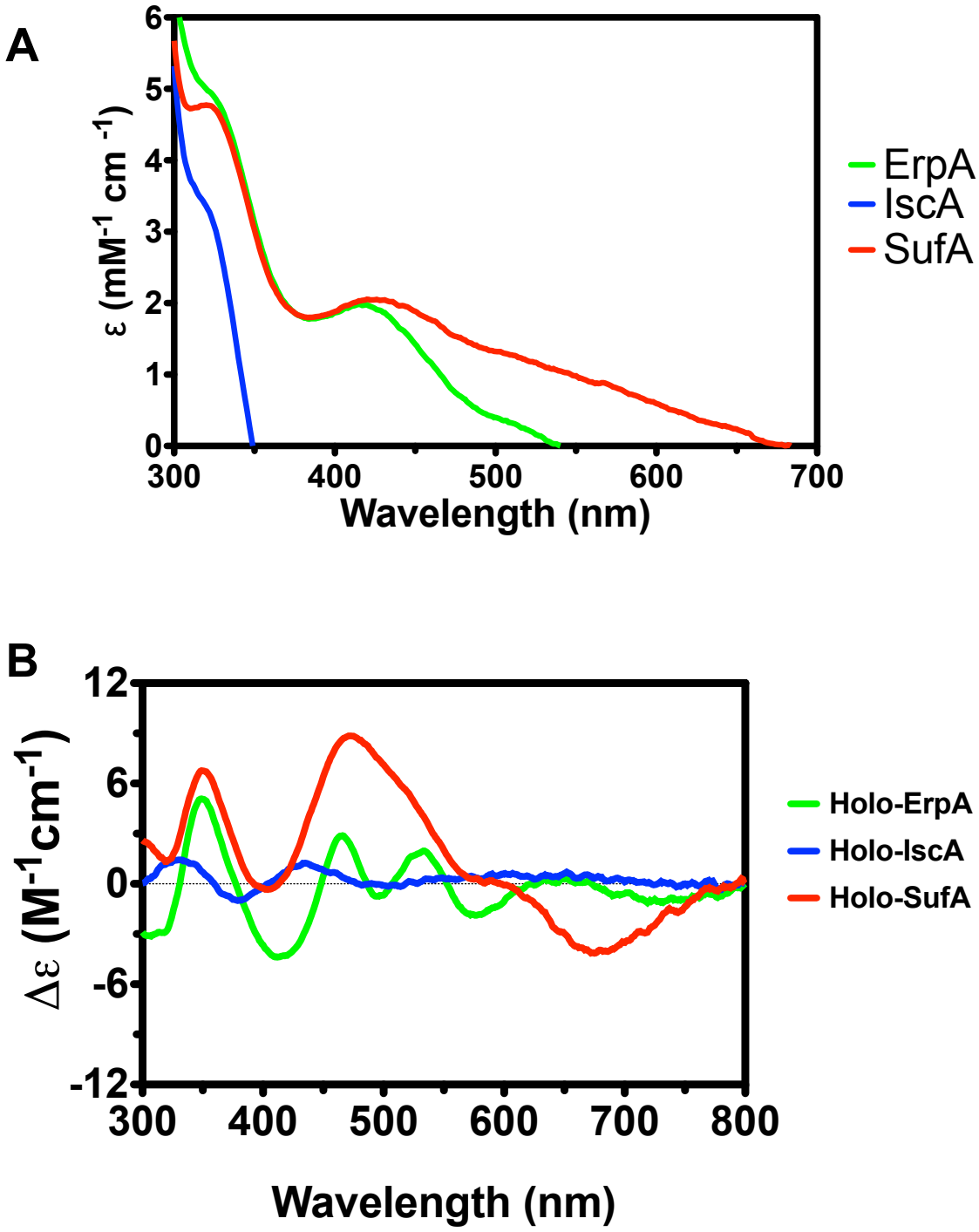

Figure 4.6 (A) Comparison of UV-visible absorption and (B) CD spectra of purified reconstituted ErpA, IscA, and SufA.

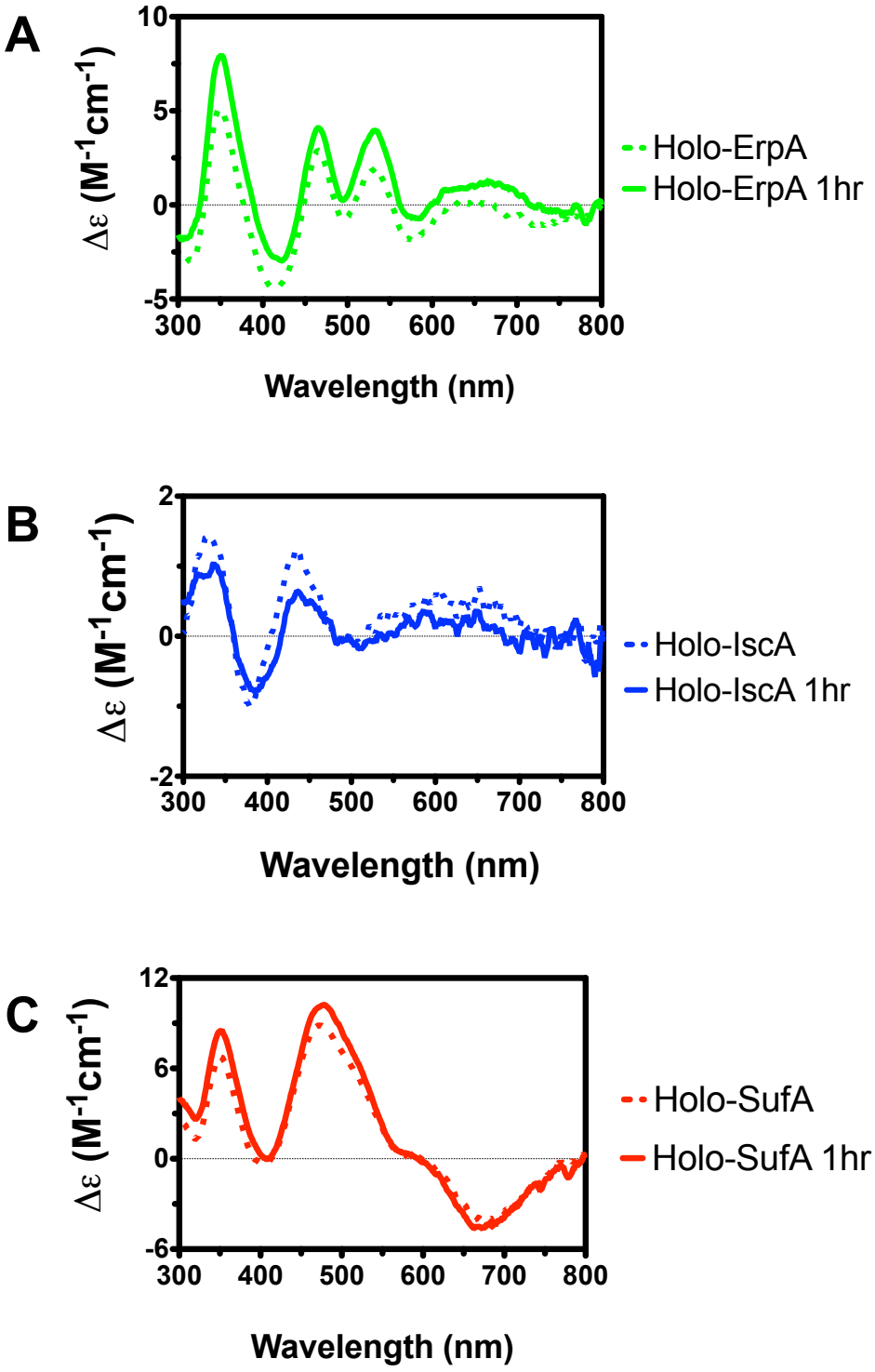

Figure 4.7 CD-monitored stability spectra of pure reconstituted (A) ErpA, (B) IscA, and (C) SufA.

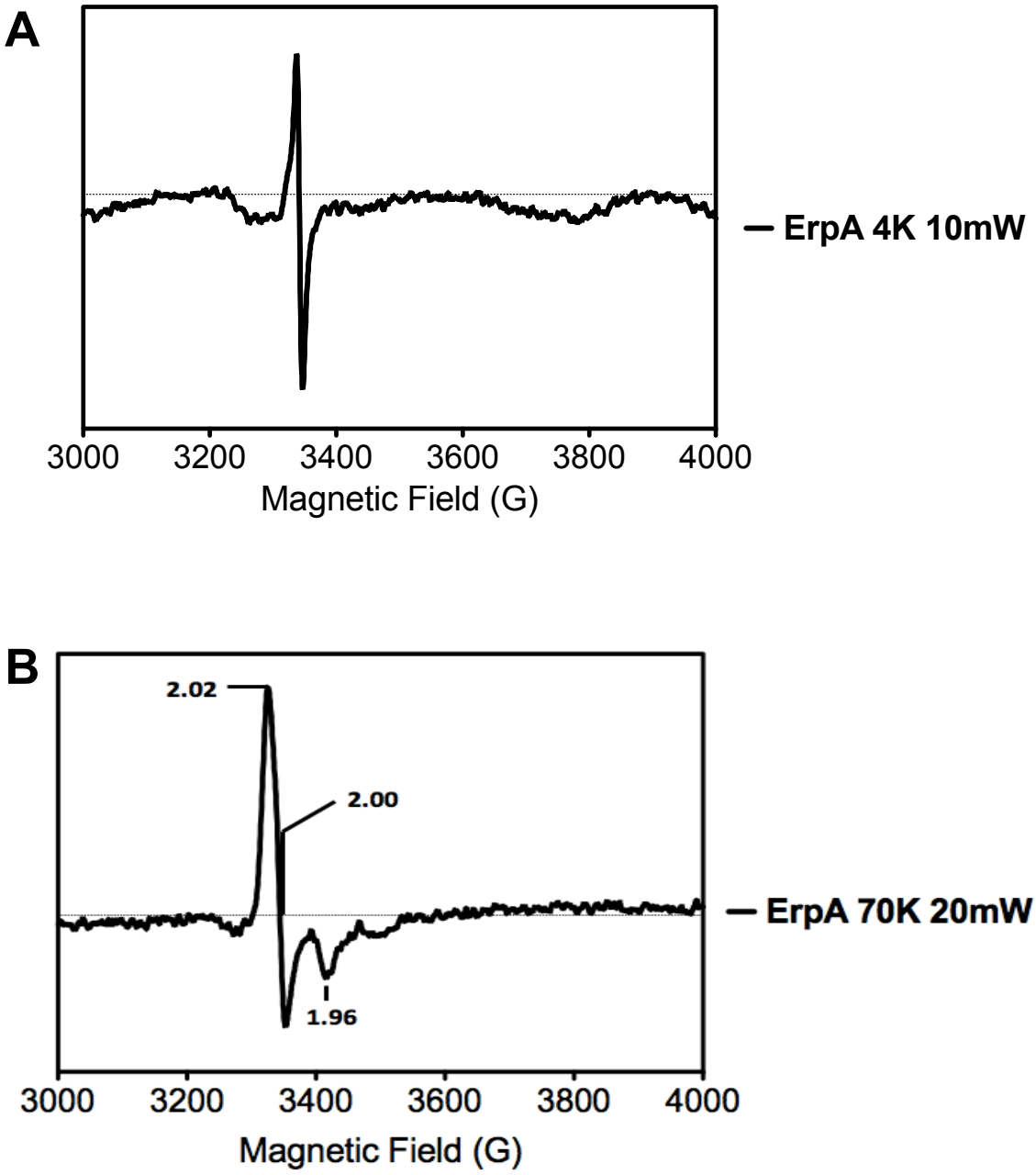

Figure 4.8 Comparison of EPR spectra of [2Fe-2S] cluster of ErpA.

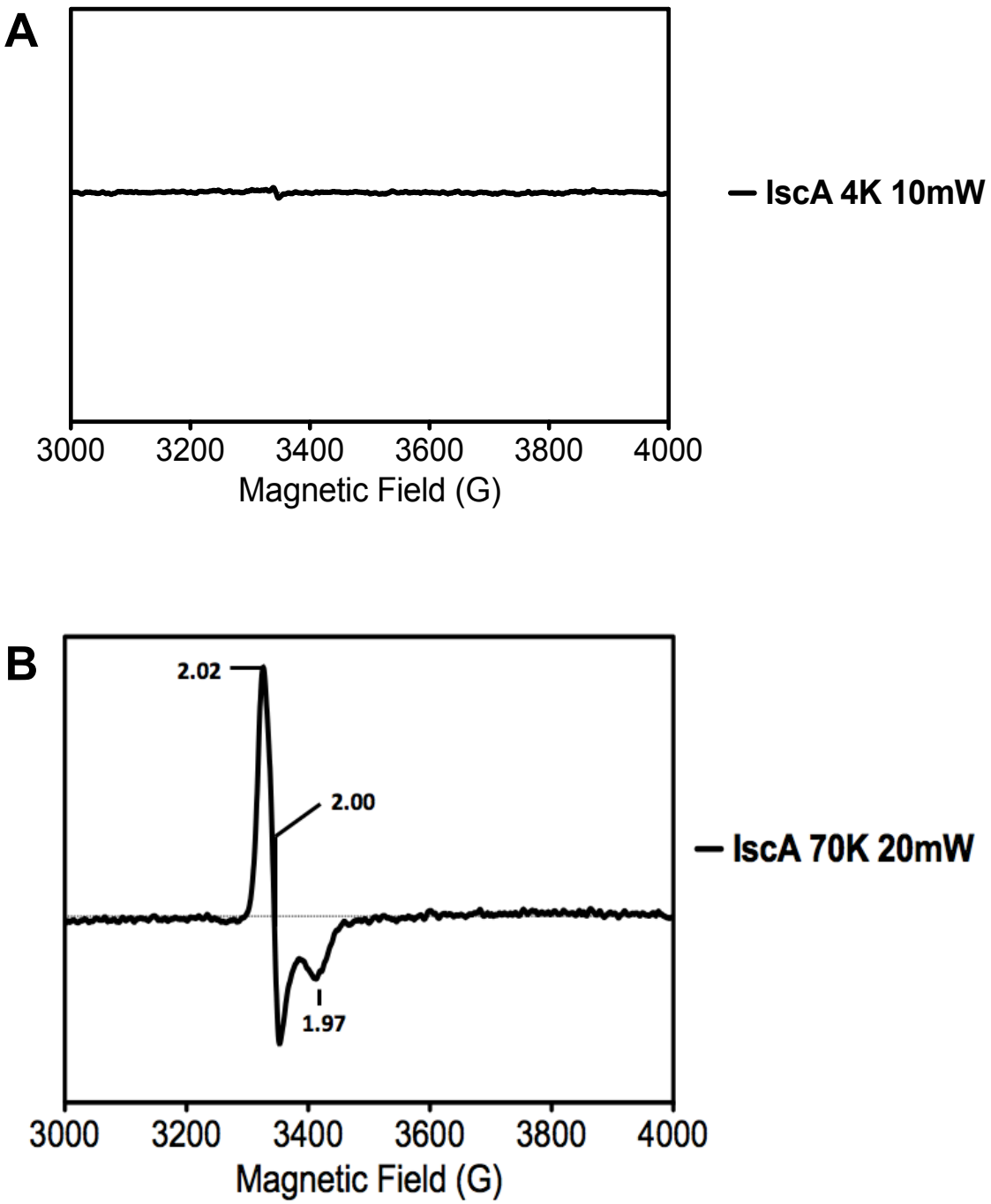

Figure 4.9 Comparison of EPR spectra of [2Fe-2S] cluster of IscA.

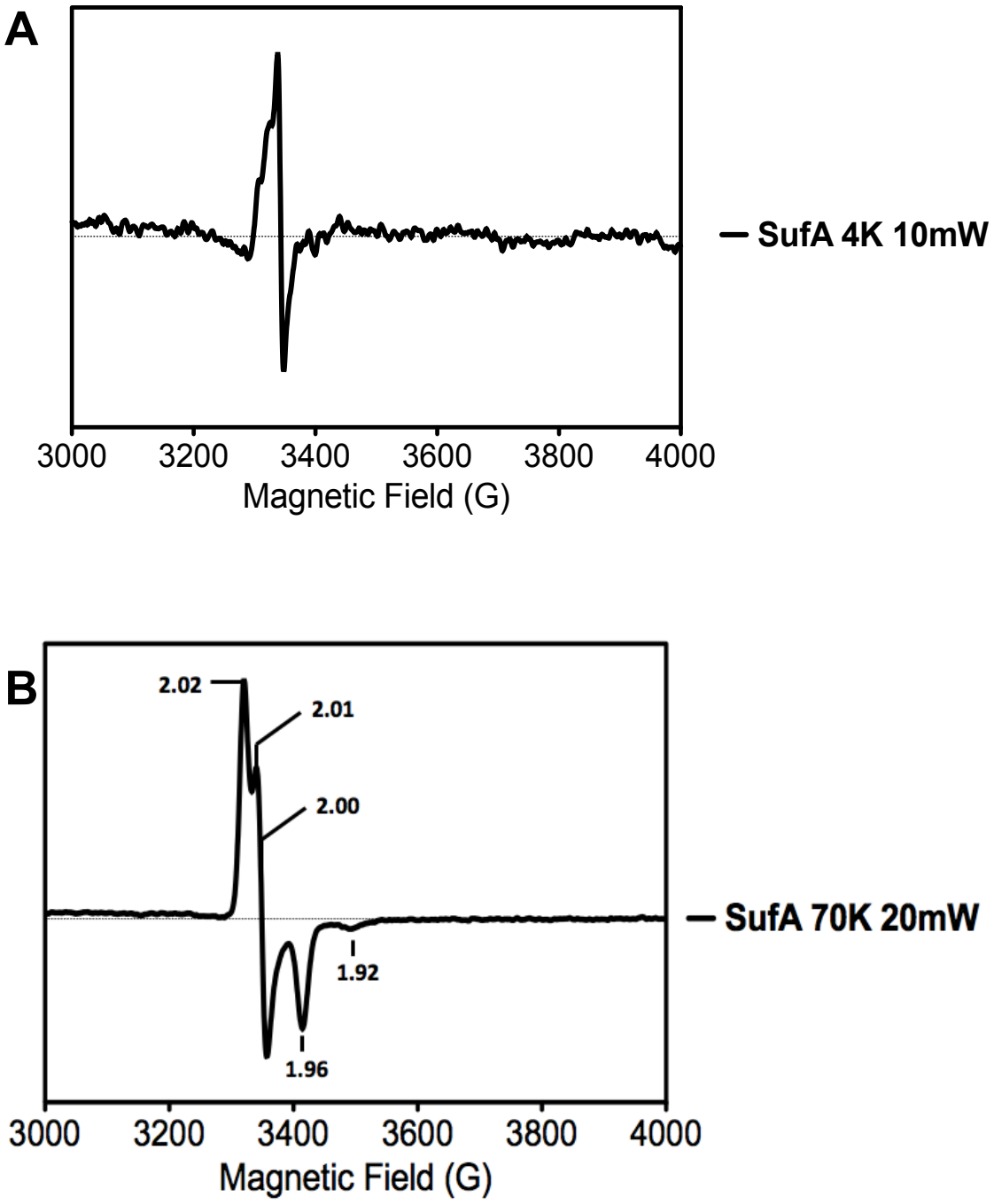

Figure 4.10 Comparison of EPR spectra of [2Fe-2S] cluster of SufA.

mM Cu EDTA standard, the spin per mole of cluster was determined for each A-type carrier protein. ErpA, IscA, and SufA treated with a 5 mM DTT (final concentration) resulted in 0.1 %, 1.7 %, and 1.3 % spin per mole of cluster, respectively.

SufBC_2D *can transfer its Fe-S cluster to either IscA or SufA*

In order to determine whether SufBC_2D preferentially assembles an Fe-S cluster onto IscA or SufA, apo-IscA or apo-SufA was mixed with SufBC_2D without DTT. The presence of DTT can assist in Fe-S cluster formation onto IscA and SufA. Therefore, each reaction mixture was set up without DTT in order to ensure that the Fe-S cluster was transferred from SufS and SufE as the sulfur source from SufBC_2D onto the A-type protein. The CD spectra of SufA and IscA alone changes minimally in the absence of SufBC_2D (Figure 4.11 A; Figure 4.12 A). The presence of SufBC_2D increasing the CD spectra intensity suggesting that an Fe-S cluster is being assembled onto the A-type carrier protein (Figure 4.11 B; Figure 4.12 B). The overall changes in the CD spectra show that SufBC_2D assists in the Fe-S cluster assembly onto SufA and IscA by 4-fold and 1.6-fold, respectively. In the first 10 minutes, the rate of Fe-S cluster assembly onto SufA is 11.6 times faster than onto IscA when using the SufBCDSE assembly system.

[2Fe-2S] clusters can be transferred to ErpA

Apo-proteins were not pre-reduced before starting transfer experiments and therefore may show reduced transfer efficiency if compared to using fully reduced apo-proteins. The CD spectra of [2Fe-2S] IscA shows an increase in the 350 nm, 450 nm, and

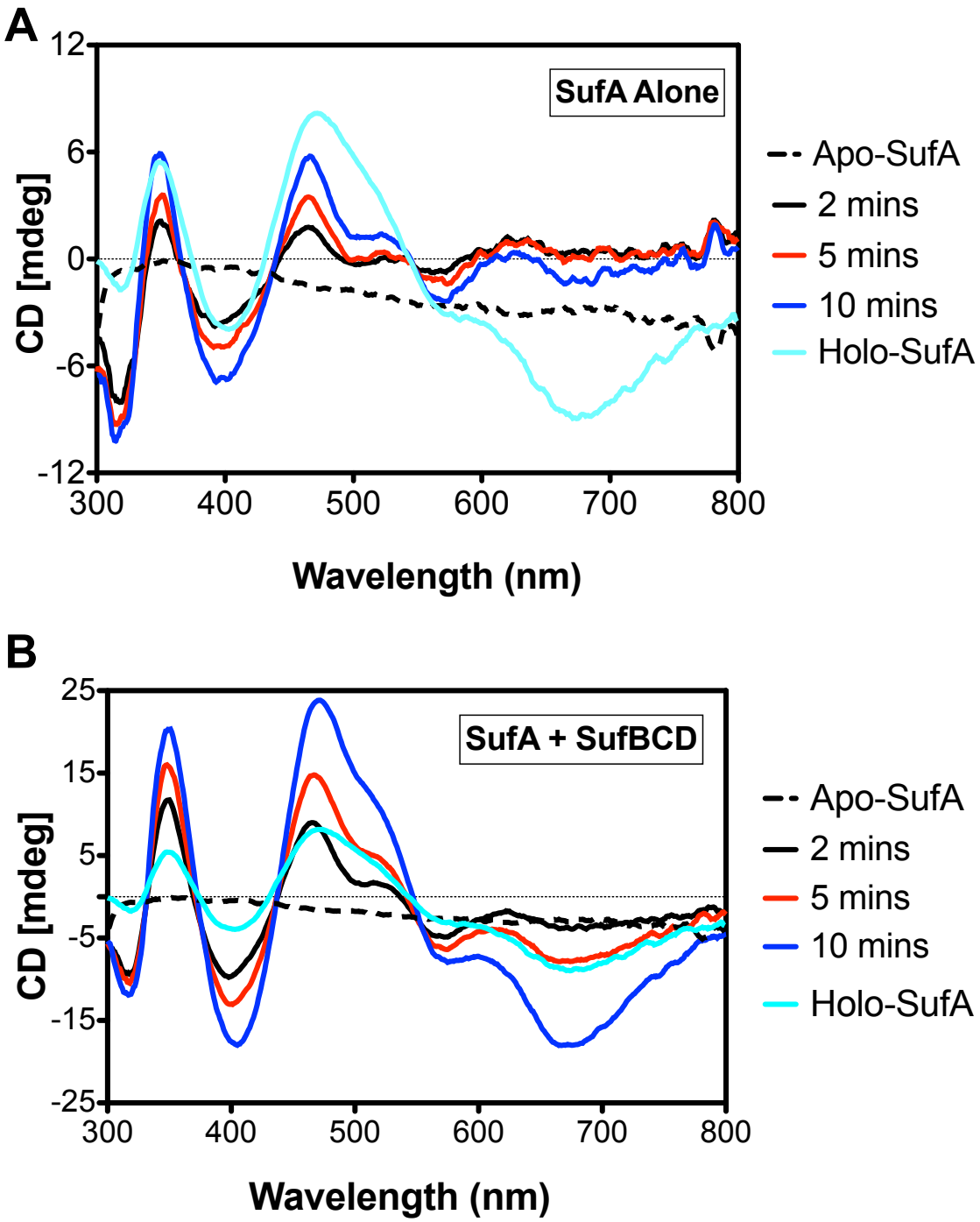

Figure 4.11 (A) CD-monitored spectra of Fe-S cluster formation onto SufA (B) in the presence of $SufBC_2D$.

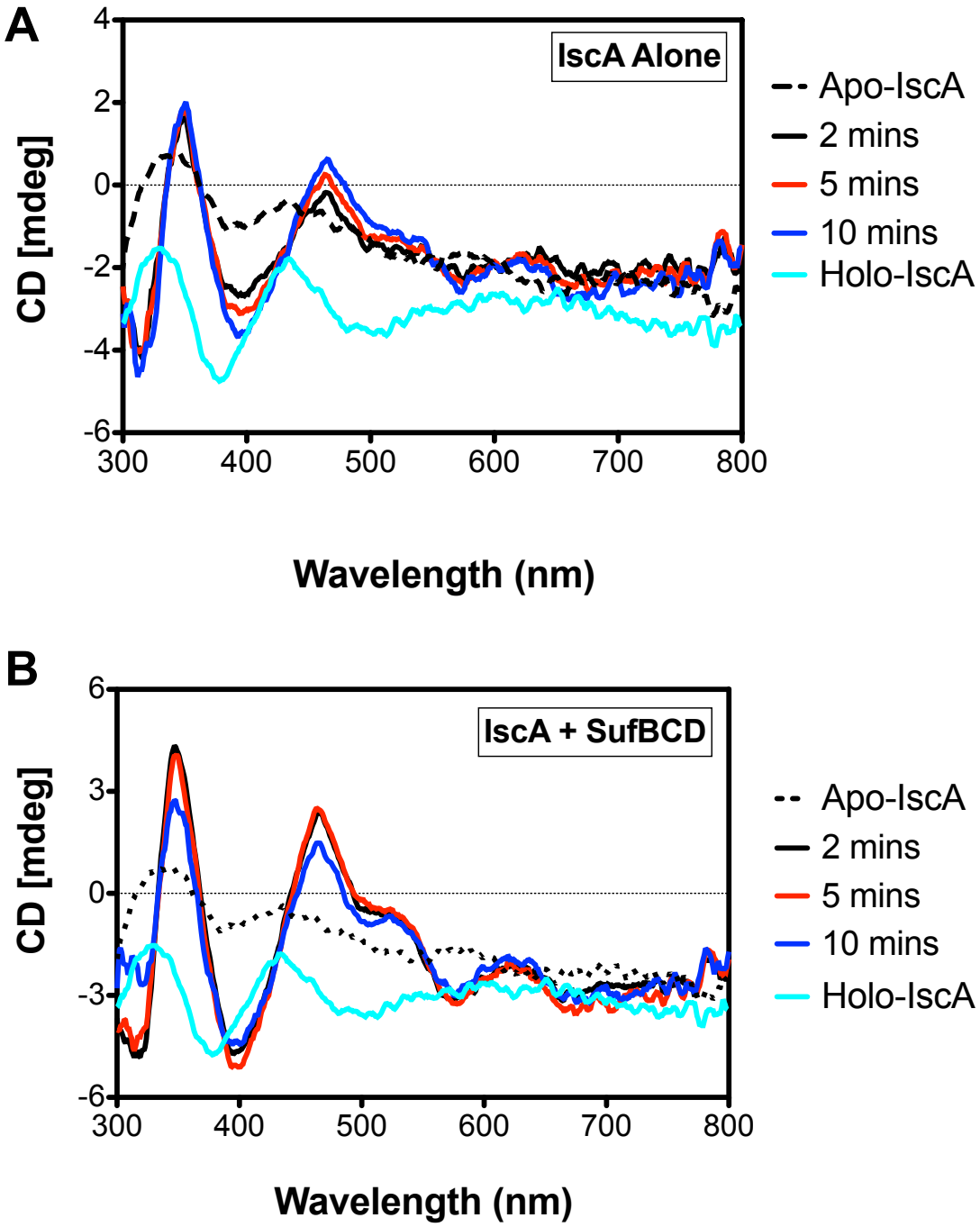

Figure 4. 12 (A) CD-monitored spectra of Fe-S cluster formation onto IscA(B) in the presence of $SufBC_2D$.

520 nm regions in the presence of apo-ErpA and apo-SufA suggesting that the cluster may partially be transferred to either protein. The overall change in the CD spectra results in approximately 70 % or 30 % of cluster transfer to apo-ErpA or apo-SufA, respectively (Figure 4.13 A and Figure 4.13 B). Kinetic data acquired for transfer from holo-IscA to apo-ErpA using an association then dissociation fit equation produced a 0.9946 correlation coefficient. Kinetic data acquired for transfer from holo-IscA to apo-SufA using a one-fit association fit equation produced a 0.9306 correlation coefficient. The K_{on} value for holo-IscA to apo-ErpA was reported in GraphPad Prism as 7995 M^{-1} cm^{-1}. The K value for holo-IscA to apo-SufA was reported in GraphPad Prism as 0.1014 min^{-1}. The concentration of cluster (M^{-1}) was used in order to calculate the K_{on} value of 2535 M^{-1} cm^{-1}. Also, the rate of transfer to apo-ErpA reaches maximum transfer after 20 minutes compared to 30 minutes with apo-SufA (Figure 4.13 A).

The CD spectra of [2Fe-2S] SufA decreases in the 450 nm range suggesting that the cluster may partially be transferred to apo-ErpA (Figure 4.14 A) and apo-IscA (Figure 4.14 B). The overall changes in CD spectra result in a maximum of 70 % transfer to apo-ErpA after 10 minutes (Figure 4.14 A) and 70 % to apo-IscA after 30 minutes (Figure 4.14 B). Kinetic data acquired for transfer from holo-SufA to apo-ErpA using an association then dissociation fit equation produced a 0.9952 correlation coefficient. Kinetic data acquired for transfer from holo-SufA to apo-SufA using a one-fit association fit equation produced a 0.9972 correlation coefficient. The K_{on} value for holo-SufA to apo-ErpA was reported in GraphPad Prism as 45421 M^{-1} cm^{-1}. The K value for holo-SufA to apo-IscA was reported in GraphPad Prism as 0.1048 min^{-1}. The concentration of cluster (M^{-1}) was used in order to calculate the K_{on} value of 24880 M^{-1} cm^{-1}.

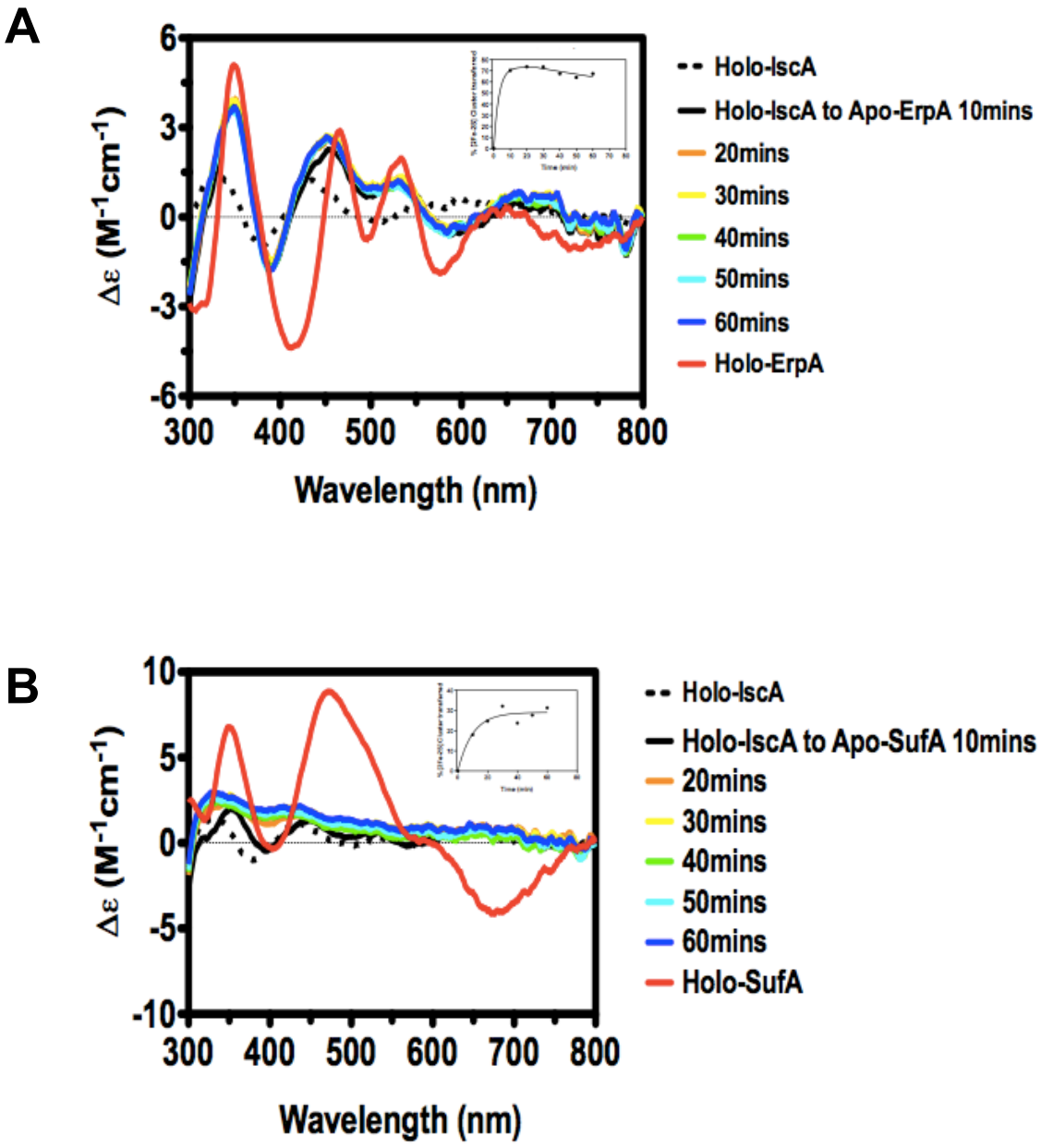

Figure 4.13 CD-monitored transfer of [2Fe-2S] IscA to (A) apo-ErpA (B) and apo-SufA.

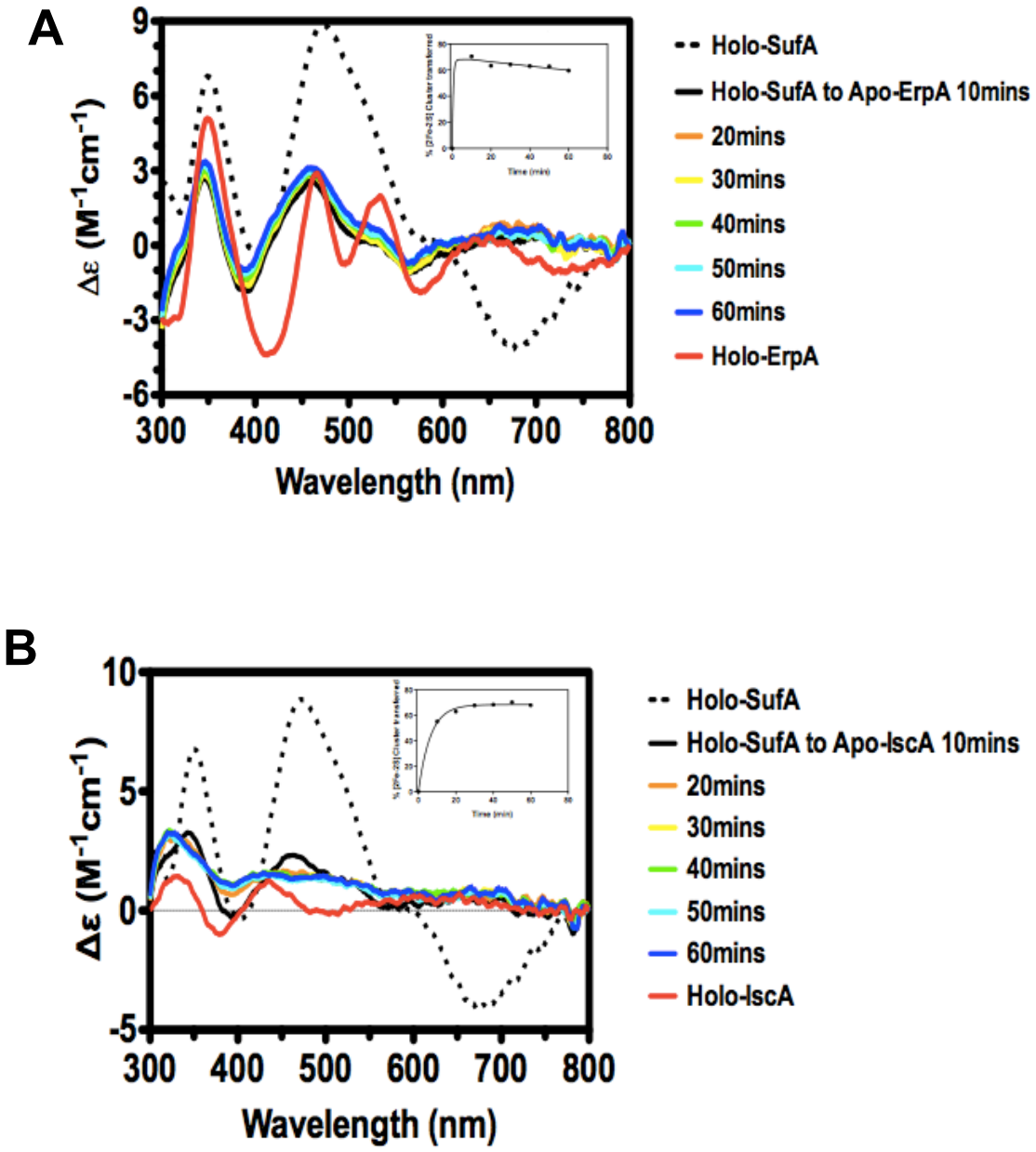

Figure 4.14 CD-monitored transfer of [2Fe-2S] SufA to (A) apo-ErpA (B) and apo-IscA.

The CD spectra of [2Fe-2S] ErpA shows a decrease in the 350 nm region in the presence of apo-IscA suggesting that the cluster may be partially be transferred to apo-IscA Figure 4.15 A). In contrast, the CD spectra of the holo-ErpA with apo-SufA shows that the cluster cannot be transferred to SufA and does not resemble that of holo-SufA (Figure 4.15 B). No model provided accurate fitting and kinetic analysis was not obtained.

DISCUSSION

It has been previously shown that bacterial IscA and SufA can coordinate a [2Fe-2S] cluster (Mapolelo et al., 2012; Gupta et al., 2009). The holo forms of IscA and SufA can be transferred to scaffold proteins (Chahal et al., 2009; Ollagnier-de-Choudens et al., 2004; Mapolelo et al., 2012). Our results showing an enhancement of Fe-S cluster formation onto SufA and IscA in the presence of the $SufBC_2D$ scaffold protein supports previous findings and the model proposed by Vinella et al., 2009 (Figure 4.2). The *suf* operon contains both *sufA* and *sufBCD*. Additionally, studies show that $SufBC_2D$ can transfer its cluster to SufA (Takahasi and Tokumoto, 2002; Chahal et al., 2009; Chahal and Outten 2012). $SufBC_2D$ has not been shown to transfer its cluster to IscA. The scaffold protein IscU can transfer its cluster to IscA (Ollagnier-de-Choudens et al., 2004). Although our results show that $SufBC_2D$ can also transfer its cluster to IscA, there is a higher transfer efficiency between $SufBC_2D$ and SufA suggesting that this may occur *in vivo*. The model also predicts that type II A-type carriers such as SufA and IscA can transfer its cluster to the type I ErpA (Figure 4.2). Our results show the holo-IscA can transfer its cluster to either ErpA or SufA. Holo-IscA preferentially transfers it cluster ErpA in comparison to SufA. Py et al., did show that ErpA has a higher affinity for IscA in comparison to SufA

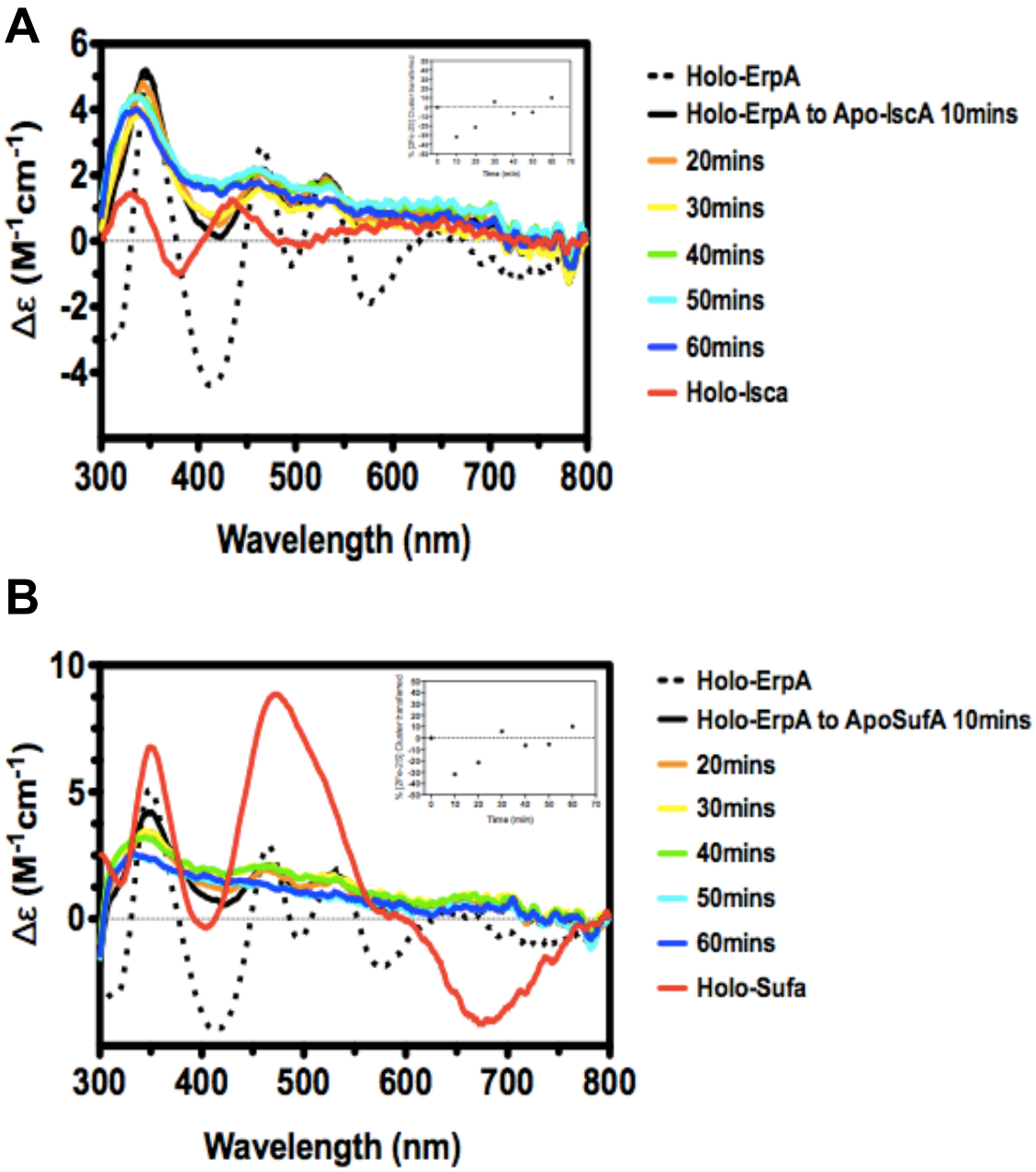

Figure 4.15 CD-monitored transfer of [2Fe-2S] ErpA to (A) apo-IscA (B) and apo-SufA

(Py et al., 2018). Holo-SufA can transfer its cluster to either ErpA or IscA but favors ErpA. According to the proposed model, it is expected that ErpA cannot transfer its cluster in the reverse direction to type II IscA and SufA. Our results show a slight decrease in the CD spectra at 350 nm of holo-ErpA in the presence of apo-IscA suggesting that ErpA may be able to transfer its cluster in the reverse direction. The lack of data fitting refutes this claim. Taken together, these findings support the model proposed by Vinella et al., 2009 and provide a more holistic view of Fe-S cluster trafficking amongst A-type carrier proteins in *E. coli* (Figure 4.16). It is noteworthy to mention that apo-proteins were not pre-reduced before starting the transfer reactions so partial transfer may be occurring or some protein may be more susceptible to oxygen. Deletion to *iscA* in combination with high oxygen exposure is lethal in bacteria (Johnson et al., 2006).

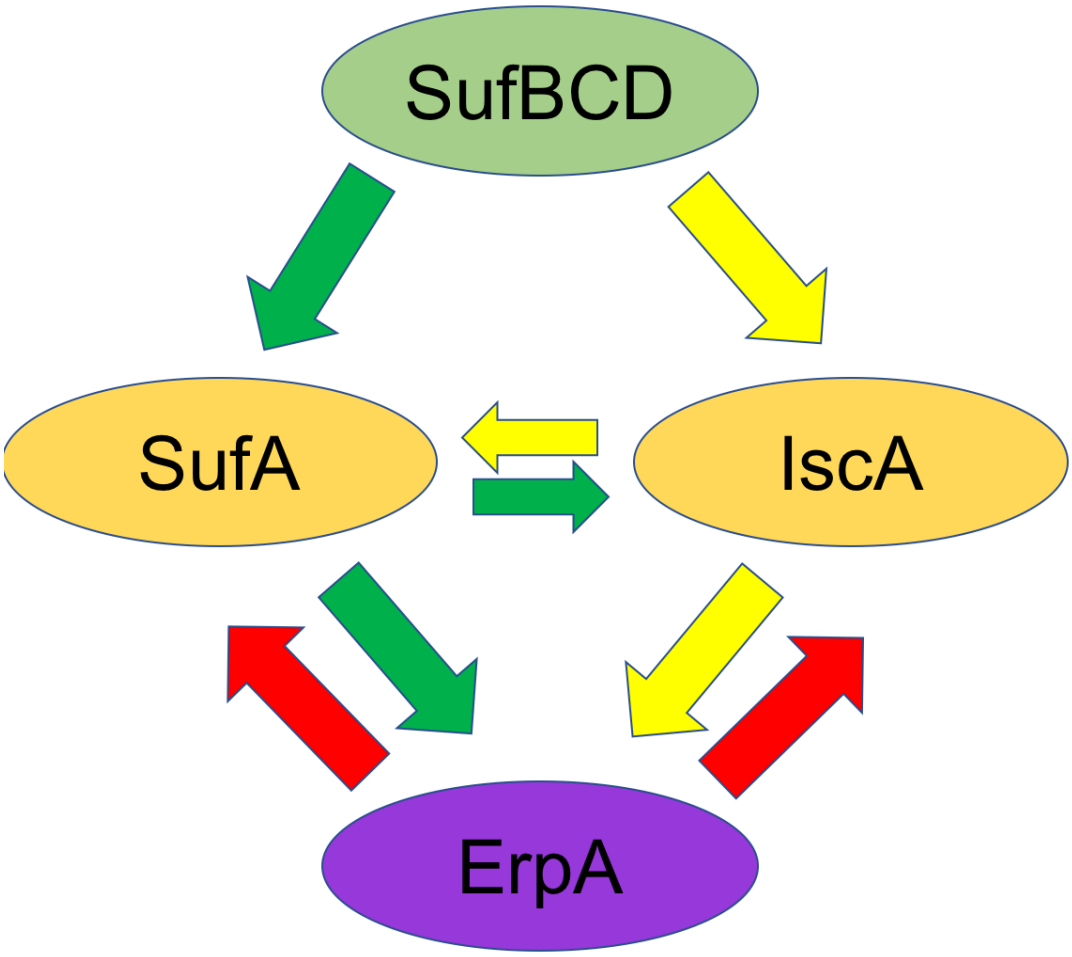

Figure 4.16 Revised directionality model of Fe-S cluster trafficking amongst $SufBC_2D$ (green: the scaffold protein), SufA, IscA (yellow: Type II A-type protein), and ErpA (purple: Type I A-type protein). The green arrows depict preferential directionality, yellow depicts a potential secondary action, and red depict a block in directionality or no transfer.

REFERENCES

1. Chahal H. K., Dai Y., Saini A., Ayala-Castro C., and Outten F. W. (2009) The $SufBC_2D$ Fe-S scaffold complex interacts with SufA for Fe-S cluster transfer. *Biochemistry* **48:** 10644-10653.

2. Chahal, H.K. and Outten, F.W. (2012) Separate Fe-S scaffold and carrier functions for $SufB_2C_2$ and SufA during *in vitro* maturation of [2Fe-2S] Fdx. *J Inorg Biochem* **116C:** 126-134.

3. Cupp-Vickery, J.R., Silberg, J.J., Ta, D.T., and Vickery, L.E. (2004) Crystal structure of IscA, an iron-sulfur cluster assembly protein from *Escherichia coli. J Mol Biol* **338:** 127-137.

4. Gupta, V., Sendra, M., Naik, S.G., Chahal, H.K., Huynh, B.H., Outten, F.W., Fontecave, M., and Ollagnier-de-Choudens, S. (2009) Native *Escherichia coli* SufA, coexpressed with $SufBC_2D$, purifies as a [2Fe-2S] protein and acts as an Fe-S transporter to Fe-S target enzymes. *J Am Chem Soc* **131:** 6149-6153.

5. Johnson, D.C., Unciuleac, M.C., and Dean, D.R. (2006) Controlled expression and functional analysis of iron-sulfur cluster biosynthetic components within *Azotobacter vinelandii. J Bacteriol* **188:** 7551-7561.

6. Kennedy, M.C. and Beinert, H. (1988) The state of cluster SH and S2- of aconitase during cluster interconversions and removal. A convenient preparation of apoenzyme. *J Biol Chem* **263:** 8194-8198.

7. Layer, G., Gaddam, S.A., Ayala-Castro, C.N., Ollagnier-de Choudens, S., Lascoux, D., Fontecave, M., and Outten, F.W. (2007) SufE transfers sulfur from SufS to SufB for iron-sulfur cluster assembly. *J Biol Chem* **282:** 13342-13350.

8. Loiseau, L., Gerez, C., Bekker, M., Ollagnier-de-Choudens, S., Py, B., Sanakis, Y., Teixeira de Mattos, J., Fontecave, M., and Barras, F. (2007) ErpA, an iron-sulfur (Fe-S) protein of the A-type essential for respiratory metabolism in *Escherichia coli. Proc Natl Sci USA* **104:** 13626-13631.

9. Mapolelo, D.T., Zhang, B., Naik, S.G., Huynh, B.H., and Johnson, M.K. (2012) Spectroscopic and functional characterization of iron-sulfur cluster bound forms of *Azotobacter vinelandii* (Nif) IscA. *Biochemistry* **51:** 8071-8084.

10. Ollagnier-de-Choudens, S., Sanakis, Y., and Fontecave, M. (2004) SufA/IscA: reactivity studies of a class of scaffold proteins involved in [Fe-S] cluster assembly. *J Biol Inorg Chem* **9:** 828-838.

11. Outten, F.W., Wood, M.J., Munoz, F.M., and Storz, G. (2003) The SufE protein and the $SufBC_2D$ complex enhance SufS cysteine desulfurase activity as part of a sulfur transfer pathway for Fe-S cluster assembly in Escherichia coli. *J Biol Chem* **278:** 45713-45719.

12. Py, B., Gerez, C., Huguenot, A., Vidaud, C., Fontecave, M., Ollagnier de Choudens, S., and Barras, F. (2018) The ErpA/NfuA complex builds an oxidation-resistant Fe-S cluster delivery pathway. *J Biol Chem* **293:** 7689-7702.

13. Riemer, J., Hoepken, H.H., Czerwinska, H., Robinson, S. R., and Dringen, R. (2004) Colorimetric ferrozine-based assay for the quantitation of iron in cultures cells. *Anal Biochem* **331:** 370-375.

14. Takahashi, Y., Tokumoto, U. (2002) A third bacterial system for the assembly of iron–sulfur clusters with homologs in archaea and plastids, *J Biol Chem* **277:** 28380-28383.

15. Vinella, D., Brochier-Armanet, C., Loiseau, L., Talla, E., and Barras, F. (2009) Iron-sulfur (Fe/S) protein biogenesis: phylogenomic and genetic studies of A-type carriers. *PLOS Genet* 5*:* e1000497.

16. Wada, K., Hasegawa, Y., Gong, Z., Minami, Y., Fukuyama, K., Takahashi, Y. (2005) Crystal structure of *Escherichia coli* SufA involved in biosynthesis of iron-sulfur clusters: implications for a functional dimer. *FEBS Lett* **579:** 6543-6548.

CHAPTER 5

GRX4 TRANSFERS A [2FE-2S] CLUSTER TO A-TYPE CARRIER PROTEINS IN *E. COLI*

ABSTRACT

Glutaredoxins are generally known as redox proteins. Biochemical studies show that monothiol glutaredoxins including *Escherichia coli* (*E. coli*) Grx4 can bind and transfer its cluster to apoproteins such as ferredoxin. The novel role of glutaredoxins in Fe-S cluster metabolism is unclear. However, understanding the role and its interactions may provide a novel therapeutic target for drug treatment. Herein, we biochemically characterize *E. coli* Grx4 using EPR and circular dichroism spectroscopies. It is shown that *E. coli* Grx4 coordinates a [2Fe-2S] cluster that can be transferred to *E. coli* A-type carrier proteins. The percentage and rate of cluster transfer suggests that Grx4 may transfer its cluster to IscA in vivo. Due to transfer rates and percentages obtained, it seems unlikely that this process is bi-directional.

INTRODUCTION

E. coli Glutaredoxin 4 is structurally similar to the yeast *Saccharomyces cerevisiae* *y*GRX5 which has been associated with Fe-S cluster metabolism (Figure 5.1 A; Herrero and Ruiz, 2007). The crystal structure of *E. coli* Grx4 also referred to as GrxD reveals a

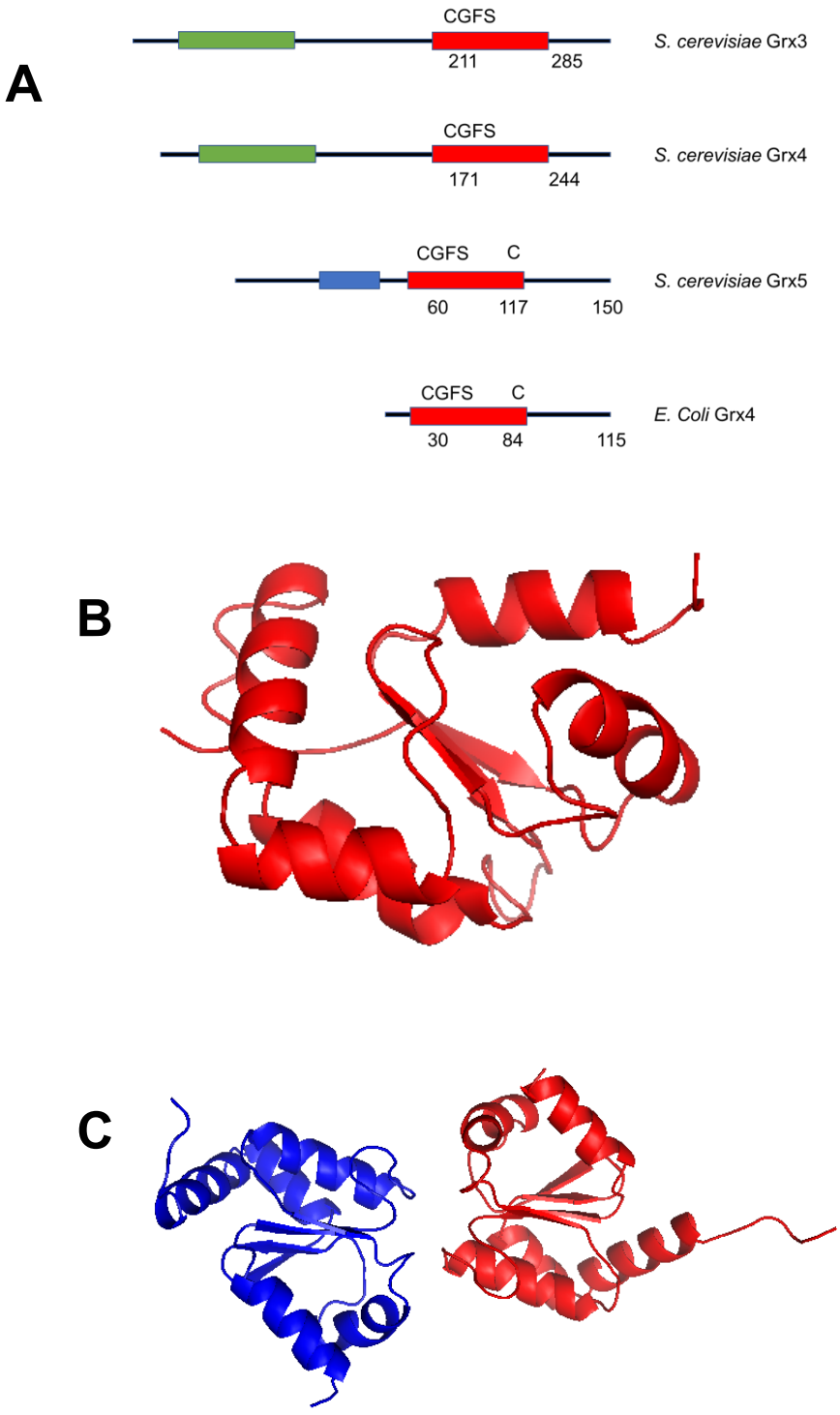

Figure 5.1 (A) Structure of monothiol glutaredoxins (green: mitochondrial targeting sequence; thioredoxin domain; blue: red: glutaredoxin domain). (B) Ribbon diagram of *E. coli* monomer and (C) dimer.

monomeric structure or homodimeric structure (Figure 5.1 B, C). The homodimer can bind two molecules of glutathione and a [2Fe-2S] cluster (Iwema et al., 2009). Glutathione assists in Fe-S cluster coordination of homodimeric glutaredoxins (Wang et al., 2012; Lillig et al., 2005; Feng et al., 2006; Johansson et al., 2007; Picciocchi et al., 2007; Rouhier et al., 2007; Bandyopadhyay et al., 2008; Couturier et al., 2009; Iwema et al., 2009; Li et al., 2010; Couturier et al., 2011; Yeung et al., 2011). This cluster can be transferred to apo-protein ferredoxin (Yeung et al., 2011; Vranish et al., 2016). Despite its ability to transfer clusters to apo-proteins, the role of Grx4 in Fe-S cluster metabolism is unclear. Genetic studies show that the deletion of *grxD* is synthetically lethal in combination with deletion of the *isc* operon (Butland et al., 2008). *E. coli* Grx4 can also rescue yeast cells deficient in Grx5 has also been associated with Fe-S cluster metabolism (Rodriguez-Manzaneque et al., 2002). Monothiol glutaredoxins found in the plant *Arabidopsis thaliana* and yeast *Saccharomyces cerevisiae* (yGrx3) have been shown to transfer its cluster to the A-type carrier IscA and SufA (Mapolelo et al., 2013). However, this has not been shown in *E. coli.* Our goal in this work is to test if *E. coli* Grx4 can also transfer its cluster to *E. coli* A-type carrier proteins thereby providing a novel Fe-S cluster trafficking pathway in *E. coli.*

MATERIALS AND METHODS

Protein Expression and Purification

The pRSF-Duet-1 (Novagen) containing the open reading frame of *E. coli grx4 (grxD)* was created by Adrienne Dlouhy (courtesy of Dr. Caryn Outten, University of South Carolina, Department of Chemistry and Biochemistry) and named "RSFDuet-1-Grx4" (Dlouhy et

al., 2016). pRSFDuet-1-Grx4 containing cells were induced via an IPTG promoter with 500 μM IPTG in order to over-express the Grx4 in BL21(DE3) cells. Four liters of cells were cultured at 37 °C to an OD 600 nm of 0.6 to 0.8 before IPTG induction at 18 °C overnight. Cells were collected via centrifugation and stored at -80 °C. Cell pellets were re-suspended in 25 mM Tris-HCl, pH 7.5, 10 mM βME, 100 mM NaCl and 1 mM phenylmethanesulfonyl fluoride (PMSF) then lysed via sonication. Cellular debris was mixed with streptomycin sulfate and centrifuged at 16,000 rpm at 4 °C. Cleared cell lysate was loaded onto a Q Sepharose ionic exchange column pre-equilibrated with 25 mM Tris-HCl, pH 7.5, 10 mM βME, and 100 mM sodium chloride (NaCl). *E. coli* Grx4 was eluted using a linear gradient starting with Buffer A (25 mM Tris-HCl, pH 7.5, 10 mM βME, and 0 M NaCl) to Buffer B (25 mM Tris-HCl, pH 7.5, 10 mM βME, and 1 M NaCl). Eluted protein was loaded onto a Phenyl FF column pre-equilibrated with 25 mM Tris-HCl, pH 7.5, 10 mM βME, and 1M NH_4SO_4 (ammonium sulfate). Grx4 was eluted using a linear gradient starting from 1 M NaCl to 0 M NH_4SO_4. SufA eluted at 75% of Buffer B (25 mM Tris-HCl, pH 7.5, 10 mM βME, and 0 M NH_4SO_4) was diluted and then loaded onto the Superdex 75 size exclusion column. Pure protein was concentrated and stored at -80 °C.

The pBADmycHisC vector containing the *sufABCDSE* operon (Outten et al., 2003) was induced via an inducible arabinose promoter with 0.2 % arabinose in order to over-express $SufBC_2D$ in BL21 (DE3) cells and purified as previously describes (Layer et al., 2007). Four liters of cells were cultured at 37 °C to an OD 600 nm of 0.6 to 0.8 before arabinose induction at 18 °C overnight. Cells were collected via centrifugation and stored at -80 °C. Cell pellets were re-suspended in 25 mM Tris-HCl, pH 7.5, 10 mM βME, 100 mM NaCl and 1 mM phenylmethanesulfonyl fluoride (PMSF) then lysed via sonication.

Cellular debris was mixed with streptomycin sulfate and centrifuged at 16,000 rpm at 4 °C. Cleared cell lysate was loaded onto a Phenyl FF column pre-equilibrated with 25 mM Tris-HCl, pH 7.5, 10 mM βME, and 1 M (ammonium sulfate) NH_4SO_4. $SufBC_2D$ was eluted using a linear gradient starting from 1 M NH_4SO_4 to 0 M NH_4SO_4. Eluted protein was diluted and then loaded onto a Q Sepharose ion exchange column pre-equilibrated with 25 mM Tris-HCl, pH 7.5, 10 mM βME, and 100 mM NaCl. $SufBC_2D$ was eluted using a linear gradient starting with Buffer A (25 mM Tris-HCl, pH 7.5, 10 mM βME) to Buffer B (25 mM Tris-HCL, pH 7.5, 10 mM βME, and 1 M NaCl). Eluted protein was concentrated and loaded onto a the Superdex 200 size exclusion column with 25 mM Tris-HCL, pH 7.5, 10 mM βME, 100 mM NaCl buffer. Pure protein was concentrated and stored at -80 °C. Protein standards (GE Healthcare) were also re-suspended in 25 mM Tris-HCl, pH 7.5, 10 mM βME, 100 mM NaCl buffer and run using the Superdex 200 size exclusion column.

In vitro Reconstitution of Grx4/GrxD

Apo-proteins or proteins that do not contain an Fe-S cluster were treated with a 50-fold molar ratio of EDTA and 20-fold molar ratio of ferricyanide between 10 to 60 minutes on ice followed by desalting (Kennedy and Beinert, 1988). Apo-protein (1 mM) was incubated in the anaerobic chamber in up to 500 µl of reconstitution buffer (25 mM Tris-HCl, pH 7.5, 10 mM βME, and 100 mM NaCl) plus 5 mM DTT and 2 mM glutathione (GSH). Then a catalytic amount of SufS and SufE (4 µM) was added before adding 8-fold excess of ferrous ammonium sulfate and a 10-fold excess of L-cysteine. After 30 minutes to an hour, cluster formation was monitored by UV-visible absorption

spectroscopy. The mixture was loaded onto a 1 ml Q FF column pre-equilibrated with 25 mM Tris-HCl, pH 7.5, 10 mM βME, and 0mM to 100 mM NaCl (without DTT). The column was washed with reconstitution buffer before elution with 25 mM Tris-HCl, pH 7.5, 10 mM βME, and 500 mM to 1 M NaCl (without DTT).

Iron content was determined using the ferrozine assay (Riemer et al., 2004). Size exclusion measurements were calibrated using known molecular weight determination standards and calculated using an equation obtained by the standard curve. UV-visible absorption spectra were recorded using a Beckman DU-800 spectrophotometer. CD spectra were recorded under anaerobic conditions using a Jasco J-815 spectropolarimeter (Jasco, Hachioji, Japan) using a 1 cm cuvette.

X-band EPR samples (300 µl total volume) containing 300 to 600 µM total iron were reduced with 5 mM DTT (final concentration) for approximately 10 minutes before storing sample in liquid nitrogen. Spectra were recorded using a Bruker EMX plus spectrometer (~9.4 GHz, Bruker, Billerica, MA) equipped with an ESR900 continuous flow cryostat (Oxford Instruments, Concord, MA) at 4 K, 35 K, and 70 K. The amount of spin for each sample was calculated under non-saturating conditions at 35 K using double integration values of the samples and 1mM Cu EDTA standard.

Fe-S Cluster Transfer Monitored by Circular Dichroism

As a control, the appropriate holo-protein (donor) alone (80 µM iron content, 40 µM cluster) was scanned at 0- and 1-hour at 25 °C in a 1 cm path length anaerobic cuvette using a JASCO J-815 spectrometer. For transfer reactions, 80 µM of apo-protein (acceptor) was added to the holo-protein donor (80 µM iron content, 40 µM cluster) at a total volume

of 300 µl in 25 mM Tris-HCl (final salt concentration between 100 to 200 mM NaCl). The Fe-S cluster transfer was monitored by CD every 10 minutes for 1 hour at 25 °C in a 1 cm path length anaerobic cuvette using a JASCO J-815 spectrometer. These same conditions were used for all combinations of holo-donor and apo-acceptor proteins shown in the Results.

RESULTS

Characterization of E. coli *Grx4*

E. coli Grx4 has a distinct UV-visible and CD (circular dichroism) spectra in the 300 nm to 600 nm range (Figure 5.2) and represents the Fe-S cluster coordination environment of the protein. As-purified Grx4 does not show distinct UV-visible peaks at 320 nm or 420 nm. The theoretical monomeric weight according to the amino acid sequence of Grx4 is approximately 12.9 kDa. Size-exclusion chromatography using protein standards of known molecular weight and diameter determined the as-purified oligomeric state of Grx4 to be a 21.6 kDa dimeric protein (Figure 5.3; Table 5.1).

Reconstitution of as-purified E. coli Grx4

As purified *E. coli* Grx4 was reconstituted by incubation with ferrous ammonium sulfate, L-cysteine, dithiothreitol, SufS, SufE, and glutathione. The UV-visible absorption spectrum was monitored over time during the reconstitution of *E. coli* Grx4 (Figure 5.4). The reconstitution reaction of Grx4 showed low-level formation of thio-ferrates, or iron-sulfur chain, byproducts. This side reaction can be monitored by an increase in absorption

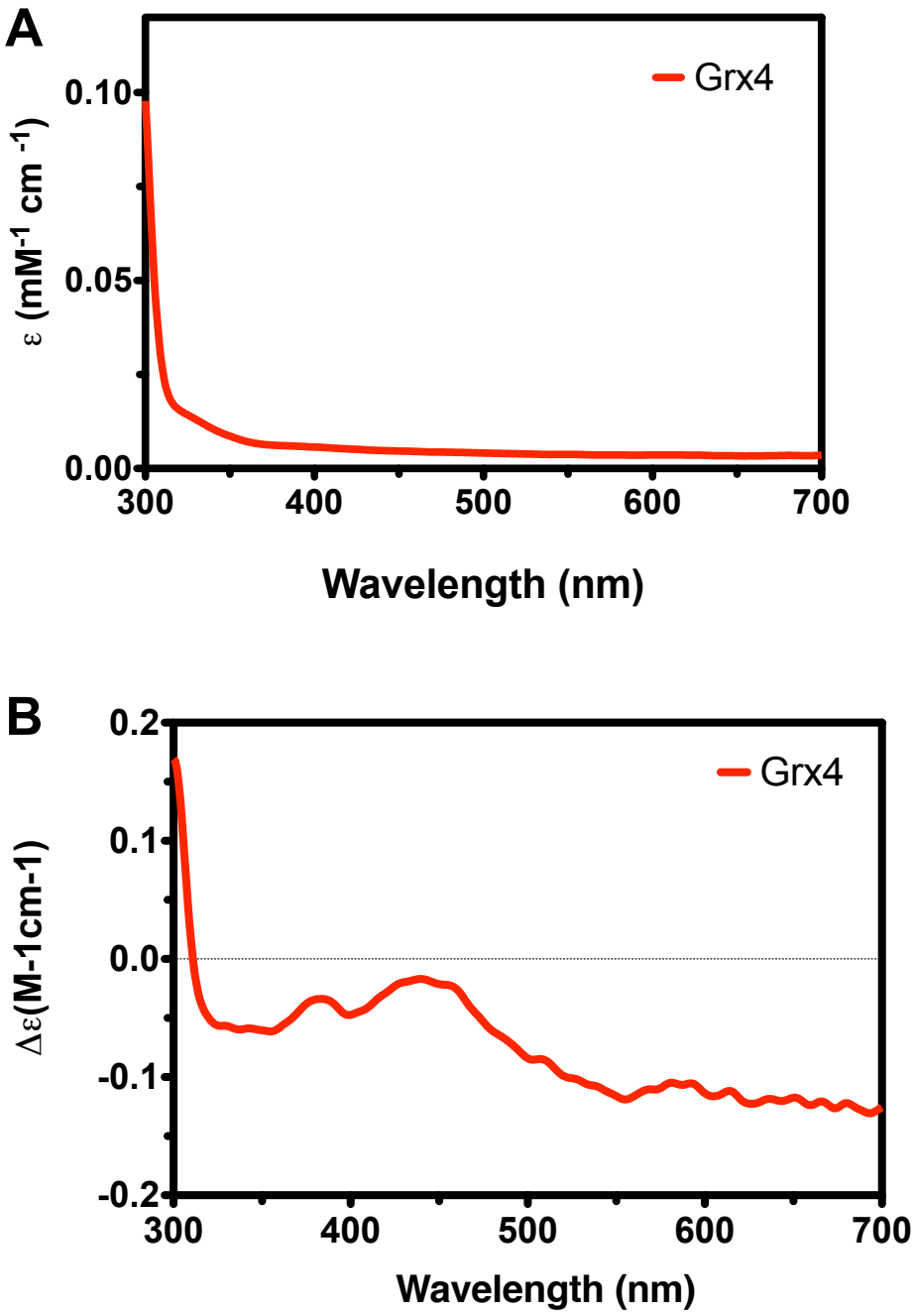

Figure 5.2 (A) Comparison of UV-visible absorption and (B) CD spectra of as-purified *E. coli* Grx4.

Table 5.1 Biochemical properties of *E. coli* Grx4

	As-purified Grx4	Reconstituted Grx4
Fe content	N/A	1.59
Complex	Dimer	N/A
Theoretical (Da)	12,878	N/A
Gel filtration (kD)	21.6	N/A

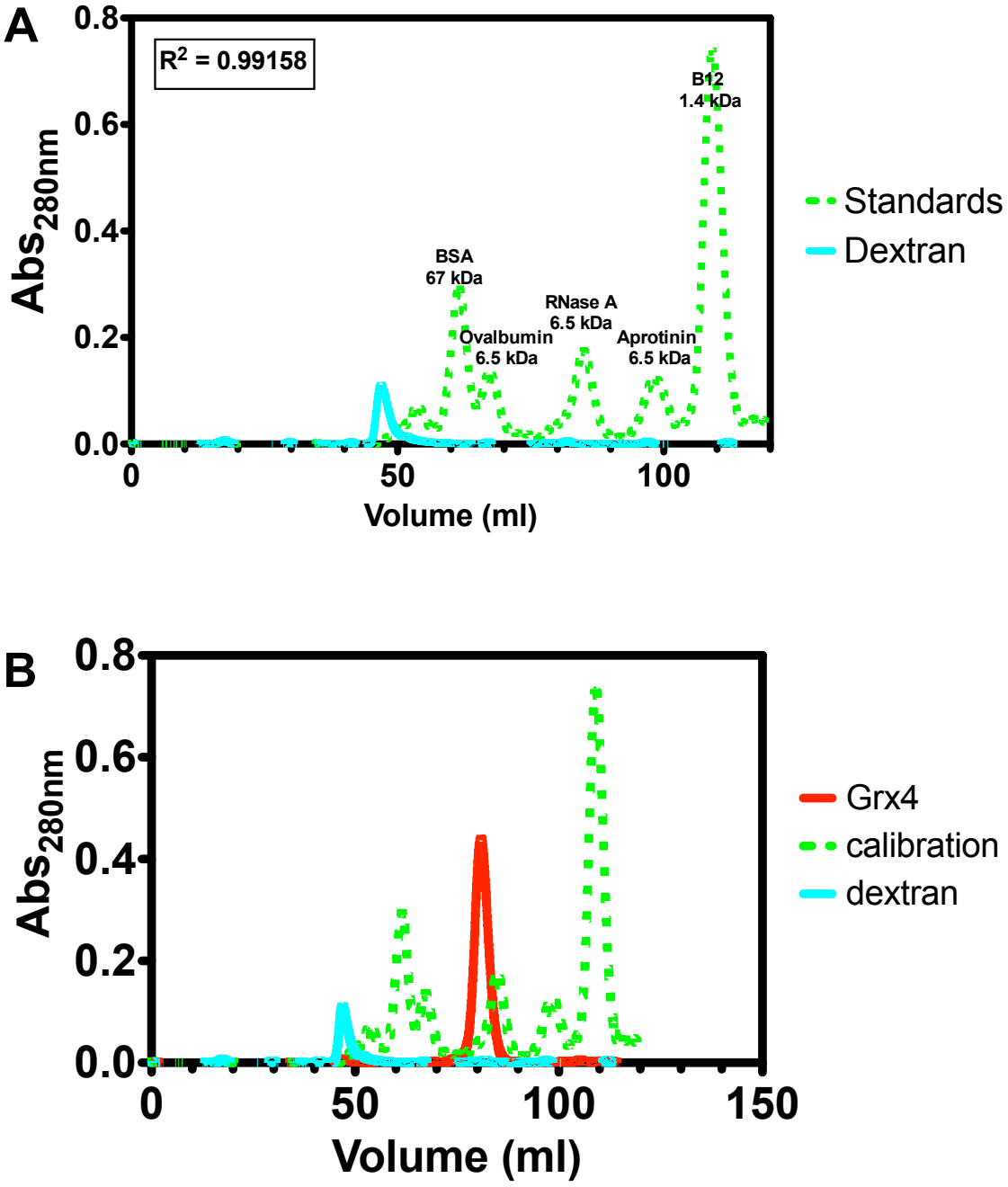

Figure 5.3 Size-exclusion chromatography of Superdex 75 (A) calibration standard proteins and (B) *E. coli* Grx4 with standards.

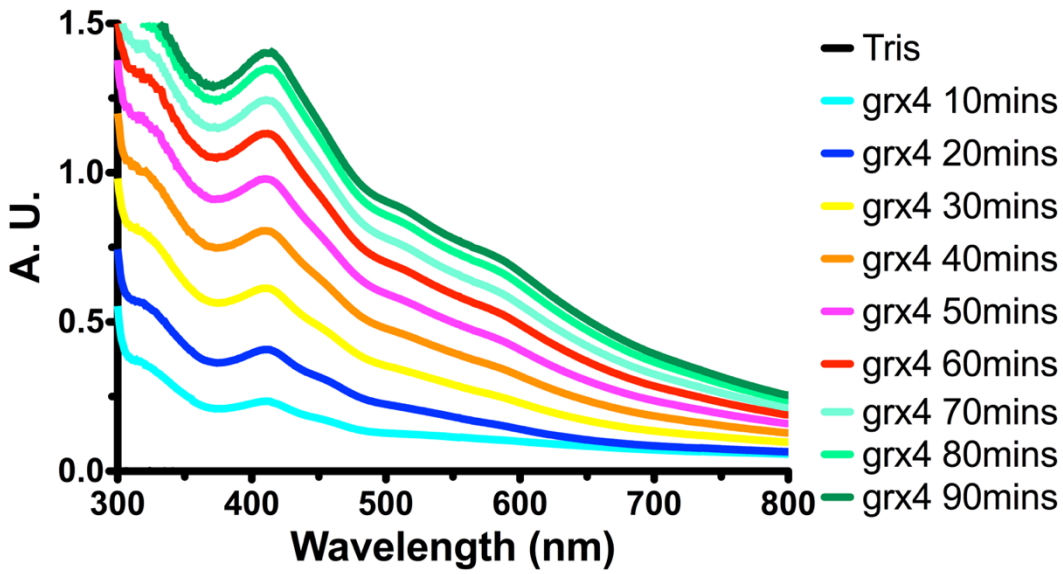

Figure 5.4 UV-visible monitored Fe-S cluster formation onto *E.coli* Grx4.

at 600 nm. *E. coli* Grx4 reconstitution reaches completion after approximately 60 minutes (Figure 5.4 A). The reaction was purified using an ionic exchange Q-Sepharose column in order remove byproducts from the reconstituted holo-protein.

Characterization of reconstituted A-Type carrier proteins

The UV-visible spectra of purified holo-Grx4 produces an intense shoulder peak at 320 nm and a peak at 420 nm which is indicative of a [2Fe-2S] cluster (Figure 5.5 A). The CD spectra of purified holo-Grx4 is more intense and shows peaks at 310 nm, 460 nm, and 555 nm suggesting that the protein contains a higher amount of iron in comparison to the as-purified sample (Figure 5.5 B). After removing byproducts, the iron per monomer of holo-Grx4 was calculated as 1.59. The stability of *E. coli* Grx4 was observed using CD after 1 hour. The CD spectra did not change indicating that *E. coli* Grx4 is stable enough at room temperature in order to proceed with further studies (Figure 5.6).

Electron paramagnetic resonance (EPR) can be used to determine the cluster type assembled onto *E. coli* Grx4. At a higher temperature of 70 K, Grx4 has more distinct features whereas the EPR spectra is saturated at 4 K. These features are indicative of a $[2Fe\text{-}2S]^{1+}$ reduced cluster which has a slower relaxation time in comparison to a [4Fe-4S] cluster (Figure 5.7). The g-values of *E. coli* Grx4 2.01, 2.01, and 1.96 produce an axial EPR spectra. Using the double integration values of a non-saturated 1 mM Cu EDTA standard, the spin per mole of cluster was determined for *E. coli* Grx4 treated with a 5 mM DTT (final concentration) for 10 minutes to produce 0.3 % spin per mole of cluster.

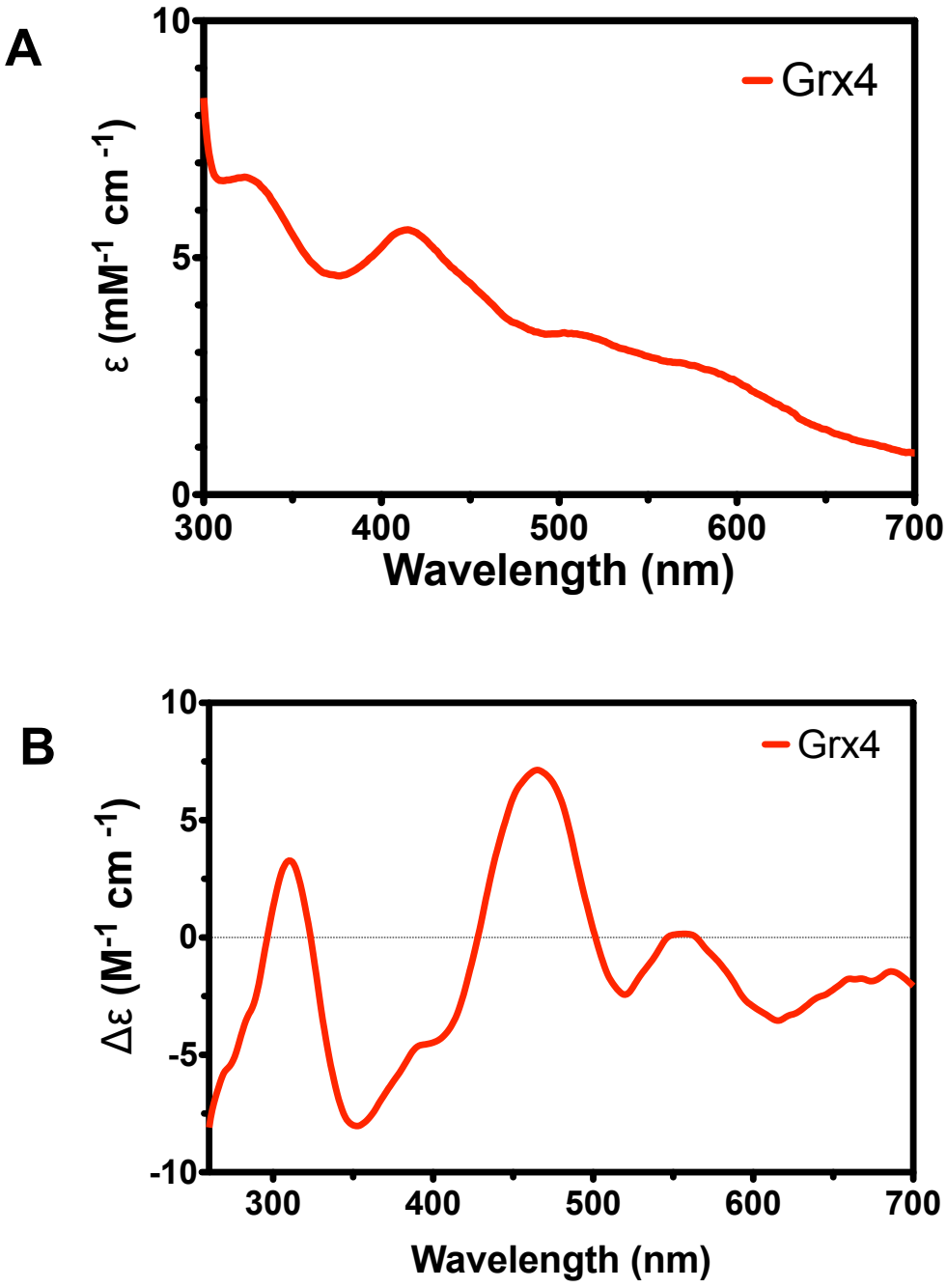

Figure 5.5 (A) UV-visible absorption and (B) CD spectra of purified reconstituted *E. coli* Grx4.

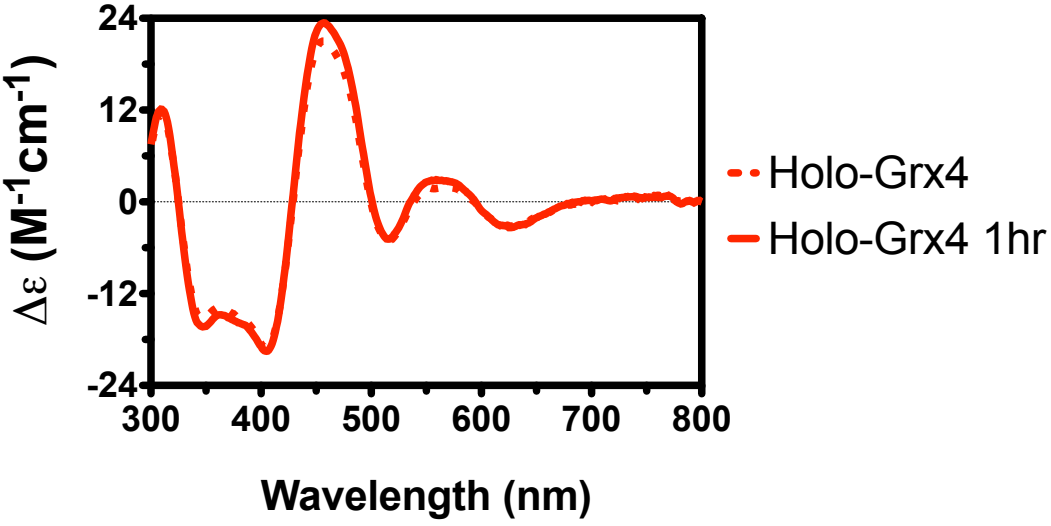

Figure 5.6 (A) CD-monitored spectra of purified reconstitution *E. coli* Grx4.

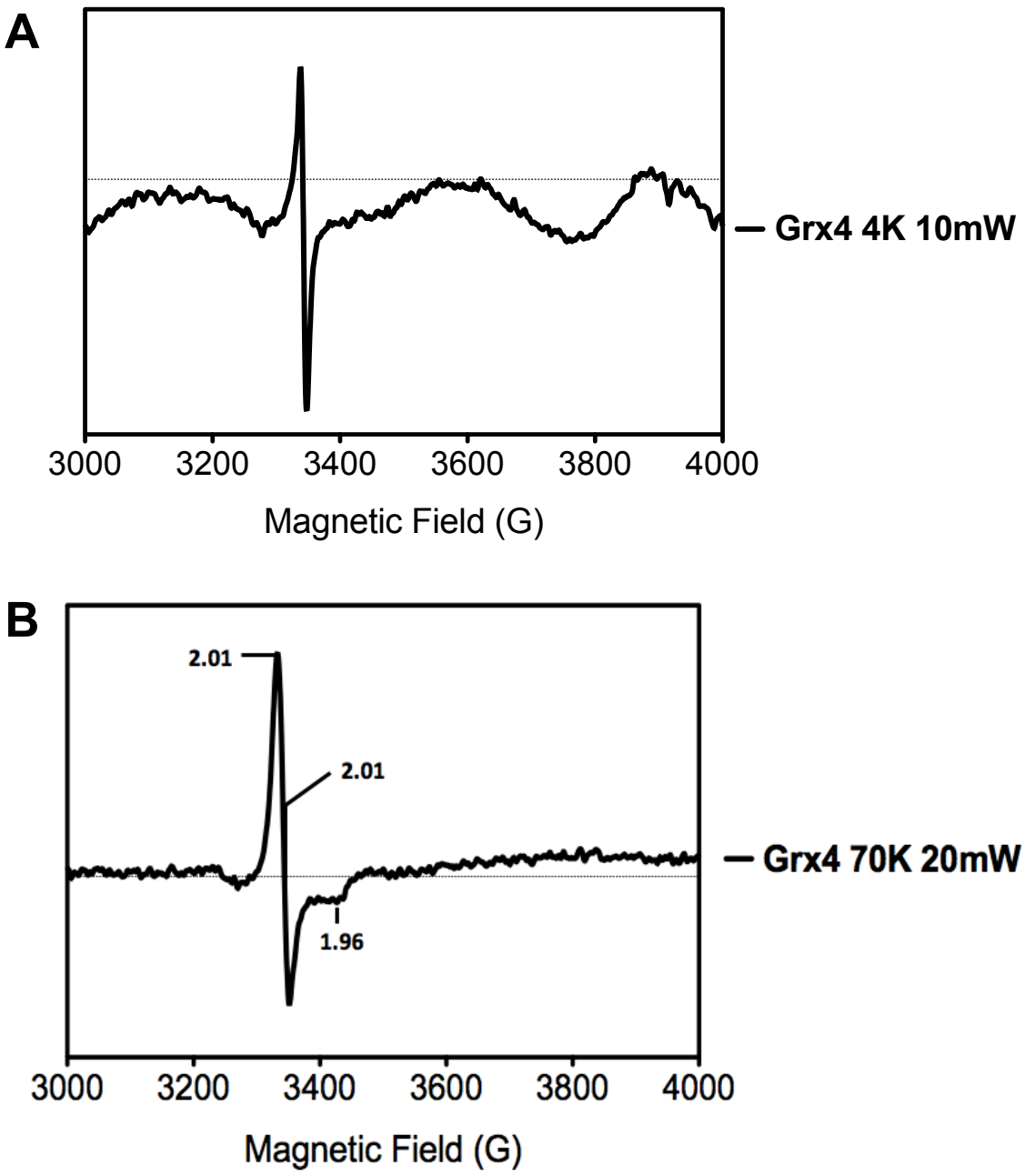

Figure 5.7 (A) Comparison of EPR spectra of [2Fe-2S] cluster of *E. coli* Grx4.

[2Fe-2S] cluster transport between E. coli Grx4

The CD spectra of [2Fe-2S] Grx4 shows a decrease in the 450 nm region in the presence of apo-ErpA suggesting that the cluster may partially be transferred to apo-ErpA (Figure 5.8 A). The overall change in CD spectra shows that 90 % of cluster can be transferred to apo-ErpA. A one-phase association curve provided a 0.9946 correlation coefficient and a K value of 0.1032. The concentration of cluster (M^{-1}) was used in order to calculate the K_{on} value of 2580 M^{-1} cm^{-1} (Figure 5.8 A). The overall change in the CD spectra shows that holo-Grx4 preferentially transfers its [2Fe-2S] cluster to IscA after 20 minutes. A one-phase association curve provided a 0.9976 correlation coefficient and a K value of 0.1729. The concentration of cluster (M^{-1}) was used in order to calculate the K_{on} value of 4323 M^{-1} cm^{-1} (Figure 5.8 B). The transfer to apo-SufA was also fit to a one-phase association curve with a correlation coefficient of 0.9941 and K value of 0.1394. The concentration of cluster (M^{-1}) was used in order to calculate the K_{on} value of 3485 M^{-1} cm^{-1} (Figure 5.8 C). The maximum percentage of transfer to apo-IscA is 100 %, 80 % to apo-SufA, and 90 % to apo-ErpA after 40 minutes (Figure 5.8).

In order to determine whether this process was bi-directional, the transfer was monitored in the reverse direction. The CD spectra of holo-ErpA did not change indicating that it was not able to transfer its cluster to apo-Grx4 (figure 5.9 A). No model provided accurate fitting and kinetic analysis was not obtained. Kinetic analysis using an association then dissociation curve of holo-IscA to apo-Grx4 resulted in a 0.9569 correlation coefficient. Also, holo-IscA was able to transfer a maximum of 9 % of its cluster to apo-Grx4 after 30 minutes (figure 5.9 B). While, holo-SufA did not show a linear increase in its CD spectra in the 450 nm region, but did show a decrease in the 320 nm region. This

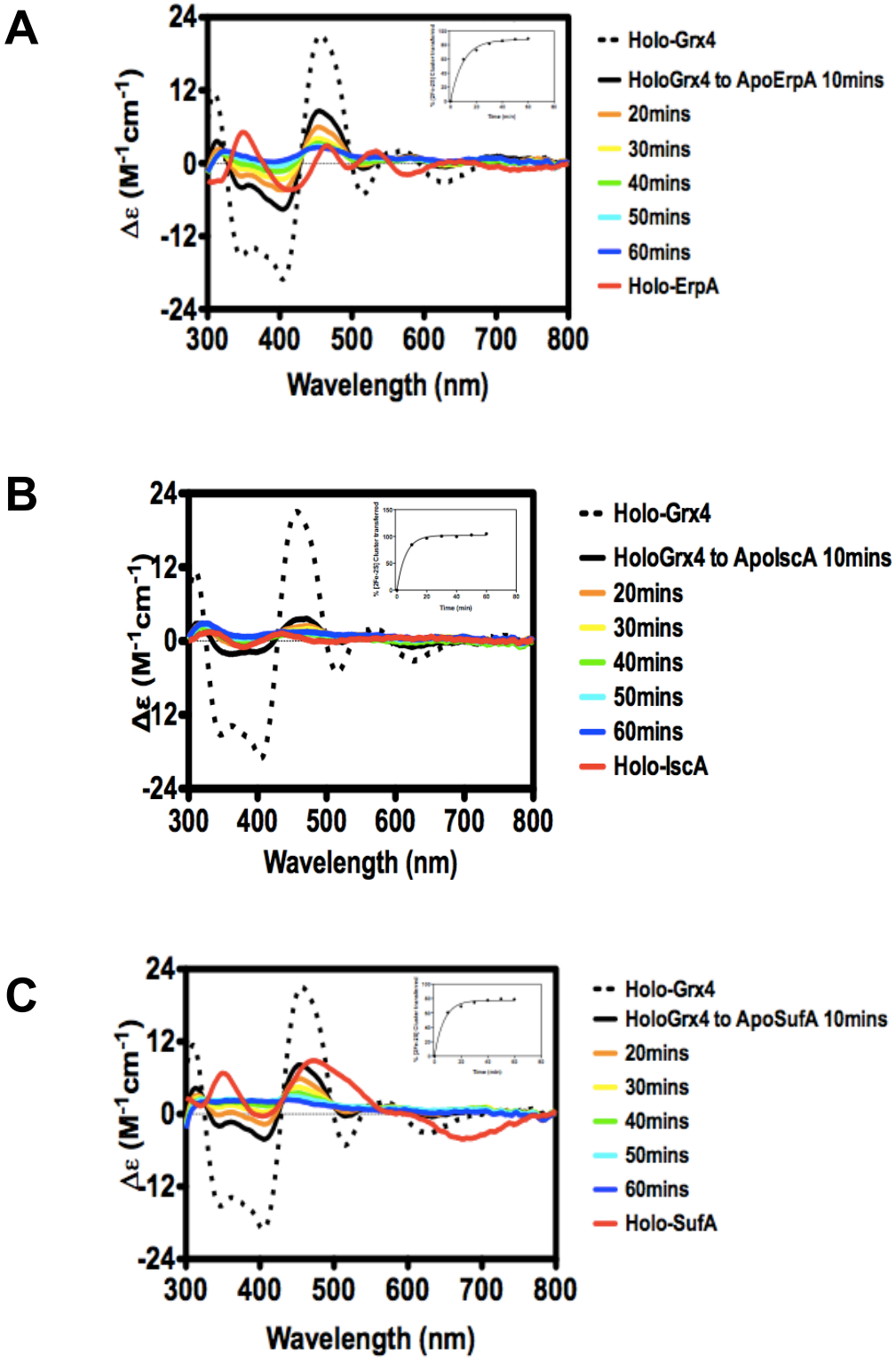

Figure 5.8 CD-monitored spectra of holo-Grx4 to (A) apo-ErpA, (B) apo-IscA, and (C) apo-SufA.

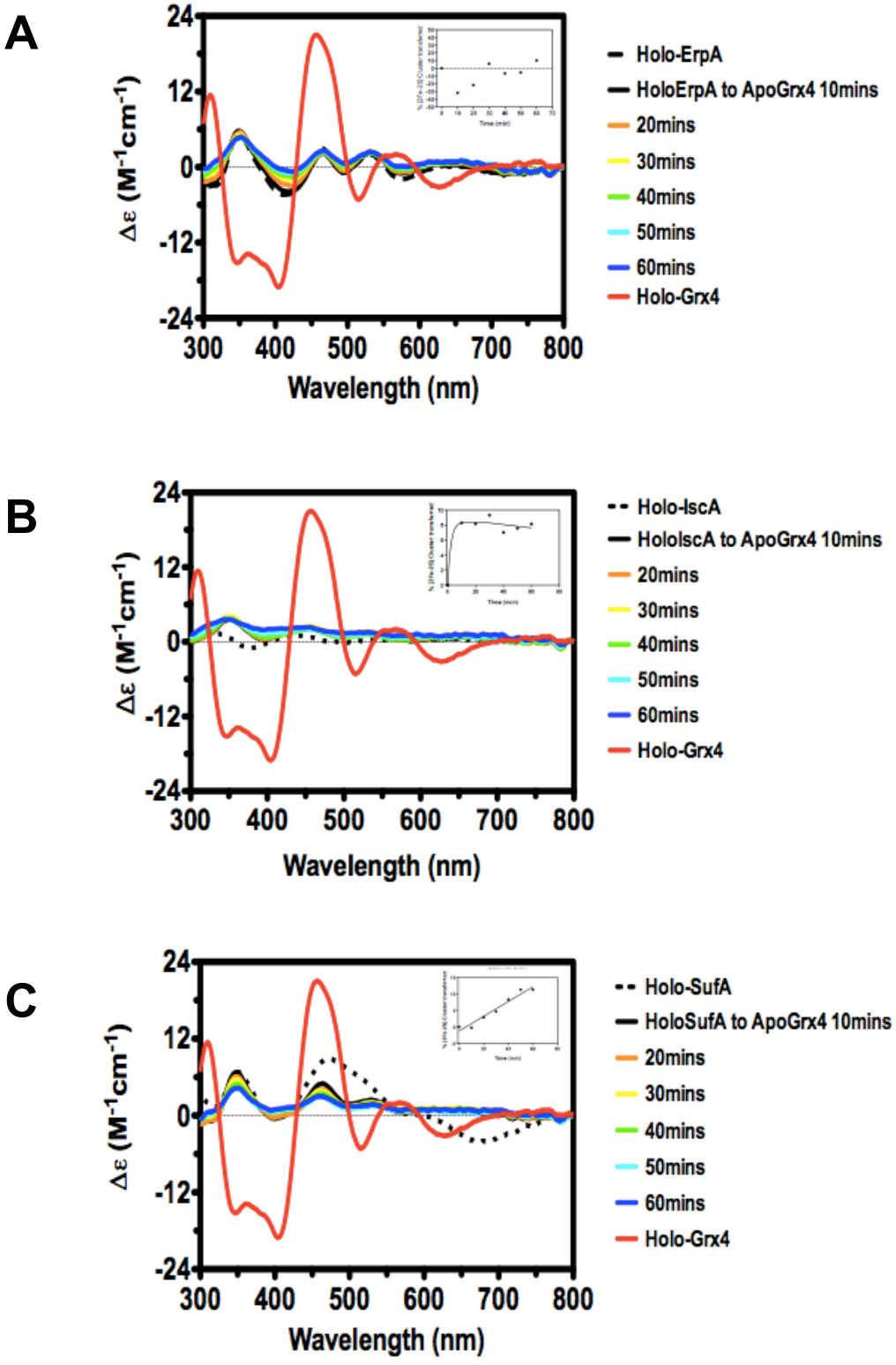

Figure 5.9 (A) CD-monitored spectra of (A) holo-ErpA, (B) holo-IscA, and (C) holo-SufA to apo-Grx4.

suggests that if holo-SufA can transfer its cluster to apo-Grx4 it is at low levels of 10 % after 60 minutes (Figure 5.9 C). No model provided accurate fitting and kinetic analysis was not obtained.

DISCUSSION

E. coli Grx4 has been previously shown to coordinate a [2Fe-2S] cluster (Dlouhy et al., 2016). Plant chloroplast *Arabidopsis thaliana (At)* GrxS14 can transfer virtually all of its [2Fe-2S] cluster to the *Arabidopsis thaliana* SufA in less than 3 minutes. The nitrogen fixation bacteria *Azotobacter vinelandii* Grx-nif can also transfer most of its [2Fe-2S] cluster to the *Azotobacter vinelandii* IscA. The rate of transfer to IscA occurs at a slower rate (Mapolelo et al., 2013). Both monothiol glutaredoxins found in plant chloroplast (GrxS14) and yeast *Saccharomyces cerevisiae* (Grx3) can transfer its cluster to the bacterial *Azotobacter vinelandii* IscA at a faster rate similar to that observed with *At* GrxS14 and *At* IscA. Similarly, our results show that *E. coli* Grx4 preferentially transfers its [2Fe-2S] cluster to apo-IscA but at a slower rate when compared to those published for *Arabidopsis thaliana (At)* GrxS14. This may be explained by incomplete reduction to apo-proteins preventing rapid transfer. Our results show that the transfer process between the A-type carrier proteins ErpA, IscA, and SufA to *E. coli* Grx4 are not bidirectional. This result is expected and is supported by the lack of cluster transfer to other monothiol glutaredoxins from reconstituted bacterial *Azotobacter vinelandii* IscA (Mapolelo et al., 2013).

REFERENCES

1. Abbaspour, N., Hurrell, R., and Kelishadi, R. (2014) Review on iron and its importance for human health. *J Res Med Sci* **19:** 164-174.

2. Aletras, V., Karaliota, A., Kamariotaki, M., Hatzipanayioti, D., and Hadjiliadis, N. (2001) Interaction of Ni(II) with 2, 3-dihydroxybenzoic acid. *Inorganica Chimica Acta* **312:** 151-162.

3. Alvarez, A., Saez, J.M., Davila Costa, J.S., Colin, V.L., Fuentes, M.S., Cuozzo, S.A., Benimelli, C.S., Polti, M.A., and Amoroso, M.J. (2017) Actinobacteria: current research and perspectives for bioremediation of pesticides and heavy metals. *Chemosphere.* **166:** 41-62.

4. Anahida, S., Yaghmaei, S., and Ghobadinejad, Z. (2011) Heavy metal tolerance of fungi. *Science Iranica* **C18:** 502-508.

5. Anbar, A. D. (2008) Oceans, Elements, and Evolution. *Science* **322**: 1481-1483.

6. Anbar, A. D., Duan, Y., Lyons, T. W., Arnold, G. L., Kendall, B., Creaser, R. A., Kaufman, A. J., Gordon, G. W., Scott, C., Garvin, J., and Buick, R. (2007) A whiff of oxygen before the Great Oxidation Event? Science **317:** 1903-1906.

7. Andrews, S.C., Robinson, A.K., and Rodriguez-Quinones, F. (2003) Bacterial iron homeostasis. *FEMS Microbiol Rev* **27:** 215-237.

8. Angerer, A., Enz, S., Ochs, M., and Braun, V. (1995) Transcriptional regulation of ferric citrate transport in *Escherichia coli* K-12. FecI belongs to a new sub-family of sigma 70–type factors that respond to extracytoplasmic stimuli. *Mol Microbiol* **19:** 163-174.

9. Ansari, M. and Malik, A. (2010) Seasonal variation of different microorganisms with nickel and cadmium in the industrial wastewater and agricultural soils. *Environ Monit Assess* **167:** 151-163.

10. Arnow, L.E. (1937) Colorimetric determination of the components of 3,4-dihydroxyphenylalanine-tyrosine mixtures. *J Biol Chem* **118:** 531-537.

11. Bandyopadhyay, S., Gama, F., Molina-Navarro, M.M., Gualberto, J.M., Claxton, R., Naik, S.G., Huynh, B.H., Herrero, E., Jacquot, J.P., Johnson, M.K., and Rouhier, N. (2008) Chloroplast monothiol glutaredoxins as scaffold proteins for the assembly and delivery of [2Fe-2S] clusters. *EMBO J* **27:** 1122-1133.

12. Baranyi, J. and Roberts, T.A. (1994). A dynamic approach to predicting bacterial growth in food. *Int J Food Microbiol* **23:** 277-294.

13. Blanc, B., Gerez, C., and Ollagnier de Choudens, S. (2015) Assembly of Fe/S proteins in bacterial systems: biochemistry of the bacterial ISC system. *Biochim Biophys Acta* **1853:** 1436-1447.

14. Bleuel, C., Grosse, C., Taudte, N., Scherer, J., Wesenberg, D., Krauss, G.J., Nies, D.H., and Grass, G. (2005) TolC is involved in enterobactin efflux across the outer membrane of *Escherichia coli*. *J Bacteriol* **187:** 6701-6707.

15. Bolton, E.T., Cowie, D.B., and Sands, M.K. (1951) Sulfur metabolism in *Escherichia coli. J Bacteriol* **63:** 309-318.

16. Boyd, E.S., Thomas, K.M., Dai, Y., Boyd, J.M., and Outten, F.W. (2014) Interplay between oxygen and Fe-S cluster biogenesis: insights from the Suf pathway. *Biochemistry* **53:** 5834-5847.

17. Braud, A., Geoffroy, V., Hoegy, F., Mislin, G.L., and Schalk, I.J. (2010) Presence of the siderophores pyoverdine and pyochelin in the extracellular medium reduces toxic metal accumulation in *Psuedomonas aeruginosa* and increases bacterial metal tolerance. *Environ Microbiol Rep* **2:** 419-425.

18. Braud, A., Hannauer, M., Mislin, G.L., and Schalk, I.J. (2009) The Pseudomonas aeruginosa pyochelin-iron uptake pathway and its metal specificity. *J Bacteriol* **191:** 3517-3525.

19. Braud, A., Hoegy, F., Jezequel, K., Lebeau, T., and Schalk IJ. (2009) New insights into the metal specificity of the Pseudomonas aeruginosa pyoverdine-iron uptake pathway. *Environ Microbiol* **11**: 1079-1091.

20. Braun, V. (1995) Energy-coupled transport and signal transduction through the gram-negative outer membrane via TonB-ExbB-ExbD-dependent receptor proteins. *FEMS Microbiol Rev* **16:** 295–307.

21. Braun, V., Mahren, S., and Ogierman, M. (2003) Regulation of the FecI-type ECF sigma factor by transmembrane signaling. *Curr Opin Microbiol* **6:** 173-180.

22. Bravo, A. and Anacona, J.R. (1998) Synthesis and characterization of metal complexes with ampicillin. *J Coordination Chem* **44:** 173-182.

23. Brickman, T.J. and McIntosh, M.A. (1992) Overexpression and purification of ferric enterobactin esterase from *Escherichia coli*. Demonstration of enzymatic hydrolysis of enterobactin and its iron complex. *J Biol Chem* **267:** 12350-12355.

24. Brown, N.C., Eliasson, R., Reichard, P., and Thelander, L. (1969) Spectrum and iron content of protein B2 from ribonucleoside diphosphate reductase. *European J Biochem* **9:** 512-518.

25. Bryce, G.F. and Brot, N. (1975) Enzymic synthesis of the cyclic trimer of 2,3-dihydroxy-N-benzoyl-L-serine in *Escherichia coli*. *Biochemistry* **11:** 1708-1715.

26. Butland, G., Babu, M., Diaz-Mejia, J. J., Bohdana, F., Phanse, S., Gold, B., Yang, W., Li, J., Gagarinova, A. G., Pogoutse, O., Mori, H., Wanner, B. L., Lo, H., Wasniewski, J., Christopolous, C., Ali, M., Venn, P., Safavi-Naini, A., Sourour, N., Caron, S., Choi, J. Y., Laigle, L., Nazarians-Armavil, A., Deshpande, A., Joe, S., Datsenko, K. A., Yamamoto, N., Andrews, B. J., Boone, C., Ding, H., Sheikh, B., Moreno-Hagelseib,

G., Greenblatt, J. F., and Emili, A. (2008) eSGA: *E. coli* synthetic genetic array analysis. *Nature Methods 5*, 789−795.

27. Caza, M., Lepine, F., and Dozois, C.M. (2011) Secretion, but not overall synthesis of catecholate siderophores contributes to virulence of extraintestinal pathogenic *Escherichia coli. Mol Microbiol* **80:** 266-282.

28. Chahal H. K., Dai Y., Saini A., Ayala-Castro C., and Outten F. W. (2009) The $SufBC_2D$ Fe-S scaffold complex interacts with SufA for Fe-S cluster transfer. *Biochemistry* **48:** 10644-10653.

29. Chahal, H.K. and Outten, F.W. (2012) Separate Fe-S scaffold and carrier functions for $SufB_2C_2$ and SufA during *in vitro* maturation of [2Fe-2S] Fdx. *J Inorg Biochem* **116C:** 126-134.

30. Chaturvedi, K.S., Hung, C.S., Crowley, J.R., Stapleton, A.E., and Henderson, J.P. (2012) The siderophore yersiniabactin binds copper to protect pathogens during infection. *Nat Chem Biol* **8:** 731-736.

31. Chen, Y., Jurkevitch, E., Bar-Ness, E., and Hadar, Y. (1993) Stability constants of pseudobactin complexes with transition metals. *Soil Sci Soc Am J* **58:** 390-396.

32. Couturier, J., Koh, C.S., Zaffagnini, M., Winger, A.M., Gualberto, J.M., Corbier, C., Decottignies, P., Jacquot, J.P., Lemaire, S.D., Didierjean, C., and Rouhier, N. (2009) Structure-function relationship of the chloroplastic glutaredoxin S12 with an atypical WCSYS active site. *J Biol Chem* **284:** 9299-9310.

33. Couturier, J., Stroher, E., Albetel, A.N., Roret, T., Muthuramalingam, M., Tarrago, L., Seidel, T., Tsan, P., Jacquot, J.P., Johnson, M.K. Dietz, K., Didierjean, C., and Rouhier, N. (2011) *Arabidopsis* chloroplastic glutaredoxin C5 as a model to explore molecular determinants fro iron-sulfur cluster binding into glutaredoxins. *J Biol Chem* **286:** 27515-27527.

34. Crosa, J. H. (1997) Signal transduction and transcriptional and posttranscriptional control of iron-regulated genes in bacteria. *Microbiol Mol Biol Rev* **61:** 319-336.

35. Crosa, J.H. and Walsh, C.T. (2002) Genetics and assembly line enzymology of siderophore biosynthesis in bacteria. *Microbiol Mol Biol Rev* **66:** 223-249.

36. Cupp-Vickery, J.R., Silberg, J.J., Ta, D.T., and Vickery, L.E. (2004) Crystal structure of IscA, an iron-sulfur cluster assembly protein from *Escherichia coli. J Mol Biol* **338:** 127-137.

37. Cupp-Vickery, J.R., Urbina, H., and Vickery, L.E. (2003) Crystal structure of IscS, a cysteine desulfurase from *Escherichia coli. J Mol Biol* **330:** 1049-1059.

38. Das, K.K., Das, S.N., and Dhundasi, S.A. (2008) Nickel, its adverse health effects and oxidative stress. *Ind J Med Res* **128:** 412-425.

39. De Pina, K., Desjardin, V., Mandrand-Berthelot, M., Giordano, G., and Wu, L. (1999) *J Bacteriol* **181:** 670-674.

40. Demple, B. (2002) Signal transduction by nitric oxide in cellular stress responses. *Mol Cell Biochem* **37:** 11-18.

41. Denkhaus, E. and Salnikow, K. (2002) Nickel essentiality, toxicity, and carcinogenicity. *Critical Rev Oncology Hematology* **42:** 35-56.

42. Ding, H. and Clark, R.J. (2004) Characterization of iron binding in IscA, an ancient iron-sulphur cluster assembly protein. *Biochem J* **379:** 433-440.

43. Ding, H., Clark, R.J., and Ding, B. (2004) IscA mediates iron delivery for assembly of iron-sulfur clusters in IscU under the limited accessible free iron conditions. *J Biol Chem* **279:** 37499-37504.

44. Dixit, R., Wasiullah, Malaviya, D., Pandiyan, K., Sing, U.B., Sahu, A., Shukla, R., Singh, B.P., Rai, J.P., Sharma, P.K., Lade, H., and Paul, D. (2015) Bioremediation of heavy metals from soil and aquatic environment: an overview of principles and criteria of fundamental processes. *Sustainability.* **7:** 2189-2212.

45. Dlouhy, A.C., Li, H., Albetel, A., Zhang, B., Mapolelo, D.T., Randeniya, S., Holland, A.A., Johnson, M.J., and Outten, C.E. (2016) The *Escherichia coli* BolA protein IbaG forms a histidine-ligated [2Fe-2S]-bridged complex with Grx4. *Biochemistry* **55:** 6869-6879.

46. Duhme, A.K., Hider, R.C., Naldrett, M.J., and Pau, R.N. (1998) The stability of the molybdenum-azotochelin complex and its effect on siderophore production in *Azotobacter vinelandii. J Biol Inorganic Chem.* **3:** 520-552.

47. Ehmann, D.E., Shaw-Reid, C.A., Losey, H.C., and Walsh, C.T. (2000) The EntF and EntE adenylation domains of *Escherichia coli* enterobactin synthetase: Sequestration and selectivity in acyl-AMP transfers to thiolation domain cosubstrates. *Proc Natl Acad Sci USA* **97:** 2509-2514.

48. Ehrenberg, A., and Reichard, P. (1972) Electron spin resonance of the iron-containing protein B2 from ribonucleotide reductase. *J Biol Chem* **247:** 3485-3488.

49. Entner, N. and Doudoroff, M. (1952) Glucose and gluconic acid oxidation of *Pseudomonas saccharophila*. *J Biol Chem* **196:** 853-862.

50. Enz, S., Braun, V., and Crosa, J. (1995) Transcription of the region encoding the ferric dicitrate-transport system in *Escherichia coli*: similarity between promoters for *fecA* and for extracytoplasmic function sigma factors. *Gene* **163:** 13-19.

51. Escolar, L., Perez-Martin, J., and de Lorenzo, V. (1998) Coordinated repression in vitro of the divergent *fepA-fes* promoters of *Escherichia coli* by the iron uptake regulation (Fur) protein. *J Bacteriol* **180:** 2579-2582.

52. Feng, Y., Zhong, N., Rouhier, N., Hase, T., Kusunoki, M., Jacquot, J.P., Jin, C., and Xia, B. (2006) Structural insight into poplar glutaredoxin C1 with bridging iron-sulfur cluster at the active site. *Biochemistry* **45:** 7998-8008.

53. Fenton, H.J.H. (1876) On a new reaction of tartaric acid. *Chem News* **33:** 190.

54. Fenton, H.J.H. (1894) The oxidation of tartaric acid in presence of iron. *J Chem Soc Proc* **10:** 157-158.

55. Fenton, H.J.H. (1896) Constitution of a new dibasic acid, resulting from the oxidation of tartaric acid. *J Chem Soc Trans* **69:** 546-562.

56. Ferguson, A.D., Hofmann, E., Coulton, J.W., Diederichs, K., and Welte, W. (1998) Siderophore-mediated iron transport: crystal structure of FhuA with bound lipopolysaccharide. *Science* **282:** 2215-2220.

57. Fernandes A.P. and Holmgren, A. (2004) Glutaredoxins: glutathione-dependent redox enzymes with functions far beyond a simple thioredoxin backup system. *Antioxidants Redox Signaling* **6:** 63-74.

58. Flint, D.H. (1993) *Escherichia coli* Fumarase A catalyzes the isomerization of enol and keto oxalacetic acid. *Biochemistry* **32:** 799-805.

59. Flint, D.H., Emptage, M.H., and Guest, J.R. (1992) Fumarase A from *Escherichia coli:* purification and characterization as an iron-sulfur cluster containing enzyme. *Biochemistry* **31:** 10331-10337.

60. Fontecave, M. (2006) Iron-sulfur clusters: ever-expanding roles. *Nat Chem Biol* **2:** 171-174.

61. Furrer, J.L., Sanders, D.N., Hook-Barnard, I.G., and McIntosh, M.A. (2002) Export of the siderophore enterobactin in *Escherichia coli*: involvement of a 43 kDa membrane exporter. *Mol Microbiol* **44:** 1225-1234.

62. Gault, M., Effantin G., and Rodrigue, A. (2016) Ni exposure impacts the pool of free fe and modifies DNA supercoiling via metal-induced oxidative stress in *Escherichia coli* K-12. *Free Radic Biol Med* **97:** 351-361.

63. Gehring, A.M., Bradley, K.A., and Walsh, C.T. (1997) Enterobactin biosynthesis in *Escherichia coli*: isochorismate lyase (EntB) is a bifunctional enzyme that is

phosphopantetheinylated by EntD and then acylated by EntE using ATP and 2,3-dihydroxybenzoate. *Biochemistry* **36:** 8495-8503.

64. Gehring, A.M., Mori, I., and Walsh, C.T. (1998) Reconstitution and characterization of the *Escherichia coli* enterobactin synthetase from EntB, EntE, and EntF. *Biochemistry* **37:** 2648- 2659.

65. Giel, J.L., Rodionov, D., Liu, M., Blattner, F.R., and Kiley, P.J. (2006) IscR-dependent gene expression links iron-sulphur cluster assembly to the control of O_2-regulated genes in *Escherichia coli*. *Mol Microbiol* **60:** 1058–1075.

66. Greenwood, K.T., and Luke, R.K. (1978) Enzymatic hydrolysis of enterochelin and its iron complex in *Escherichia coli* K-12. Properties of enterochelin esterase. *Biochim Biophys Acta.* **525:** 209-218.

67. Gupta, V., Sendra, M., Naik, S.G., Chahal, H.K., Huynh, B.H., Outten, F.W., Fontecave, M., and Ollagnier-de-Choudens, S. (2009) Native *Escherichia coli* SufA, coexpressed with $SufBC_2D$, purifies as a [2Fe-2S] protein and acts as an Fe-S transporter to Fe-S target enzymes. *J Am Chem Soc* **131:** 6149-6153.

68. Haber, F. and Weiss, (1932) J. Über die Katalyse des Hydroperoxydes. *Naturwiss* **51:** 948-950.

69. Hantke, K. (1990) Dihydroxybenzolyserine—a siderophore for *E. coli. FEMS Microbiol Lett* **67:** 5-8.

70. Harle, C., Kim, I., Angerer, A., and Braun, V. (1995) Signal transfer through three compartments: transcription initiation of *Escherichia coli* ferric dicitrate transport system from the cell surface. *EMBO J.* **14:** 1430-1438.

71. Harrison, F. and Bucking, A. (2009) Siderophore production and biofilm formation as linked traits. *ISME J* **3:** 632-634.

72. Herrero, E., Torre-Ruiz, M.A. (2007) Monothiol glutaredoxins: a common domain for multiple functions. *Cell Mol Life Sci 64:* 1518-1530.

73. Hoff, K.G., Silberg, J.J., Vickery, L.E. (2000) Interaction of the iron-sulfur cluster assembly protein IscU with the Hsc66/Hsc20 molecular chaperone system of *Escherichia coli. Proc Natl Acad Sci USA* **97:** 7790-7795.

74. Hu, X. and Boyer, G.L. (1996) Siderophore-mediated aluminum uptake by *Bacillus magaterium* ATCC 19213. *Appl Environ Microbiol.* **62:** 4044-4048.

75. Hunsicker-Wang, L.M., Heine, A., Chen, Y., Luna, E.P., Todaro, T., Zhang, Y.M., Williams, P.A. McRee, D.E., Hirst, J., Stout, C.D., and Fee, J.A. (2003) High-resolution structure of the soluble, respiratory-type Rieske protein from *Thermus thermophiles:* analysis and comparison. *Biochemisry* **42:** 7303-7317.

76. Hunt, M.D., Pettis, G.S., and McIntosh, M.A. (1994) Promoter and operator determinants for fur-mediated iron regulation in the bidirectional *fepA-fes* control region of the *Escherichia coli* enterobactin gene system. *J Bacteriol* **176:** 3944-3955.

77. Ilbert, M. and Bonnefov, V. (2013) Insight into the evolution of the iron oxidation pathways. *Biochim Biophys Acta* **1827:** 161-175.

78. Imlay, J. (2015) Diagnosing oxidative stress in bacteria: not as easy as you might think. *Curr Opin Microbiol* **24:** 124-131.

79. Irving, H. and Williams, R.J.P. (1953) The stability of transition-metal complexes. *J Chem Soc* **0:** 3192-3210.

80. Itoh, Y., Sugita-Konishi, Y., Kasuga, F., Iwaki, M., Hara-Kudo, Y., Saito, N., Noguchi, Y., Konuma, H., and Kumagai, S. (1998) Enterohemorrhagic *Escherichia coli* O157: H7 present in radish sprouts. *Appl Environ Microbiol* **64:** 1532-1535.

81. Iwema, T., Picciocchi, A., Traore, D.A.K., Ferrer, J., Chauvat, F., and Jacquamet, L. (2009) Structural basis for deleivery of the intact [Fe2S2] cluster by monothiol glutaredoxin. *Biochemistry* **48:** 6041-6043.

82. Iwig, J.S., Rowe, J.L., and Chivers, P.T. (2006) Nickel homeostasis in *Escherichia coli* – the RcnR-RcnA efflux pathway and its linkage to NikR function. *Mol Microbiol* **62:** 252-262.

83. Johansson, C., Kavanagh, K.L., Gileadi, O., and Oppermann, U. (2007) Reversible sequestration of active site cysteines in a 2Fe-2S-bridged dimer provides a mechanism for glutaredoxin 2 regulation in human mitochondria. *J Biol Chem* **282:** 3077-3082.

84. Johnson, D.C., Dean, D.R., Smith, A.D., and Johnson, M.K. (2005) Structure, function, and formation of biological iron-sulfur clusters. *Annu Rev Biochem* **74:** 247-281.

85. Johnson, D.C., Unciuleac, M.C., and Dean, D.R. (2006) Controlled expression and functional analysis of iron-sulfur cluster biosynthetic components within *Azotobacter vinelandii. J Bacteriol* **188:** 7551-7561.

86. Kambampati, R. and Lauhon, C.T. (1999) IscS is a sulfurtransferase for the in vitro biosynthesis of 4-thiouridine in Escherichia coli tRNA. Biochemistry. **38:** 16561-16568.

87. Kammler, M., Schon, C., and Hantke, K. (1993) Characterization of the ferrous iron uptake system of *Escherichia coli. J Bacteriol* **175:** 6212-6219.

88. Kashket, E.R. and Brodie, A.F. (1963) Oxidative phosphorylation in fractionated bacterial systems. *J Biol Chem* **238:** 2564-2570.

89. Kasprzak, K.S., Sunderman, F.W., Jr., and Salnikow, K. (2003) Nickel carcinogenesis. *Mutat Res.* **533:** 67-97.

90. Kawano, M., Oshima, T., Kasai, H., and Mori, H. (2002) Molecular characterization of long direct repeat (LDR) sequences expressing a stable mRNA encoding for a 35-amino-acid cell-killing peptide and a *cis*-encoded small antisense RNA in *Escherichia coli*. *Mol Microbiol* **45:** 333-349.

91. Kennedy, M.C. and Beinert, H. (1988) The state of cluster SH and S2- of aconitase during cluster interconversions and removal. A convenient preparation of apoenzyme. *J Biol Chem* **263:** 8194-8198.

92. Keseler, I.M., Collado-Vides, J., Santos-Zavaleta, A., Peralta-Gil, M., Gama-Castro, S., Muniz-Rascado, L., Bonavides-Martinez, C., Paley, S., Krummenacker M., Altman, T., Kaipa, P., Spaulding, A., Pacheco, J., Latendresse, M., Fulcher, C., Sarker, M., Shearer, A.G., Mackie, A., Paulsen, I., Gunsalus, R.P., and Karp, P.D. (2011) EcoCyc: a comprehensive database of *Escherichia coli* biology. *Nucleic Acids Res* **39:** D583-590.

93. Kiley, P.J. and Beinert, H. (2003) The role of Fe-S proteins in sensing and regulation in bacteria. *Curr Opin Microbiol* **6:** 181-185.

94. Koh, E. and Henderson, J.P. (2015) Microbial copper-binding siderophores at the host-pathogen interface. *J Biol Chem* **290:** 18967-18974.

95. Koppenol, W.H. (1993) The centennial of the Fenton reaction. *Free Radic Biol Med* **15:** 645-651.

96. Koppenol, W.H. (2001) The Haber-Weiss cycle — 70 years later, *Redox Rep* **6:** 229-234.

97. Kumar, V., Mishra, R.K., Kaur, G., and Dutta, D. (2017) Cobalt and nickel impair DNA metabolism by the oxidative stress independent pathway. *Metallomics* **9:** 1596-1609.

98. Langman, L., Young, I. G., Frost, G. E., Rosenberg, H., and Gibson, F. (1972) Enterochelin system of iron transport in *Escherichia coli*: mutations affecting ferric-enterochelin esterase. *J Bacteriol* **112:** 1142-1149.

99. Larsen, R.A., Foster-Hartnett, D., McIntosh, M.A., and Postle, K. (1997) Regions of *Escherichia coli* TonB and FepA proteins essential for *in vivo* physical interactions. *J Bacteriol* **179:** 3213-3221.

100. Lauble, H., Kennedy, M.C., Beinert, H., and Stout, C.D. (1992) Crystal structures of aconitase with isocitrate and nitroisocitrate bound. *Biochemistry* **31:** 2735-2748.

101. Layer, G., Gaddam, S.A., Ayala-Castro, C.N., Ollagnier-de Choudens, S., Lascoux, D., Fontecave, M., and Outten, F.W. (2007) SufE transfers sulfur from SufS to SufB for iron-sulfur cluster assembly. *J Biol Chem* **282:** 13342-13350.

102. Li, L., Cheng, N., Hirschi, K.D., and Wang, X. (2010) Structure of *Arabidopsis* chloroplastic monothiol glutaredoxin *At*GRXcp. *Acta Crystallogr D Biol Crystallogr* **66:** 725-732.

103. Lillig, C.H., Berndt, C., and Holmgren, A. (2008) Glutaredoxin systems. *Biochim Biophys Acta* **1780:** 1304-1317.

104. Lillig, C.H., Berndt, C., Vergnolle, O., Lonn, M.E., Hudemann, C., Bill, E., and Holmgren, A. (2005) Characterization of human glutaredoxin 2 as iron-sulfur protein: a possible role as redox sensor. *Proc Natl Acad Sci USA* **102:** 8168-8173.

105. Lin, H., Fischbach, M.A., Liu, D.R., and Walsh, C.T. (2005) In vitro characterization of salmochelin and enterobactin trilactone hydrolases IroD, IroE, and Fes. *J Am Chem Soc* **10:** 11075-11084.

106. Locher, K.P., Rees, B., Koebnik, R., Mitschler, A., Moulinier, L., Rosenbusch, J.P., Moras, D. (1998) Transmembrane signaling across the ligand-gated FhuA receptor: crystal structures of free and ferrichrome-bound states reveal allosteric changes. *Cell* **95:** 771-778.

107. Loiseau, L., Gerez, C., Bekker, M., Ollagnier-de-Choudens, S., Py, B., Sanakis, Y., Teixeira de Mattos, J., Fontecave, M., and Barras, F. (2007) ErpA, an iron-sulfur (Fe-S) protein of the A-type essential for respiratory metabolism in *Escherichia coli. Proc Natl Sci USA* **104:** 13626-13631.

108. Lu, J., Jian, J., Huang, W., Lin, H., Li, J., and Zhou, M. (2016) Experimental and theoretical identification of the Fe(VII) oxidation state in FeO4-. *Phys Chem Chemical Phys* **18:** 31125-31131.

109. Ma, L. and Payne, S.M. (2012) AhpC is required for optimal production of enterobactin by *Escherichia coli. J Bacteriol* **194:** 6748-6757.

110. Macomber, L. and Hausinger, R.P. (2011) Mechanisms of nickel toxicity in microorganisms. *Metallomics* **3:** 1153-1162.

111. Macomber, L., and Imlay, J.A. (2009) The iron-sulfur clusters of dehydratases are primary intracellular targets of copper toxicity. *Proc Natl Acad Sci USA* **20:** 8344-8349.

112. Macomber, L., Elsey, S.P., Hausinger, R.P. (2011) Fructose-1, 6-bisphosphate aldolase (class II) is the primary site of nickel toxicity in *Escherichia coli*. *Mol Microbiol* **82:** 1291-1300.

113. Mansy, S.S., Wu, G., Surerus, K.K., and Cowan, J.A. (2002) Iron-sulfur cluster biogenesis *Thermatoga maritima* IscU is a structured iron-sulfur cluster assembly protein. *J Biol Chem* **227:** 21397-21404.

114. Mapolelo, D.T., Zhang, B., Naik, S.G., Huynh, B.H., and Johnson, M.K. (2012) Spectroscopic and functional characterization of iron-sulfur cluster bound forms of *Azotobacter vinelandii* (Nif) IscA. *Biochemistry* **51:** 8071-8084.

115. Mapolelo, D.T., Zhang, B., Randeniya, S., Albetel, A., Li, H., Couturier, J., Outten, C.E., Rouhier, N., and Johnson, M.K. (2013) Monothiol glutaredoxins and A-type proteins: partners in Fe-S cluster trafficking. *Dalton Trans.* **42:** 3107-3115.

116. Marti, S., Chabane, Y.N., Alexandre, S., Coquet, L., Vila, J., Jouenne, T., and De, E. (2011) *PLOS One* 6(10): e26030.

117. McCandliss, R.J. and Herrmann, K.M. (1978) Iron, an essential element for biosynthesis of aromatic compounds. *Proc Natl Sci USA* **75:** 4810-4813.

118. McCandliss, R.J., Poling, M.D., and Herrmann, K.M. (1978) 3-deoxy-d-arabino-heptulosonate 7-phosphate synthase. *J Biol Chem* **253:** 4259-4265.

119. McHugh, J.P., Rodriguez-Quinones, F., Abdul-Tehrani, H., Svistunenko, D.A., Poole, R.K., Cooper, C.E., and Andrews, S.C. (2003) Global iron-dependent gene regulation in *Escherichia coli.* A new mechanism for iron homeostasis. *J Biol Chem* **278:** 29478-29486.

120. Mehi, O., Bogos, B., Csorgo, B., Pal, F., Nyerges, A., Papp, B., and Pal, C. (2014) Pertubration of iron homeostasis promotes the evolution of antibiotic resistance. *Mol Biol Evol* **31:** 2793-2804.

121. Messenger, A.J. and Barclay, R. (1983) Bacteria, iron, and pathogenicity. *Biochem Education* **11:** 54-63.

122. Mettert, E.L. and Kiley PJ. (2014) Coordinate regulation of the Suf and Isc Fe-S cluster biogenesis pathways by IscR is essential for viability of *Escherichia coli*. *J Bacteriol* **196:** 4315-4323.

123. Mettert, E.L. and Kiley, P.J. (2015) How is Fe-S cluster formation regulated? *Annu Rev Microbiol* **69:** 505-526.

124. Miethke, M. and Marahiel, M.A. (2007) Siderophore-based iron acquisition and pathogen control. *Microbiol Mol Biol Rev* **71:** 413-451.

125. Miller, J.H. (1972). Experiments in molecular genetics. Cold Spring Harbor Laboratory, Cold Spring Harbory, NY.

126. Mukherjee, G. and Ghosh, T. (1995) Metal ion interaction with penicillins –Part VII: Mixed-ligand complex formation of cobalt (II), nickel(II), copper(II), and zinc(II) with ampicillin and nucleic bases. *J Inorg Biochem* **59:** 827-833.

127. Nishio, K. and Nakai, M. (2000) Transfer of iron-sulfur cluster from NifU to apoferredoxin. *J Biol Chem* **275:** 22615-22618.

128. Nriagu, J.O. (1980) A silent epidemic of environmental metal poisoning? *Environ Pollution* **50:** 139-161.

129. O'Brien, I.G. and Gibson, F. (1970) The structure of enterochelin and related 2,3-dihydroxy-n-benzoylserine conjugates from *Escherichia coli*. *Biochim Biophys Acta* **215:** 393-402.

130. Ochs, M., Angerer, A., Enz, S., and Braun, V. (1996) Surface signaling in transcription regulation of the ferric citrate transport system of *Escherichia coli*: mutational analysis of the alternative sigma factor FecI supports its essential role in *fec* transport gene transcription. *Mol Gen Genet* **250:** 455-465.

131. Ochs, M., Veitinger, S., Kim, I., Welz, D., Angerer, A., and Braun, V. (1995) Regulation of citrate dependent iron transport system in *Escherichia coli*: FecR is required for transcriptional activation by FecI. *Mol Microbiol* **15:** 119-132.

132. Ollagnier-de-Choudens, S., Lascoux, D., Loiseau, L., Barras, F., Forest, E., and Fontecave, M. (2003) Mechanistic studies of the SufS-SufE cysteine desulfurase: evidence for sulfur transfer from SufS to SufE. *FEBS Lett* **555:** 263-267.

133. Ollagnier-de-Choudens, S., Mattioli, T., Takahashi, Y., and Fontecave, M. (2001) Iron-sulfur cluster assembly characterizaztion of IscA and evidence for a specific and functional complex with ferredoxin. *J Biol Chem* **276:** 22604-22607.

134. Ollagnier-de-Choudens, S., Nachin, L., Sanakis, Y., Loiseau, L., Barras, F., and Fontecave, M. (2003) SufA from *Erwinia chrysanthemi.* Characterization of a scaffold protein required for iron-sulfur cluster assembly. *J Biol Chem* **278:** 17993-18001.

135. Ollagnier-de-Choudens, S., Sanakis, Y., and Fontecave, M. (2004) SufA/IscA: reactivity studies of a class of scaffold proteins involved in [Fe-S] cluster assembly. *J Biol Inorg Chem* **9:** 828-838.

136. Outten, F.W. (2015). Recent advances in the Suf Fe-S cluster biogenesis pathway: beyond the *Proteobacteria*. *Biochim. Biophys. Acta* **1853:**1464-1469.

137. Outten, F.W., Wood, M.J., Munoz, F.M., and Storz, G. (2003) The SufE protein and the $SufBC_2D$ complex enhance SufS cysteine desulfurase activity as part of a sulfur

transfer pathway for Fe-S cluster assembly in Escherichia coli. *J Biol Chem* **278:** 45713-45719.

138. Outten. F.W., Djaman, O., and Storz, G. (2004) A *suf* operon requirement for Fe-S cluster assembly during iron starvation in *Escherichia coli*. *Mol Microbiol* **52:** 861-872.

139. Peekhaus, N. and Conway, T. (1998) What's for dinner?: Entner-Doudoroff metabolism in *Escherichia coli. J Bacteriol* **180:** 3495-3502.

140. Picciocchi, A., Saguez, C., Boussac, A., Cassier-Chauvat, C., and Chauvat, F. (2007) CGFS-type monothiol glutaredoxins from the cyanobacterium Synechocystis PCC6803 and othr evolutionary distant model organisms possess a glutathione-ligated [2Fe-2S] cluster. *Biochemistry* **46:** 15018-15026.

141. Polti, M.A., Atjian, M.C., Amoroso, M.J., and Abate, C.M. (2011) Soil chromium bioremediation: synergic activity of actinobactera and plants. *International Biodeterior Biodegrad* **65:** 1175-1181.

142. Pomposiello, P.J. and Demple, B. (2001) Redox-operated genetic switches: the SoxR and OxyR transcription factors. *Trends Biotechnol* **19:** 109-114.

143. Pressler, U., Staudenmaier, H., Zimmermann, L., and Braun, V. (1988) Genetics of the iron dicitrate transport system of *Escherichia coli. J Bacteriol* **170:** 2716-2724.

144. Py, B. and Barras, F. (2010) Building Fe-S proteins: bacterial strategies. *Nat Rev Microbiol* **8:** 436-446.

145. Py, B., Gerez, C., Huguenot, A., Vidaud, C., Fontecave, M., Ollagnier de Choudens, S., and Barras, F. (2018) The ErpA/NfuA complex builds an oxidation-resistant Fe-S cluster delivery pathway. *J Biol Chem* **293:** 7689-7702.

146. Rainnie, D.J. and Bragg, P.D. (1973) The effect of iron deficiency on respiration and energy-coupling in *Escherichia coli. J Gen Microbiol* **77:** 339-349.

147. Ranquet, C., Ollagnier-de-Choudens S., Loiseau L., Barras F., and Fontecave M. (2007) Cobalt stress in *Escherichia coli*: The effect on the iron-sulfur proteins. *J Biol Chem* **282:** 30442-30451.

148. Rasha, F.M. (2017) Intracellular siderophore detection in an Egyptian, cobalt-treated *F. solani* isolate using SEM-EDX with reference to its tolerance. *Polish J Microbiol* **66:** 235-243.

149. Ratledge, C. and Dover, L.G. (2000) Iron metabolism in pathogenic bacteria. *Annu Rev Microbiol* **54:** 881-941.

150. Ray, J.M. and Bauerle, R. (1991) Purification and properties of tryptophan-sensitive 3-deoxy-d-arabino-heptulosonate 7-phosphate synthase from *Escherichia coli. J Bacteriol* **173:** 1894-1901.

151. Riemer, J., Hoepken, H.H., Czerwinska, H., Robinson, S. R., and Dringen, R. (2004) Colorimetric ferrozine-based assay for the quantitation of iron in cultures cells. *Anal Biochem* **331:** 370-375.

152. Robbins, A.H. and Stout, C.D. (1989) Structure of activated aconitase: formation of the [4Fe-4S] cluster in the crystal. *Proc Natl Acad Sci USA* **86:** 3639-3643.

153. Robbins, A.H. and Stout, C.D. (1989) The structure of aconitase. *Proteins* **5:** 289-312.

154. Roche, B., Aussel, L., Ezraty, B., Mandin, P., Py, B., and Barras, F. (2013) Iron/sulfur proteins biogenesis in prokaryotes: formation, regulation and diversity. *Biochim Biophys Acta* **1827:** 455-469.

155. Rodriguez-Manzaneque, M.T., Tamarit, J., Belli, G., Ros, J., Herrero, E. (2002) Grx5 is a mitochondrial glutaredoxin required for the activity of iron/sulfur clusters. *Mol Biol Cell* 13: 1109-1121.

156. Rolfe, M.D., Rice, C.J., Lucchini, S., Pin, C., Thompson, A., Cameron, A.D., Alston, M., Stringer, M.F., Betts, R.P., Baranyi, J., Peck, M.W., and Hinton, J.C. (2012)

Lag phase is a distinct growth phase that prepares bacteria for exponential growth and involves transient metal accumulation. *J Bacteriol* **194:** 686-701.

157. Roth, V. (2006). Doubling Time. (http://www.doubling-time.com/compute.php

158. Rouhier, N., Unno, H., Banfyopadhyay, S., Masip, L., Kim, S.K., Hirasawa, M., Gualberto, J.M., Lattard, V., Kusunoki, M., Knaff, D.B., Georgiou, G., Hase, T., Johnson, M.K., and Jacquot, J.P. (2007) Functional, structural, and spectroscopic characterization of a glutathione-ligated [2Fe-2S] cluster in poplar glutaredoxin C1. *Proc Natl Acad Sci USA* **104:** 7379-7384.

159. Schultz-Hauser, G., Koster, W., Schwarz, H., and Braun, V. (1992) Iron (III) hydroxamate transport in *Escherichia coli* K-12: FhuB-mediated membrane association of the FhuC protein and negative complementation of fhuC mutants. *J Bacteriol* **174:** 2305-2311.

160. Schwartz, C.J., Djaman, O., Imlay, J.A., and Kiley, P.J. (2000) The cysteine desulfurase, IscS, has a major role in *in vivo* Fe-S cluster formation in *Escherichia coli*. *Proc Natl Acad Sci USA* **97:** 9009-9014.

161. Schwartz, C.J., Giel, J.L., Patschkowski, T., Luther, C., Ruzicka, F.J., Beinert, H., Kiley, and P.J. (2001) IscR, an Fe-S cluster-containing transcription factor, represses expression of *Escherichia coli* genes encoding Fe-S cluster assembly proteins. *Proc Natl Acad Sci USA* **98:** 14895-14900.

162. Semsey, S., Andersson, A.M.C., Krishna, S., Jensen, M.H., Masse, E., and Sneppen, K. (2006) Genetic regulation of fluxes: iron homeostasis of *Escherichia coli. Nucleic Acids Res* **34:** 4960-4967.

163. Seo, S.W., Kim, D., Latif, H., O'Brien, E.J., Szubin, R., and Palsson, B.O. (2014) Deciphering Fur transcriptional regulatory network highlights its complex role beyond iron metabolism in *Escherichia coli. Nat Commun* **5:** 4910.

164. Shaw-Reid, C.A., Kelleher, N.L., Losey, H.C., Gehring, A.M., Berg, C., and Walsh, C.T. (1999) Assembly line enzymology by multimodular nonribosomal peptide

synthetases: the thioesterase domain of *E. coli* EntF catalyzes both elongation and cyclolactonization. *Chem Biol* **6**: 385-400.

165. Singh, H., Dai, Y., Outten, F.W., and Busenlehner, L.S. (2013) *Escherichia coli* SufE sulfur transfer protein modulates the SufS cysteine desulfurase through allosteric conformational dynamics. *J Biol Chem* **288:** 36189-36200.

166. Smith, A.D., Agar, J.N., Johnson, K.A., Frazzon, J., Amster, I.J., Dean, D.R., and Johnson, M.K. (2001) Sulfur transfer from IscS to IscU: the first step in iron-sulfur cluster biosynthesis. *J Am Chem Soc* **123:** 11103-11104.

167. Smith, A.D., Frazzon, J., Dean, D.R., and Johnson, M.K. (2005) Role of conserved cysteines in mediating sulfur transfer from IscS to IscU. *FEBS Lett* **579:** 5236-5240.

168. Solomon, E.B., Yaron, S., and Matthews, K.R. (2002) Transmission of *Escherichia coli* O157:H7 from contaminated manure and irrigation water to lettuce plant tissue and its subsequent internalization. *Appl Environ Microbiol* **68:** 397-400.

169. Staudenmaier, H., Van Hove, B., Yaraghi, Z., and Braun, V. (1989) Nucleotide sequences of the fecBCDE genes and locations of the proteins suggest a periplasmic-binding-protein-dependent transport mechanism for iron (III) dicitrate in *Escherichia coli. J Baceteriol* **171:** 2626-2633.

170. Stephens, C.M. and Bauerle, R. (1991) Analysis of the metal requirement of 3-deoxy-d-arabino-heptulosonate 7-phosphate synthase from *Escherichia coli. J Biol Chem* **266:** 20810-20817.

171. Takahashi, Y., Tokumoto, U. (2002) A third bacterial system for the assembly of iron–sulfur clusters with homologs in archaea and plastids, *J Biol Chem* **277:** 28380-28383.

172. Tseng, B.S., Zhang, W., Harrison, J.J., Quach, T.P., Song, J.L., Penterman, J., Singh, P.K., Chopp, D.L., Packman, A.I., and Parsek, M.R. (2013) The extracellular matrix protects *Pseudomonas aeruginosa* biofilms by limiting the penetration of tobramycin. *Environ Microbiol* **15:** 2865-2878.

173. Urbina, H.D., Silberg, J.J., Hoff, K.G., and Vickery, L.E. (2001) Transfer of sulfur from IscS to IscU during Fe/S cluster assembly. *J Biol Chem* **276:** 44521-6

174. Van Elsas, J.D., Semenov, A.V., Costa, R., and Trevors, J.T. (2011) Survival of *Escherichia coli* in the environment: fundamental and public health aspects. *ISME J* **5:** 173-183.

175. Van Hove, B., Staudenmaier, H., and Braun, V. (1990) Novel two-component transmembrane transcription control: regulation of iron dicitrate transport in *Escherichia coli* K-12. *J Bacteriol* **172:** 6749-6758.

176. Vinella, D., Brochier-Armanet, C., Loiseau, L., Talla, E., and Barras, F. (2009) Iron-sulfur (Fe/S) protein biogenesis: phylogenomic and genetic studies of A-type carriers. *PLOS Genet* **5:** e1000497.

177. Visca, P., Colotti, G., Serino, L., Verzili, D., Orsi, N., and Chiancone, E. (1992) Metal regulation of siderophore synthesis in *Pseudomonas aeruginosa* and functional effects of siderophore-metal complexes. *Appl Environ Microbiol* **58:** 2886-2893.

178. Vranish, J.N., Das, Deepika, Barondeau, D.P. (2016) Real-time kinetic probes support monothiol glutaredoxins as intermediate carriers in Fe-S cluster biosynthetic pathwyas. *ACS Chem Biol 11:* 3114-3121.

179. Wada, K., Hasegawa, Y., Gong, Z., Minami, Y., Fukuyama, K., Takahashi, Y. (2005) Crystal structure of *Escherichia coli* SufA involved in biosynthesis of iron-sulfur clusters: implications for a functional dimer. *FEBS Lett* **579:** 6543-8.

180. Wade, H.E. (1952) Observations on the growth phases of *Escherichia coli*, American Type 'B'. *J Gen Microbiol* **7:** 18-23.

181. Wagegg, W. and Braun, V. (1981) Ferric citrate transport in *Escherichia coli* requires outer membrane receptor protein fecA. *J Bacteriol* **145:** 156-163.

182. Walsh, C.T., Liu, J., Rusnak, F., and Sakaitani, M. (1990) Molecular studies on enzymes in chorismate metabolism and the enterobactin biosynthetic pathway. *Chem Rev* **90:** 1105-1129.

183. Wang, W., Qiu, Z., Tan, H., Cao, L. (2014) Siderophore production by actinobacteria. *Biometals* **27:** 623-631.

184. Welz, D. and Braun, V. (1998) Ferric citrate transport of *Escherichia coli:* functional regions of the FecR transmembrane regulatory protein. *J Bacteriol* **180:** 2387-2394.

185. Winkelmann, G., Cansier, A., Beck, W., and Jung, G. (1994) HPLC separation of enterobactin amd linear 2,3-dihydroxybenzoylserine derivatives: a study on mutants of *Escherichia coli* defective in regulation (*fur*), esterase (*fes*) and transport (*fepA*). *Biometals* **7:** 149-154.

186. Wu, S. and Cowan, J.A. (2003) Iron-sulfur cluster biosynthesis. A comparative kinetic analysis of native and cys-substituted ISA-mediated $[2Fe\text{-}2S]^{2+}$ cluster transfer to an apoferredoxin target. *Biochemistry* **42:** 5784-5791.

187. Wu, S., Wu, G., Surerus, K.K., and Cowan, J.A. (2002) Iron-sulfur cluster biosynthesis. Kinetic analysis of [2Fe-2S] cluster transfer from holo IscU to apo Fd: role of redox chemistry and a conserved aspartate. *Biochemistry* **41:** 8876-8885.

188. Xu, F.F. and Imlay, J.A. (2012) Silver(I), mercury(II), cadmium(II), and zinc(I) target exposed enzymic iron-sulfur clusters when they toxify *Escherichia coli. Appl Environ Microbiol* **78:** 3614-3621.

189. Ye, J., Nadar, S.V., Li, J., and Rosen, B.P. (2014) Structure of *Escherichia coli* Grx2 in complex with glutathione: a dual-function hybrid of glutaredoxin and glutathione S-transferase. *Acta Crystallogr C Biol Crystallogr* **70:** 1907-1913.

190. Yeo, W.S., Lee, J.H., Lee, K.C., Roe, J.H. (2006) IscR acts as an activator in response to oxidative stress for the *suf* operon encoding Fe-S assembly proteins. *Mol Microbiol* **61:** 206-218.

191. Yeung, N., Gold, B., Liu, N.L., Prathapam, R., Sterling, H.J., Williams, E.R., and Butland, G. (2011) The *E. coli* monothiol glutaredoxin GrxD forms homodimeric and heterodimeric FeS cluster containing complexes. *Biochemistry* **50:** 8957-8969.

192. Zheng, M., Wang, X., Templeton, L.J., Smulskim D.R., LaRossam, R.A., and Storz, G. (2001) DNA microarray-mediated transcriptional profiling of the *Escherichia coli* response to hydrogen peroxide. *J Bacteriol* **183:** 4562-4570.